INFORMATION TO USERS

This manuscript has been reproduced from the microfilm master. UMI films the text directly from the original or copy submitted. Thus, some thesis and dissertation copies are in typewriter face, while others may be from any type of computer printer.

The quality of this reproduction is dependent upon the quality of the copy submitted. Broken or indistinct print, colored or poor quality illustrations and photographs, print bleedthrough, substandard margins, and improper alignment can adversely affect reproduction.

In the unlikely event that the author did not send UMI a complete manuscript and there are missing pages, these will be noted. Also, if unauthorized copyright material had to be removed, a note will indicate the deletion.

Oversize materials (e.g., maps, drawings, charts) are reproduced by sectioning the original, beginning at the upper left-hand corner and continuing from left to right in equal sections with small overlaps. Each original is also photographed in one exposure and is included in reduced form at the back of the book.

Photographs included in the original manuscript have been reproduced xerographically in this copy. Higher quality 6" x 9" black and white photographic prints are available for any photographs or illustrations appearing in this copy for an additional charge. Contact UMI directly to order.

UMI®

Bell & Howell Information and Learning
300 North Zeeb Road, Ann Arbor, MI 48106-1346 USA
800-521-0600

IMPROVEMENT OF INELASTIC PERFORMANCE FOR FRICTION DAMPED ASYMMETRIC BUILDINGS

Hatem Bedair

A Thesis

in

School For Building (Civil Engineering)

Presented in Partial Fulfillment of the Requirements

for the Degree of Master of Applied Science at

Concordia University

Montreal, Quebec, Canada

August 1998

ABSTRACT

IMPROVEMENT OF INELASTIC PERFORMANCE FOR FRICTION DAMPED ASYMMETRIC BUILDINGS

HATEM BEDAIR

This thesis investigates the effect of having brace strength eccentricity (slip load eccentricity) negative that of stiffness eccentricity on the performance of friction damped braced frames, in an effort to improve the efficiency of friction damped braced frames in single and multi-storey buildings.

Firstly, multi-storey models having stiffness ratio (brace stiffness to frame stiffness) of three and strength ratio (brace strength to frame strength) of unity are subjected to an ensemble of earthquakes over a wide range of stiffness eccentricity e_s such that $0 < e_s < 1.2$ and a range of slip load e_{pb} such that $-e_s < e_{pb} < e_s$. The results demonstrate that as the slip load eccentricity e_{pb} moves from the stiff side to the flexible side of the structure, maximum displacement and ductility demands are reduced and more storeys participate in dissipating energy. Maximum improvement is obtained when $e_{pb} = -e_s$.

The inelastic behavior of single-storey model is studied using the history of base shear and torque. A single storey model with stiffness ratio of three and strength ratio of one is subjected to an earthquake over the range of slip load and stiffness eccentricity indicated above. The results show that as e_{pb} shifted to the flexible side of the structure the maximum base torque is decreased.

The energies imparted and dissipated by brace slippage and frame yield of the single

storey model indicated above are studied. The results demonstrate that the energy dissipated by the braces increases as the slip load eccentricity moves to the flexible side of the structure.

The research demonstrates that the slip load eccentricity must be considered in the design of friction bracing.

DEDICATION

I dedicated this work to the person who has affected my life the most, the person who teach me faith and self dependency. To my father with my love and respect.

ACKNOLEDGMENTS

I wish to thank my supervisor Dr. O. A. Pekau for his assistance and useful suggestions throughout the work. His knowledge about the subject as well as his curiosity have directed me to finish this work. The financial support for this work was provided by Natural Sciences and Engineering Research Council of Canada under Grant No. A8258.

Thanks are also extended to my numerous friends Yaser and Ahmad for their friendship and help. I would like also to express my sincere thanks to my parents and my sisters Marwa and Nermin for their love and long waiting.

Last but not least I would like to thank my fiance Doaa for her encouragement. Her patience and understanding are gratefully acknowledged

TABLE OF CONTENTS

Description Page

LIST OF FIGURES

Description Page

LIST OF TABLES

NOTATIONS

a	distance from center of mass to resisting elements in the direction of excitation
BST	base shear and torque surface
CM	center of mass of floor under consideration
CR	center of strength for arrangement of resisting elements
CR_F	center of resistance of frame
CR_B	center of resistance of brace
CS	center of stiffness of floor under consideration
d	distance from center of mass to resisting elements oriented along X-axis
D	plan dimension parallel to excitation
D_n	plan dimension perpendicular to excitation
e_p	strength eccentricity of combined system
e_{pb}	slip load eccentricity of braces
e_{pf}	strength eccentricity of unbraced frame
e_{pb}^*	normalized slip load eccentricity of braces
e_{pf}^*	normalized strength eccentricity of unbraced frame
e_s	stiffness eccentricity of combined system
e_{sb}	stiffness eccentricity of braces
e_{sf}	stiffness eccentricity of unbraced frame
e_s^*	normalized eccentricity of combined system

e_{sb}^*	normalized stiffness eccentricity of braces
e_{sf}^*	normalized stiffness eccentricity of unbraced frame
E_{brace}	energy dissipated by friction braces
E_{frame}	energy dissipated by frame yield
E_k	kinetic energy
E_s	strain energy
E_t	input energy of the system
E_ξ	the energy dissipated in viscous damping
FDBF	friction damped braced frame
K_{iy}	stiffness of individual resisting element
KB	lateral stiffness of brace
KF	lateral stiffness of unbraced frame
Ky	total lateral stiffness of the resisting elements
K_θ	torsional rigidity of the structure about center of mass
$K_{\theta s}$	torsional rigidity of the structure about center of stiffness
m	mass of structure
R	the code force modification factor (in current study R=4)
$R_{elastic}$	the theoretical maximum elastic seismically induced force
RByi	yield load of single resisting element
RB	resistance of brace
RF	resistance of unbraced frame
R_y	total resistance of the structure in the direction of excitation

R_{yi}	the yield resistance of the individual element
V_y	base shear in the y-direction
$V_y max$	maximum shear capacity of the system
T	period of structure
T_θ	base torque
$T_\theta max$	maximum torque capacity of the system
Δ_i	the i^{th} frame maximum displacement
Δ_{iy}	the i^{th} frame yield displacement
γ	relative torsional stiffness
ρ	radius of gyration about the center of mass
ω_y	uncoupled lateral frequency
ω_θ	uncoupled torsional frequency
$\omega_{1,2}$	coupled natural frequencies of the system
Ω_0	uncoupled torsional-lateral frequency ratio

CHAPTER 1

INTRODUCTION

The philosophy of the earthquake protection of buildings concentrate fundamentally on preventing collapse of the main structure during a severe earthquake. In recent years many researchers have been concerned with the development of new seismic structural systems that can improve the seismic performance of buildings. One of these systems is the friction damped braced frames (FDBF) which was introduced by Pall and Marsh in 1982. In this system the tension compression cross-braces are replaced by a mechanism containing a friction device in the intersection of the cross-braces. The friction damping device helps to absorb the extra energy input of severe earthquake excitations [1]. Because of the fact that costs combined with the repair and rehabilitation of buildings and their non-structural components in the outcome of an earthquake could be prohibitive, the idea of the friction damping device arose to overcome this deficiency. Friction dampers have successfully performed in other configurations of the bracing, namely in single diagonal braces and K-bracing for new construction as well as in retrofit of existing buildings[2].

As a good tool in governing structural response due to seismic excitations, friction damped braced frames have fascinated researchers to study the optimization procedure that would ensure maximum energy dissipation while minimizing lateral and torsional displacements. Early studies have concentrated on demonstrating the optimum ratios of stiffness and strength between the friction damped braces and the unbraced frames [3, 4]. Later attention has been given to the plan-wise distribution of strength and

stiffness between the device-equipped resisting braces [6].

This thesis studies the effect of slip load distribution on the displacement and ductility of the multi-storey structural models and on the base shear and torque as well as the energy dissipated by friction in the single-storey structure model, as an effort to determine a method for redistributing the slip load that would be easy to apply in order to improve the response.

The buildings studied in this thesis are 3-dimensional eccentric shear buildings of intermediate height. The resisting elements are moment resisting frames with friction damper braces. This study examines the inelastic behavior of eccentric buildings that have eccentricity up to 40 percent of the plan dimension due to variation of brace strength distribution (slip load eccentricity).

It should be noted that the analysis of the single and multi-storey stiffness eccentric models is made by using the two dimensional dynamic analysis program DRAIN-2D [14]. Therefore, all 3-D models have been converted to equivalent 2-D models. These 2-D models are explained in chapter 2. Moreover all definitions and formulation are described in chapter 2.

The research presented herein consists of three phases: the first phase deals with the effects of slip load distribution on the displacements and ductility demands of a multi-storey structural models; the second phase briefly addresses the effect that slip load distribution has on the base shear and torque of a single-storey structural model; and the third phase examines the effect of the slip load distribution on the amount of energy that the reconfigured braces will be expected to dissipate of a single storey model.

Phase I evaluates the previous single-storey model used [5,6] and its ability to provide responses over the full range chosen of slip load distributions. Suitable multi-storey models are then chosen consisting of five and ten typical single-storey models introduced in [5] and used in [6], and maximum displacements and ductility demands are obtained for a wide range of eccentricities and an ensemble of earthquakes, namely, the 1940 El Centro N-S excitation, the artificial Newmark-Blume-Kapur earthquake, the 1952 Taft S69E excitation, and the 1977 Romania N-S excitation. Comparisons are also made with the results of other researchers [6] to determine potential benefits of slip load redistribution. Particular attention is given to those structures having the center of strength of the unbraced structure coincident with the center of stiffness of the braced structure.

Phase II applies the slip load distribution used in phase I for the single-storey model, and the base shear and torque are obtained for the full range selected of stiffness eccentricity and strength distribution. The time history used was 1940 El Centro N-S excitation.

Phase III uses the same slip load and stiffness distribution of the single-storey model of the previous phase to report the amount of energy that will be imparted to the structures considered as well as the amount of energy that will be dissipated by the braces and by frame yield.

A review of the literature serving as a foundation of this research is presented below. Other relevant literature is given at appropriate points in each of the chapters.

1.1 LITERATURE REVIEW

Since Pall and Marsh introduced the friction dampers in 1982 [1], many researchers studied their performance in both single and multi-storey buildings for symmetric and asymmetric structures. Collectively, these studies have agreed with the fact that in order to optimize structure efficiency, tuning of the friction damped braces must be done with respect to both the stiffness and the slip load of the braces. Initially Baktash carried out the study of the ratio of brace strength to frame strength and demonstrated that the friction device offers maximum energy dissipation under pseudostatic loading when the brace strength equals to that of the unbraced frame in which it was added to [3]. Baktash simplified the analysis by studying a symmetric structure which required the analysis of only one friction damped braced frame (FDBF).

Later, Pekau and Guimond studied the effectiveness of FDBF in directing the seismic response of asymmetric structures. They studied the effectiveness of the ratio of the brace stiffness to the frame stiffness [4]. They demonstrated that an optimum response to seismic excitation will occur when this ratio exceeds seven. Pekau and Guimond established a single storey mass eccentric model containing two identical friction damped braced frames which the creation of the eccentricity of the model was achieved by moving the FDBF so that the center of stiffness of the structure, lying halfway between the two FDBF, no longer coincided with the center of mass of the deck.

For friction damped model with high stiffness of the brace (more than seven), the enhanced performance accompanying slip load redistribution has been presented by Martin and Pekau. However, such magnitude of brace stiffness to frame stiffness (KB/KB = 10) while desirable may not necessarily be realizable in practice owing to architectural layout requirements. For this reason Martin and Pekau evaluate the effectiveness of the reduced bracing to frame stiffness given by KB/KF = 3.

This study requires a model that can handle a wide range of stiffness eccentricity as well as the redistribution of slip load eccentricity. Therefore the unbraced single storey structure, created by Goel and Chopra [5], has been selected since it is an appropriate numerical model when analyzing the response of buildings subjected to coupled lateral torsional motions. The research of Goel and Chopra did not consider the effect of introducing friction damped braces into the systems.

To modify those sections of the Mexico building code belonging to earthquake resistant design, Tso and Ying [8], and Sadek and Tso [9] studied the optimization of the strength and stiffness distribution between resisting frames. Their studies showed that structures having strength eccentricity negative that of the stiffness eccentricity have a better performance under seismic loading than structures having their strength eccentricity limited to the positive range only. They further suggested that future modifications of the code should consider taking advantage of this phenomenon.

The previous research of the unbraced structures was the foundation of the work done by Martin and Pekau [7]. They studied the effect of the slip load distribution on the displacement and ductility demand of single-storey asymmetric friction damped structures. Martin and Pekau [7] demonstrated that improvement in performance of friction damped braced frames (FDBF) may be obtained by properly tuning the devices with respect to the slip load distribution between the resisting braces. For varying slip load distribution in asymmetric structures, optimum responses have been obtained when the slip load eccentricity is opposite that of the structure stiffness eccentricity [7].

Emphasizing the use of storey shear and torque histories as a tool to study the inelastic seismic behavior of asymmetric buildings, De La Llera and Chopra showed that the base shear and torque (BST) surface, in conjunction with the base shear and torque histories,

provides a useful conceptual framework for understanding the behavior of asymmetric systems [10]. They showed that changes in the planwise distribution of strength produces changes in the torsional capacity of the system and in the length of the constant base torque branch of the BST surface corresponding to predominantly torsional mechanisms of the structure [10]. Stiffness and strength asymmetry may be effectively used to control the torsional performance of a structure [12].

1.2 PHASE I: SLIP LOAD DISTRIBUTION IN MULTI-STOREY STRUCTURES

The ratio of brace strength to frame strength RB / RF was determined by Baktash [3], while the ratio of brace stiffness to frame stiffness KB / KF was established by Guimond [4]. Afterwards, Martin [6] proved that a reduction in KB / KF is acceptable. In Chapter 3 an attempt is made at determining how these limits may be set within the structure. The multi-storey models investigated are five and ten-storey models. Each storey is assigned global values of RB / RF = 1.0 and KB / KF = 3, and the models were strength eccentric models. These strength eccentric models are designed so that the strength eccentricity of the frames is equal the stiffness eccentricity of the structure, or the center of strength of the frames coincides with the center of stiffness of the structure ($e_{pf} = e_s$). At first, the slip load eccentricity was identical with the stiffness eccentricity, i. e. the total required slip load of the structure is concentrated on the stiff side of the model, then the slip load of the flexible side is increased and that of the stiff side is decreased while maintaining RB / RF the value of one. The slip load eccentricity, e_{pb}, is expected to vary between $-e_s$ and e_s. The results obtained were identical with those obtained by Tso and Ying [8] for unbraced single storey structures. That is, the optimum

responses occur when $e_{pb} < 0$. They also reflect the results obtained by Martin and Pekau for friction damped braced frames of single-storey structure.

The results obtained demonstrate that as the slip load eccentricity moves from the stiff side to the flexible side of the structure, more storeys will participate in dissipating energy and the optimum responses occur when $e_{pb} = -e_s$.

1.3 PHASE II: EFFECT OF SLIP LOAD DISTRIBUTION ON THE BASE SHEAR AND TORQUE HISTORY OF SINGLE-STOREY STRUCTURES.

Chapter 4 investigates the effect of slip load distribution on the inelastic seismic behavior of asymmetric single storey structures with friction dampers using the histories of base shear and torque. The first step in understanding this behavior is to construct the base shear and torque surface (BST) for the model, which represents all combinations of shear and torque that applied statically lead to collapse of the structure.

Considering the single storey model used by Martin [6], the value of RB / RF was set to be equal to unity and KB/KF = 3.

For the full range of stiffness eccentricity (from 0.0 to 1.2), the slip load is expected to vary between $-e_s$ and e_s. It was observed that the maximum base torque deceases as the slip load eccentricity move from the stiff side to the flexible side of the structure. Furthermore, strength eccentricity controls the width and skewness of the BST surface.

1.4 PHASE III: ENERGY ABSORPTION

The final phase of this study deals with the energy imparted and dissipated by the single storey model used in the previous phase. Chapter 5 looks at the effect of the redistribution of brace slip loads on the ability of the models to dissipate the inelastic energy by friction braces and by the frame yield. The energy input and dissipated time-histories are calculated for three cases of slip load eccentricity ($e_{pb}^* = e_s^*$, $e_{pb}^* = 0$ and $e_{pb}^* = -e_s^*$) with the full range chosen of stiffness eccentricity (e_s^* from 0 to 1.2). The results obtained reflect those of phase 1 & 2 in which the maximum energy dissipated by brace slippage is in the case of $e_{pb}^* = -e_s^*$.

Analysis of the overall results obtained shows that the improved optimum performance of the FDBF occurs when the slip load eccentricity equals the stiffness eccentricity but on the other side of the structure.

CHAPTER 2

DESCRIPTION OF THE MODEL

2.1 INTRODUCTION

This chapter depicts the single-storey structural model which will be used to investigate the effects of the slip load redistribution between the friction device equipped braces on the inelastic seismic behavior of asymmetric buildings and on the energy imparted and dissipated by the system. Also described in this chapter are the multi-storey models that will be used to study the effect of slip load distribution on the maximum edge displacements and element ductility demands. The multi-storey models are used in the early part of the investigation as an extension of the work by Martin [6] for a single-storey model.

The single-storey model is the stiffness eccentric model used by Goel and Chopra [5]. The model has four resisting elements as shown in Figure 2.1, two elements in the direction of excitation and two resisting elements in the orthogonal direction. A special case of this model is the case with only two resisting elements in the direction of excitation which have been used in most of this study. The model with two elements in the direction orthogonal to the excitation has been used in one case during the current investigation when the torsional rigidity of the structure need to be increased. The two elements in the direction of excitation are friction damped braced frames (FDBF), while the two resisting elements in the orthogonal direction, if they exist, are assumed to be elastic elements, i. e. all models used have two FDBF in the direction of excitation.

2.2 DESCRIPTION OF THE SINGLE-STOREY MODEL (Without Braces)

The single-storey stiffness eccentric model described in this section was originally introduced by Goel and Chopra [5] and selected by Martin [6] to study the effect of slip load distribution on the maximum response and ductility demand of single -storey structures. This model has the ability to simulate a wide range of slip load and stiffness distribution that will be used in the study.

The basic structure consists of a rigid rectangular deck of mass m and dimensions D_n by D, supported by two massless frame elements as imaged in Figure 2.2. The dimensions are chosen to be a function of the mass radius of gyration ρ as follow:

$$D_n = 3\rho \tag{2-1}$$

$$D = \sqrt{3} \cdot \rho \tag{2-2}$$

The aspect ratio (D_n/D) is thus chosen to be 1.732. According to Tso [15] an aspect ratio less than unity gives higher response but in fact it is less likely to occur than the aspect ratio chosen. Moreover it is important that the values of the deck dimension chosen follow the mathematical relation for the mass radius of gyration:

$$\rho^2 = \frac{I_j}{A} \tag{2-3}$$

$$\rho^2 = \frac{I_x + I_y}{A} = \frac{1}{D_n \cdot D} \cdot \left(\frac{D_n \cdot D^3}{12} + \frac{D \cdot D_n^3}{12} \right) \tag{2-4}$$

$$\rho^2 = \frac{(D_n^2 + D^2)}{12} \tag{2-5}$$

For simplicity the model is symmetric about the X-axis and lateral movement of

the center of mass in the X-direction is prevented. For Y-direction earthquake excitation, the result is a simple model with only two degrees of freedom: the translation displacement, y, of the center of mass, CM, relative to the ground in the Y-direction and a rotation, θ, about a vertical axis passing through the center of mass of the model. Figure 2.2 shows the general layout of the single-storey model or the typical floor of the multi-storey models; as can be seen two resisting elements (1 & 2) in the direction of excitation (Y-direction) are located at a distance of (a) to either side of CM along the X-axis. One special case of this study dealt with a torsionally rigid structure; in this case, high torsional rigidity was set up by the introduction of the two resisting elements in the orthogonal direction (elements 3 & 4 of Figure 2.1). Elements 3 and 4 are located at a distance of (d) to either side of CM along the Y-axis. The elements in the orthogonal direction are assumed to remain elastic, which means that the two models of Figures 2.1 and 2.2 are similar in that they both have two friction damped braced frames in the direction of excitation, the difference being that the model with elements in the orthogonal direction has a wider range of increased torsional rigidity.

Lateral and torsional rigidities of the model are given by:

$$K_y = \sum_i K_{iy} \tag{2-6}$$

$$K_x = \sum_j K_{jx} \tag{2-7}$$

$$K_\theta = \sum_i K_{jy} a_i^2 + \sum_i K_{jx} d_i^2 + \sum_i K_{i\theta} \tag{2-8}$$

$$K_{\theta s} = K_\theta - e_s^2 K_y \tag{2-9}$$

where K_y is the total lateral stiffness of the resisting elements in the direction of

excitation (the Y-direction), K_x is the total lateral stiffness of the elements in the orthogonal direction (the X-direction), $K_{i\theta}$ is the torsional rigidity of an element about its own axis (can be neglected for planar members), K_θ is the torsional rigidity of the structure about the center of mass, CM, and $K_{\theta s}$ is the torsional rigidity of the structure about the center of stiffness, CS. In equation 2-8 the second term exists only for systems with elements in the X-direction.

The yield strength of the frame element is assumed proportional to stiffness. That means that the center of resistance of the frame, CR_F, coincides with the center of stiffness of the structure. The center of stiffness of a structure, is defined as that point along the deck where the resultant of the lateral force passes through without any rotation of the deck. The center of resistance, CR, of a structure is defined as that point along the deck where the resultant of the lateral load of sufficient magnitude causes yielding in all resisting elements at the same instant. The distance measured from the center of stiffness to the center of mass is the elastic stiffness eccentricity and is denoted by e_s. The other eccentricity that will be used in this study is the plastic eccentricity or the strength eccentricity. The plastic eccentricity denoted by e_p can be defined as the distance measured from the center of resistance to the center of mass. Accordingly, four eccentricities can be defined for the model:

$$e_s = \frac{1}{K_y}\sum_i K_{iy} a_i \qquad (2\text{-}10)$$

$$e_p = \frac{1}{R_y}\sum_i R_{yi} a_i \qquad (1\text{-}11)$$

$$e_s^* = \frac{e_s}{\rho} \tag{2-12}$$

$$e_p^* = \frac{e_p}{\rho} \tag{2-13}$$

where e_s^* represents the static stiffness eccentricity, normalized with respect to the radius of gyration about the center of mass ρ, coming from an irregular distribution of stiffness and mass, and e_p^* expresses the normalized static strength eccentricity due to the variation of yield strength of the resisting elements. R_y depicts the total resistance of the structure in the direction of excitation and is given by:

$$R_y = \sum_i R_{yi} \tag{2-14}$$

where R_{yi} is the yield resistance of the individual elements. The occurrence of yielding of the resisting elements is ensured by limiting the maximum induced elastic resistance of the element to the ratio of the theoretical maximum elastic seismically induced force, $R_{elastic}$, to the code force modification factor, R. Thus, R_y is represented as:

$$R_y = \frac{R_{elastic}}{R} \tag{2-15}$$

In this study a value of R = 4.0 was used, which depicts the maximum allowable modification factor for structures that have high level of ductility according to the 1995 NBCC [16]. The uncoupled lateral frequency and the uncoupled torsional frequency about the center of mass can now be defined as:

$$\omega_y = \left(\frac{K_y}{m}\right)^{\frac{1}{2}} \tag{2.16 a}$$

$$\omega_x = \left(\frac{K_x}{m}\right)^{\frac{1}{2}} \tag{2-16 b}$$

$$\omega_\theta = \left(\frac{K_\theta}{m\rho^2}\right)^{\frac{1}{2}} \tag{2-17}$$

Two other torsional frequencies which have been used in the literature are [11]:

$$\omega_{\theta s} = \left(\frac{K_{\theta s}}{mr^2}\right)^{\frac{1}{2}} \tag{2-18}$$

$$\omega_{\theta o} = \left(\frac{K_{\theta s}}{m\rho^2}\right)^{\frac{1}{2}} \tag{2-19}$$

where r is the mass radius of gyration about the center of resistance, CR, of the structure. Consequently, three uncoupled torsional to lateral frequency ratios, can be defined:

$$\Omega^2_{CM} = \frac{\omega^2_\theta}{\omega^2_y} \tag{2.20}$$

$$\Omega^2_{CR} = \frac{\omega^2_{\theta s}}{\omega^2_y} \tag{2-21}$$

$$\Omega^2_o = \frac{\omega^2_{\theta o}}{\omega^2_y} \tag{2-22}$$

The uncoupled torsional to lateral frequency ratio Ω_o is a significant feature that allows direct comparison of the results as long as it is constant and independent of the eccentricity of the structure.

Moreover the two coupled natural frequency of the system can be calculated from the following equation [11]:

$$\frac{\omega_{1,2}^2}{\omega_y^2} = \frac{1+\Omega_{CM}^2}{2} \pm \sqrt{\frac{\left[1-\Omega_{CM}^2\right]^2}{4} + (e_s^*)^2} \qquad (2\text{-}23)$$

Because of the fact that friction dampers are considered to be most advantageous to multi-storey buildings of moderate height, a period of vibration of T = 1.0 sec. is specified. In addition, since the lateral-torsional coupling in elastic structures is most critical when the torsional to lateral frequency ratio is near unity, therefore, $\Omega_o = 0.9$ will be adopted for the models used in this study. The remaining variables are thereby adjusted to ensure the specified T and Ω_o. The dimensions of the model with two resisting elements in the direction of excitation together with the large eccentricity (e_s = 1.2) used in this study are not allowing Ω_o grater than 0.9. Therefore, the resisting elements in the orthogonal direction have been introduced when Ω_o needed to be more than 0.9.

2.2.1 Positioning the Resisting Elements

The single-storey stiffness eccentric structure of Figure 2.1 shows the general layout of the single-storey model or the typical floor of the multi-storey models. The model has two resisting elements in the direction of excitation (Y-direction) and two resisting elements in the orthogonal direction (X-direction). The center of mass coincides with the geometric centroid of the deck and the resisting elements are placed at equal distance either side of CM in both directions. The eccentricity is created by assigning different stiffness to the resisting elements in the direction of excitation. Determining the

actual in-plan position of the resisting elements is done according to the equations set forth in reference [5]. Considering the generalized system of Figure 2.1, the resisting elements of this stiffness eccentric system are located according to:

$$\frac{d}{\rho} = \frac{\sqrt{\gamma_x}\Omega_o}{\omega_x/\omega_y} \tag{2-24}$$

$$\frac{a}{\rho} = \sqrt{(1-\gamma_x)\Omega_0^2 + (e_s{}^*)^2} \tag{2-25}$$

where ω_x / ω_y is the lateral vibration frequency ratio equal to $(K_x / K_y)^{1/2}$ and γ_x is defined as the relative torsional stiffness of frames oriented along the X-direction to the torsional stiffness and is given by:

$$\gamma_x = \frac{\left(\sum_i K_{ix} d^2{}_i\right)}{K_{\theta s}} \tag{2-26}$$

The stiffness of each element are given by:

$$\frac{K_{1y}}{m} = \frac{\omega_y^2}{2}\left(1 - \frac{e_s{}^*}{a/\rho}\right) \tag{2-27}$$

$$\frac{K_{2y}}{m} = \frac{\omega_y^2}{2}\left(1 + \frac{e_s{}^*}{a/\rho}\right) \tag{2-28}$$

$$\frac{K_{3x}}{m} = \frac{K_{4x}}{m} = \frac{\omega_y^2}{2}\left(\frac{\omega_x}{\omega_y}\right)^2 \tag{2-29}$$

If the elements of the orthogonal direction do not exist, "d" will be zero and equation 2-25 will be as follows:

$$\frac{a^2}{\rho^2} = \Omega_0^2 + (e_s{}^*)^2 \tag{2-30}$$

2.2.2 Adding Friction Damper Equipped Braces

A friction damper device basically consists of series of steel plates with slotted holes (Figure 2.4). The plates are specially treated to develop most reliable friction [24]. They are clamped together with high strength bolts and allowed to slip at a predetermined load.

Braces and frames are alike in that they have particular strength and stiffness features. The difference between traditional X or K bracing and friction damper equipped braces is that the friction damper does not undergo traditional yielding. It starts to slip at predetermined load equal to the yield point of traditional bracing. Only if the friction damper bracing reaches its maximum slip displacement, then it can practice yielding. During an earthquake, the friction dampers start to slip and dissipate energy at the predetermined load just before the structural elements undergo yielding deformation [3]. After the earthquake the strain energy of the framed structure brings the friction damper to their near original alignment.

Because of this likeness between braces and frames, the equations introduced earlier are applied to the bracing as well. In order to remove the confusion between the strength, stiffness and slip load eccentricity of the frame and bracing, the following notations are used for each of the frame and bracing properties. Hence, the frame stiffness and strength eccentricity can be defined as:

$$e_{sf} = \frac{1}{KF_y} \sum_i KF_{iy} a_i \tag{2-31}$$

$$e_{pf} = \frac{1}{RF_y} \sum_i RF_{yi} a_i \tag{2-32}$$

and the brace stiffness and slip load eccentricity can be formulated as:

$$e_{sb} = \frac{1}{KB_y} \sum_i KB_{iy} a_i \tag{2-33}$$

$$e_{pb} = \frac{1}{RB_y} \sum_i RB_{yi} a_i \tag{2-34}$$

where e_{sb} is the stiffness eccentricity of the braces measured from the center of mass to the center of rigidity of the braces, and e_{pb} is the strength eccentricity or the slip load eccentricity of the braces measured from the center of mass of the structure and the slip load center of the braces. The slip load center of the braces is defined as that point along the deck where the application of a force of sufficient magnitude causes all the braces to slip at the same time. Figure 2.3 shows the position of center of stiffness and center of resistance for the frames and braces due to different distribution of slip load, frame resistance and stiffness.

The stiffness is defined (for both the braced and the unbraced frames) as the load that results a storey drift of unity. The individual frame resistance, RF_{yi} is defined as the force required for the resisting element to start yielding, and the individual brace strength, RB_{yi}, is defined as the force needed for one friction damper to start slippage at constant load.

Two new variables of particular interest can be introduced: the ratio of total brace stiffness to total frame stiffness, KB / KF, and the ratio of total brace strength to total frame strength, RB / RF.

Several studies have been dealt with the optimization of KB / KF and RB / RF by other researchers and will not be reproduced here [3, 4, 6, 7, 11]. Baktash [3] and Pekau

and Guimond [4] used two dimensional analysis and made some simplifying assumptions to examine the ratio of total strength or stiffness. One common assumption in both studies was that the resisting frames would be identical in stiffness and strength, and that the braces assigned to each frame would also have identical slip loads and stiffnesses. Guimond [11] established the ratio of braces stiffness to frame stiffness KB / KF to be grater than seven. Later Martin and Pekau showed that KB /KF = 3 is adequate. From these studies, it was concluded that the optimum response of a structure would be obtained when the RB / RF ratio was near unity and KB / KF of three is satisfactory. The current research studies the effect of changes in distribution of RB_{yi} and KB_{iy} while RB / RF and KB / KF remain constant.

2.2.3 Computer Modeling of the Single-storey Structures Considered

The single-storey model used is that with only two FDBF in the direction of excitation. The analysis of this single-storey stiffness eccentric model made by using the two dimensional dynamic analysis program DRAIN-2D [14]. Therefore, the system has been converted to an equivalent 2-D model. Figure 2.2 represents the layout of the structure to be modeled. The rigid deck is replaced by beam element with infinite rigidity. The infinite rigidity of the beam is insured by selecting suitable material property which reflects that of the deck. A simple truss element was chosen to model the frame and braces. The truss elements have the stiffness and yielding properties of the frame, or the stiffness and the slip load property of the friction dampers. Figure 2.6 shows the idealized single-storey model and figure 2.8 shows the idealized translational and rotational deformations.

The mass of each floor is assumed to be lumped at the floor level. Thus it is easy to assign the center of mass to the control node in the model of the beam which is assumed to be the center of mass. This point was prevented from horizontal movement. The application of beam elements for modeling the deck and truss elements for modeling the resisting elements is verified by the design assumptions that have been made. The truss elements carry only tension or compression which is compatible with the assumption that frames act as massless tension compression spring. Control points are located at the edges of the model, at the location of the resisting elements, and at the CM point. Finally, positioning of the resisting elements and the structural properties governing their behavior is dictated by equations (2.1) to (2.31).

It should be noted that if an element (frame or brace) does not exist, it will be assigned either a KB or RB value of zero.

To study the maximum edge displacement and ductility demands of the single storey structures (chapter 3), the models used were subjected to four earthquake records (1940 EL Centro N-S, the Newmark-Blume-Kapur artificial excitation, 1952 Taft S69-E, 1977 Romania N90-W).

In chapter 4 this idealized single-storey model was subjected to 1940 El-Centro N-S earthquake record to study the inelastic seismic behavior of single-storey structure using histories of base shear and torque.

To study the energy input and dissipated by the system (chapter 5), the model was subjected to 1977 Romania N90W earthquake excitation.

2.3 MULTI-STOREY MODELS

In addition to the translational motions, buildings subjected to earthquakes often undergo a torsional motion. The torsional motion arises because of the eccentricity between the center of mass and the center of stiffness at various floors of the building.

It is simple to estimate the center of mass of a building. Therefore the analysis of the structure will be straightforward if the requirement is to apply the seismic force through the center of mass. However, if the load application point is the center of stiffness, hence the position of the center of stiffness must be determined. In this study a ground excitation is applied to multi-storey eccentric friction damped braced frame to study the response due to different stiffness eccentricities (0.0, 0.3, 0.5, 0.75, 0.9 and 1.2). Therefore the center of stiffness has to be known.

For multi-storey buildings there is no exact definition for the center of stiffness. It is possible to define the center of stiffness at any floor level as the point that when applying a lateral force through it, the floor level under consideration has no rotation, but the other floor levels may rotate.

In this study the center of stiffness and the center of mass of each floor level are set to lie on two vertical lines and the stiffness eccentricity e_s is assumed to be the distance between the two lines.

2.3.1 Description of Multi-storey Stiffness Eccentric Model

In the multi-storey models (five and ten Storey) the floor level of each storey consists of a rigid rectangular deck of mass m, that is supported by two massless, planar frame elements. The deck dimensions and aspect ratio are as the same as the single-storey

model. The center of mass and resistance are set to lie on two vertical lines. At each floor level, the multi-storey models have two degrees of freedom: translation y in the y-direction and rotation θ about the vertical axis through the center of mass. As a single-storey model each floor is assumed to be symmetric about the x-axis; however there is unsymmetry about the y-axes.

As the case for single storey model, the multi-storey models under consideration are strength eccentric models where the strength eccentricity of the unbraced frame equals the stiffness eccentricity i.e. $e_p = e_s$. In this case the yield strength of the resisting frame elements RF is assumed proportional to stiffness, therefore, the CR of all floor levels lie on one vertical line coincident with the CS vertical line.

The strength of unbraced structure RF is calculated from the elastic response of the symmetric structure, for which the maximum base shear is $R_{elastic}$. Employing the code force modification factor R, $RF_y = R_{elastic}/R$.

In this study a value of R=4 is considered which represents the reduction factor for ductile systems according to 1995 NBCC. The frame elements of all storeys are assumed to be identical.

2.3.2 Position of Resisting Elements

The centers of mass of the floor levels of the multi-storey model lie on one vertical line. At each floor level the resisting elements are position symmetrically about the CM which coincides with the geometric centroid of the deck. Determining the actual in-plan position of the resisting elements for each floor level is done according to the set of equations (2.23 to 2.28)

The stiffness eccentricity normalized with respect to the mass radius of gyration ρ was allowed to vary over the range (0 to 1.2) while the slip load eccentricity normalized with respect to the mass radius of gyration ρ was allowed to vary over the range ($-e_s^*$ to e_s^*) i.e.

$$0 \le (e^*_s = e_s/\rho) \le 1.2 \tag{2-35}$$

$$-1.2 \le (e^*_{pb} = e_{pb}/\rho) \le 1.2 \tag{2-36}$$

The computer program DRAIN-2D [14] was used for the analysis of the multi-storey models with five percent viscous damping and time step $\Delta t=0.01$ sec. Four earthquake records were used as the seismic input base excitation: 1940 El-Centro N-S; the Newmark-Blume-Kapur artificially generated ground motion; 1952 Taft; 1977 Romania N90W Figure 2.10 shows the acceleration time history of this ensemble.

The eccentricity in the x-direction between the center of mass and center of stiffness is represented by e_s and is constant throughout the height, for each floor level the stiffness eccentricity is calculated from equation 2.10. A period of vibration of T=1.0 sec. and a torsional to lateral frequency ratio is $\Omega_o=0.9$ are specified. The SAP90 program was used to calculate the period of vibration and the lateral and torsional frequencies, several iterations being used to adjust the variables to ensure the specified T and Ω_o. Simply the properties of the one storey model are used for each floor level of the multi-storey models and using SAP90 program, the mode shapes, frequencies, and fundamental periods are calculated. Then the properties were readjusted by the ratio of the calculated fundamental period and 1.0.

To check the uncoupled torsional to translational frequency ratio, equation 2.23 is

used to calculate the ratio of ω_2 / ω_1 for each eccentricity of the single storey model. Then SAP90 was used to calculate the same ratio for each eccentricity of the multi-storey models to ensure that they are identical with the values of one storey model.

2.3.4 Computer Modeling of Structures Considered

The lateral analysis of asymmetric building structures usually requires a full three dimensional computer procedure. It is acceptable to reduce the size of the problem by neglecting less significant degrees of freedom, for instance normal bending and torsion of columns and beam, and by taking advantage of the particular structural and geometric features of the building [25].

Analysis of the multi-storey models will be done through the use of DRAIN-2D, a two dimensional dynamic analysis program [14]. Therefore, as single-storey model, the multi-storey models have been converted to equivalent two dimensional multi-storey models as shown in Figures 2.9 and 2.10. The idealized multi-storey computer model of Figure 2.9 represents the case in which the model has only two FDBF resisting elements in the direction of excitation, while Figure 2.10 depicts the case that has two more elastic elements in the orthogonal direction.

For each floor level of the multi-storey models the rigid deck is modeled as a series of beam elements with infinite rigidity and material properties reflecting those of the rigid deck, the lengths of the beam elements are chosen to be equal to the distance between control nodes. The frames and braces are modeled as truss elements, each having the lateral stiffness and yielding properties of the resisting elements. For the friction brace, the yield resistance specified for the truss element equals the slip load of the brace.

The mass of each floor level is assumed to be concentrated at the centroid of the deck, therefore, it is possible to assign the total mass of a floor level to that point in the center of the rigid beam and considered as the center of mass CM of that floor level. The center of mass of each floor level was prevented from horizontal movement.

The rigid beam of all floors and the lumped mass assigned to the center of the beam of each floor are assumed to be identical for all floors. Moreover the frames and braces properties (stiffness and strength or slip load) of each side of the model are identical for all floors since the centers of stiffness and the centers of resistance of all floor are lay on two vertical lines.

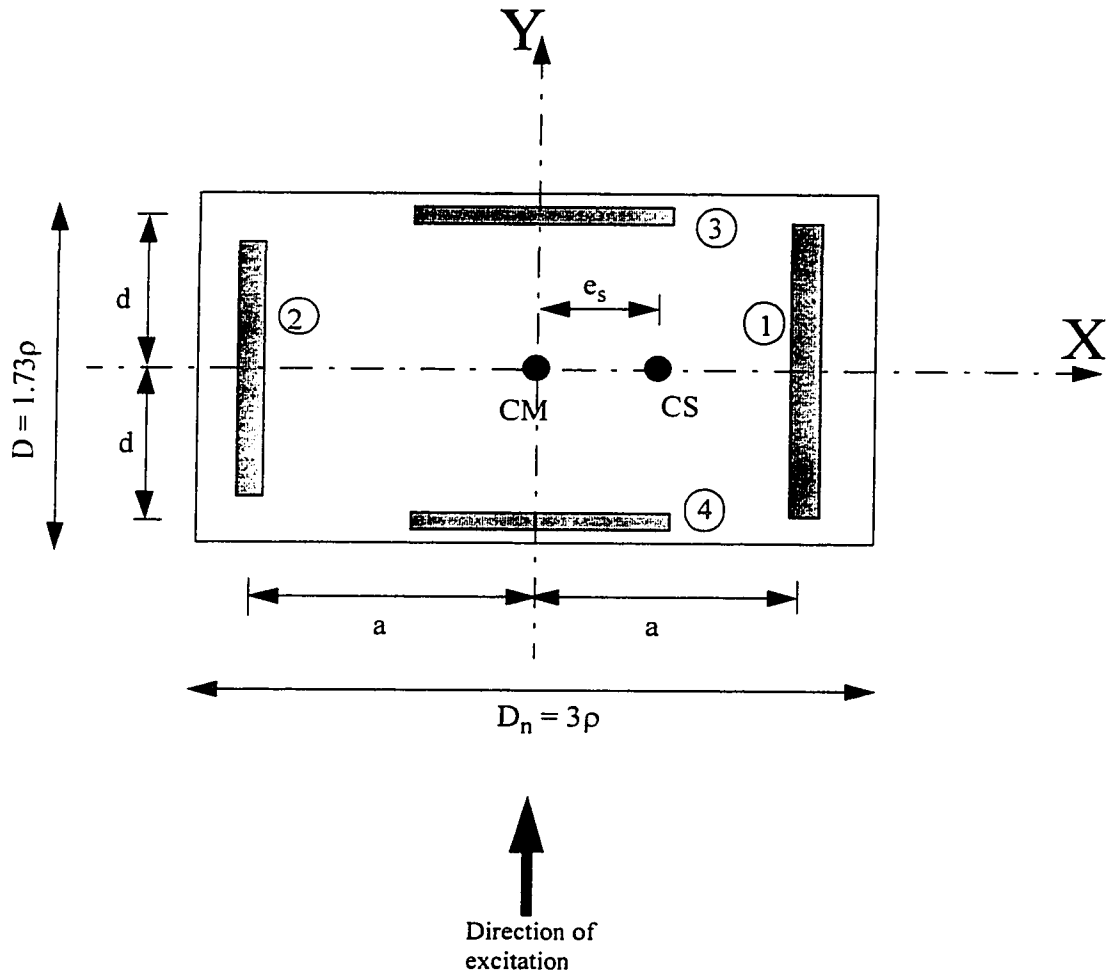

Figure 2.1 Generalized stiffness eccentric model with two FDBF in the direction of excitation and two elastic elements in the orthogonal direction

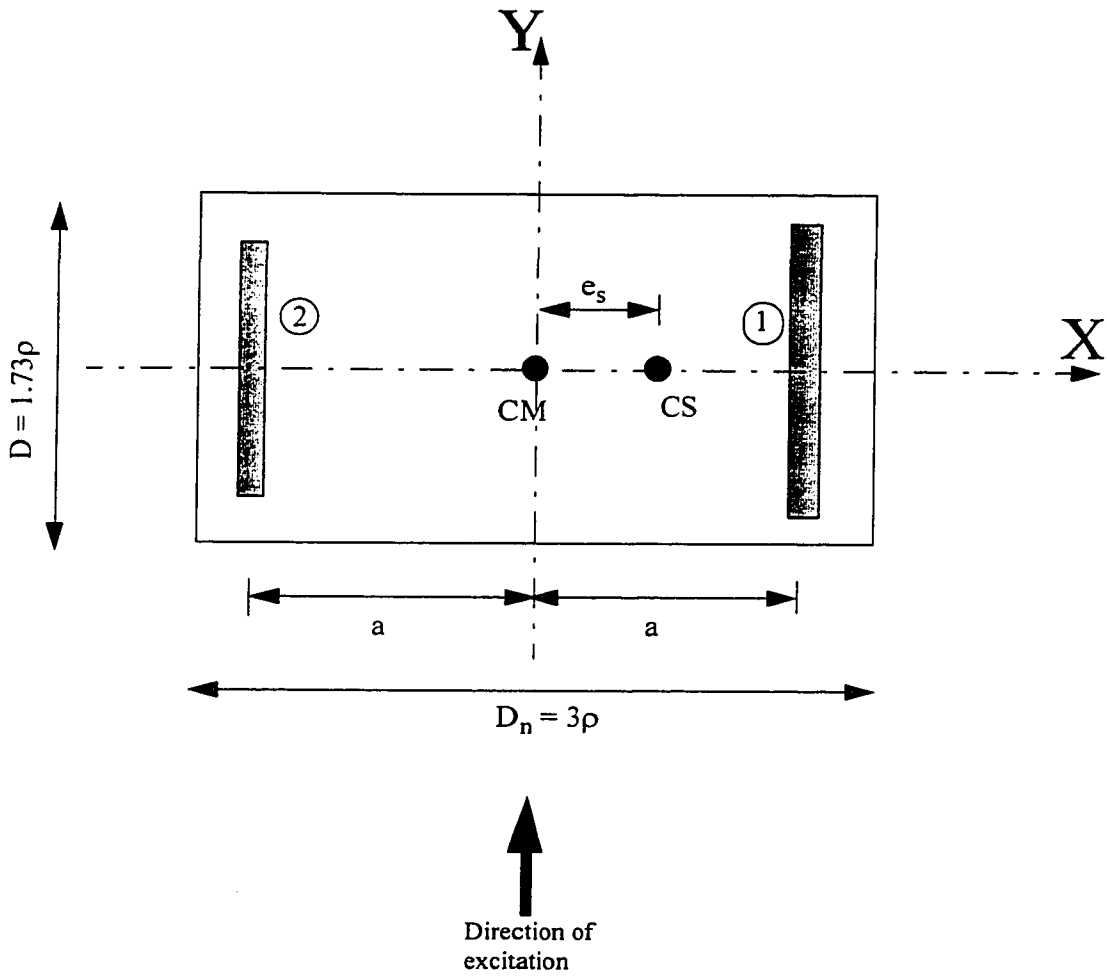

Figure 2.2 Generalized stiffness eccentric model with two FDBF in the direction of excitation

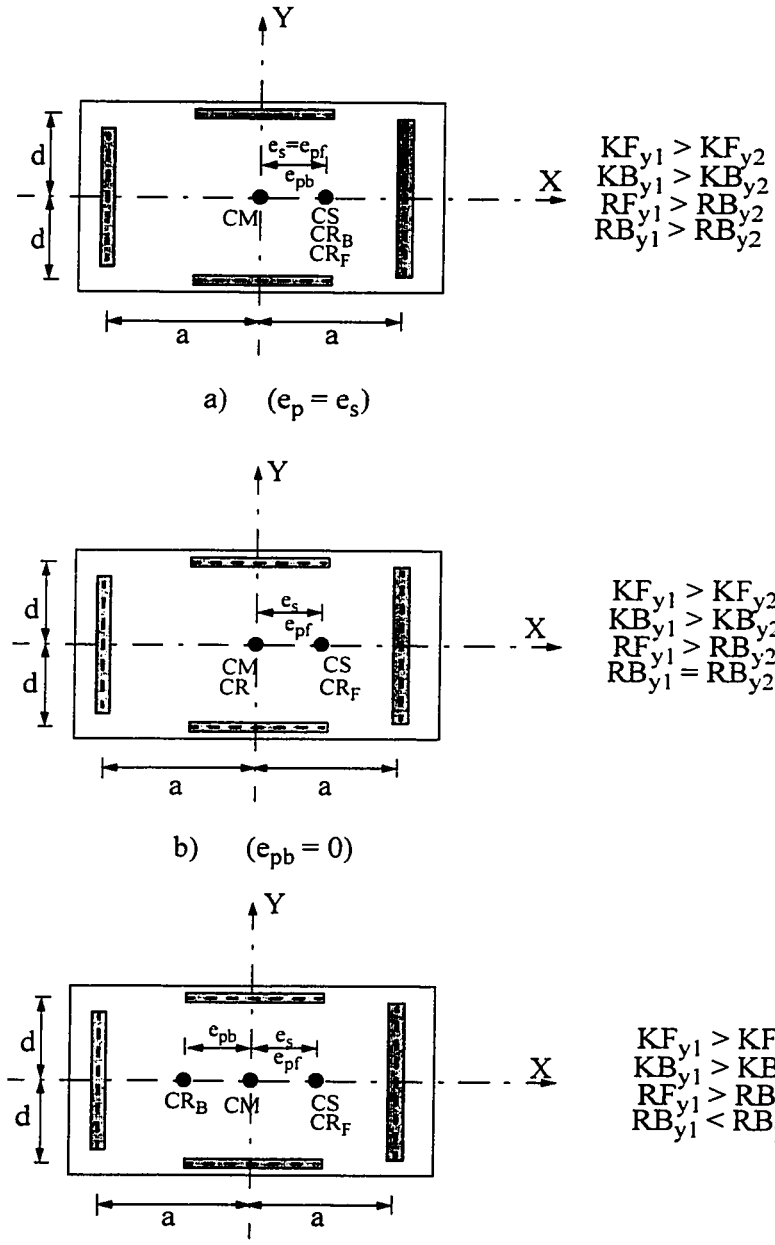

Figure 2.3 Positions of CS, CM, CR_F, CR_B due to different slip load distribution

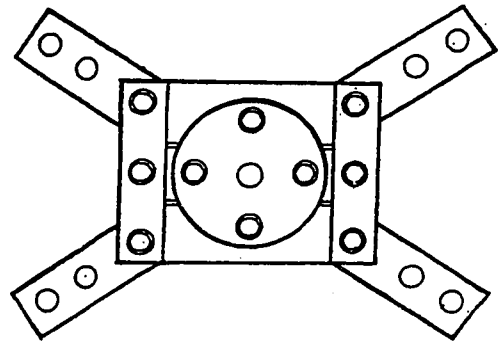

Figure 2.4 Typical friction device [3].

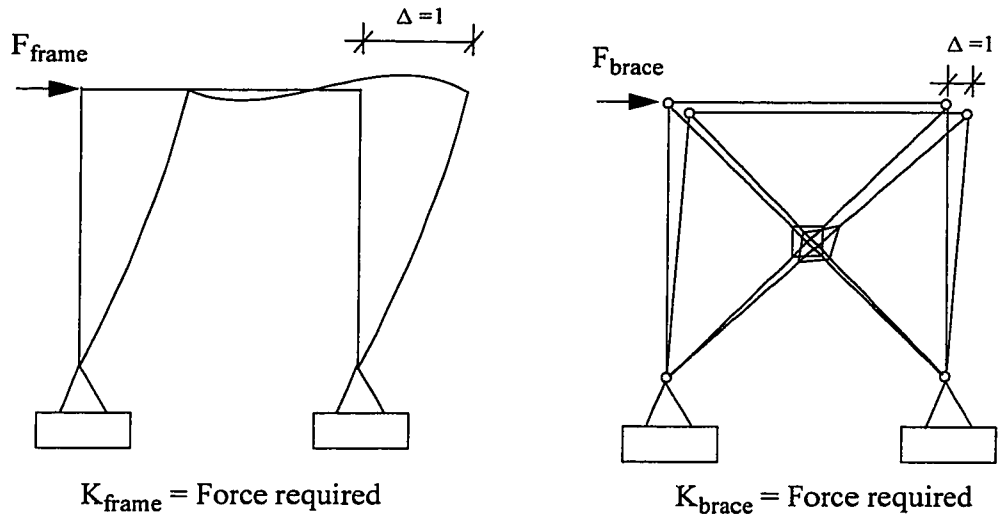

Figure 2.5 Definition of stiffness [11]

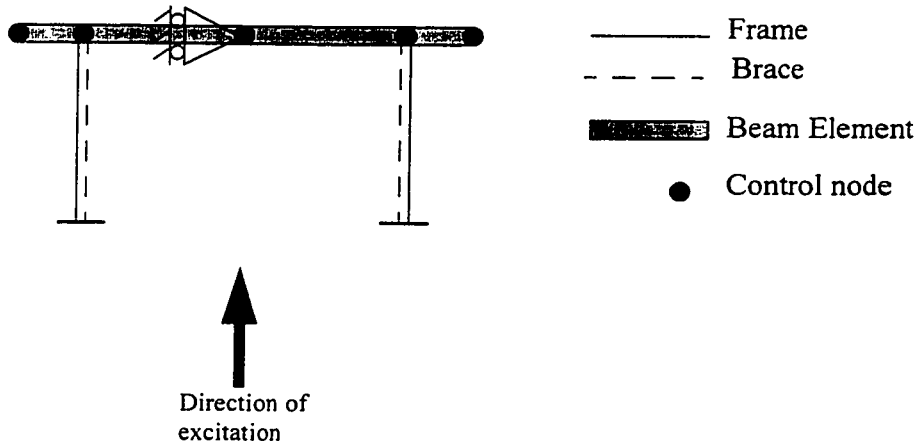

Figure 2.6 The idealized single-storey model and typical floor of the multi-storey models with two FDBF in the direction of excitation

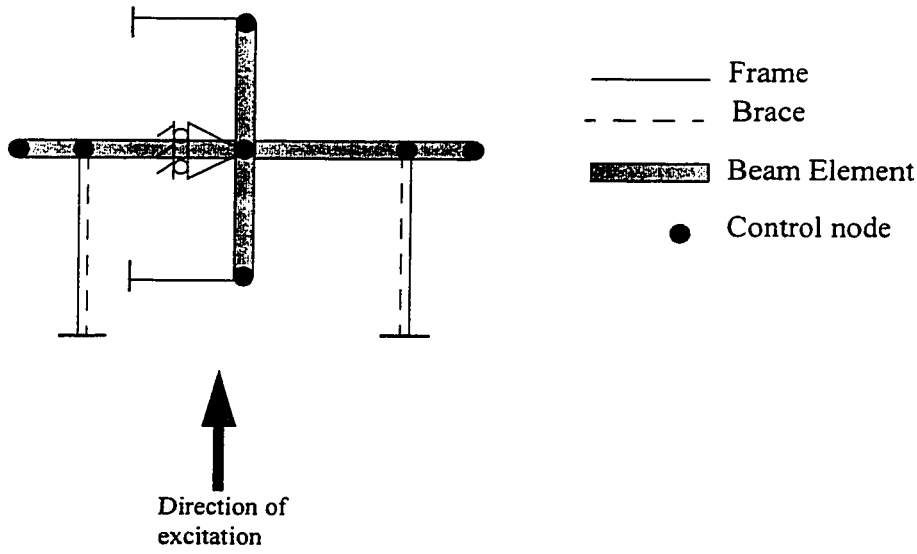

Figure 2.7 The idealized typical floor level of the multi-storey model with two FDBF in the direction of excitation and two elastic elements in the orthogonal direction

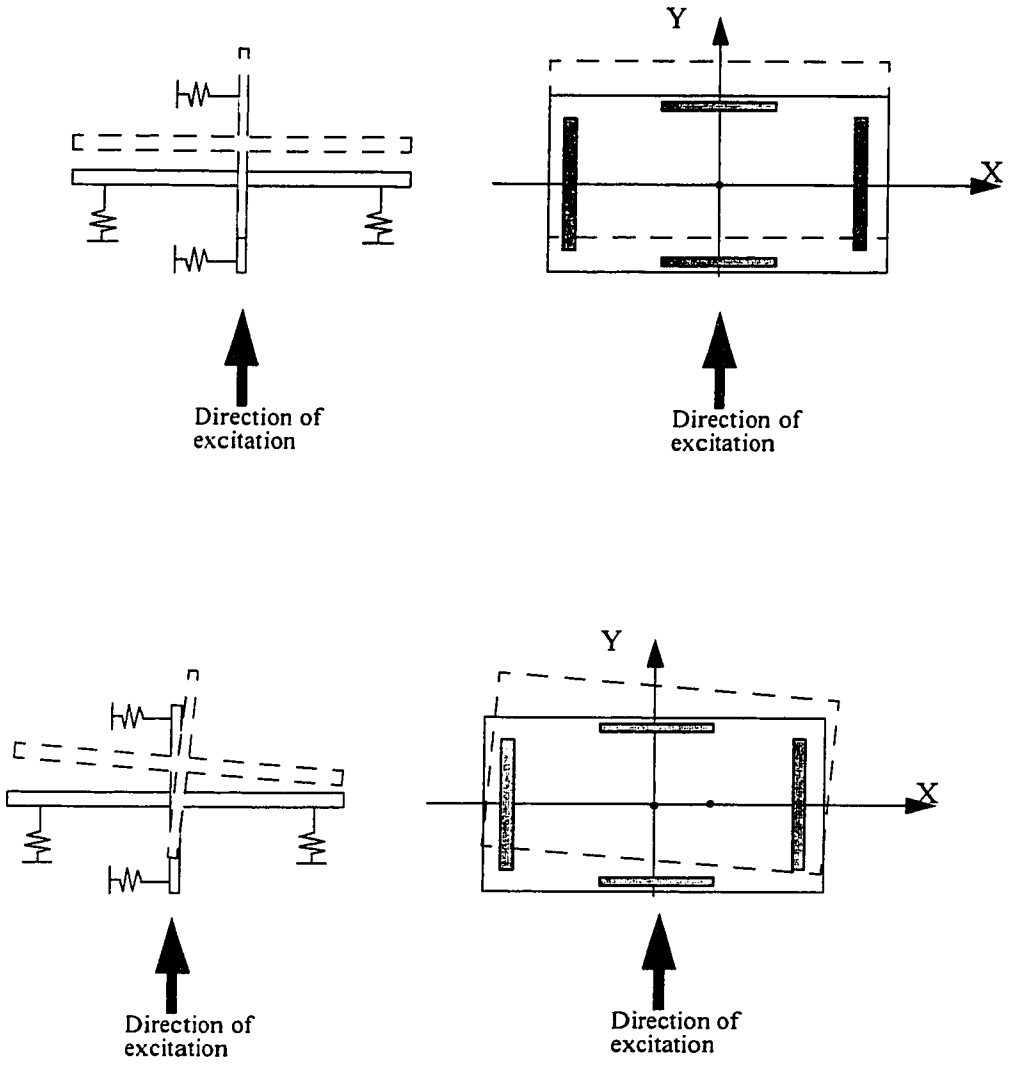

Figure 2.8 The idealized translation and rotation for symmetric and asymmetric models

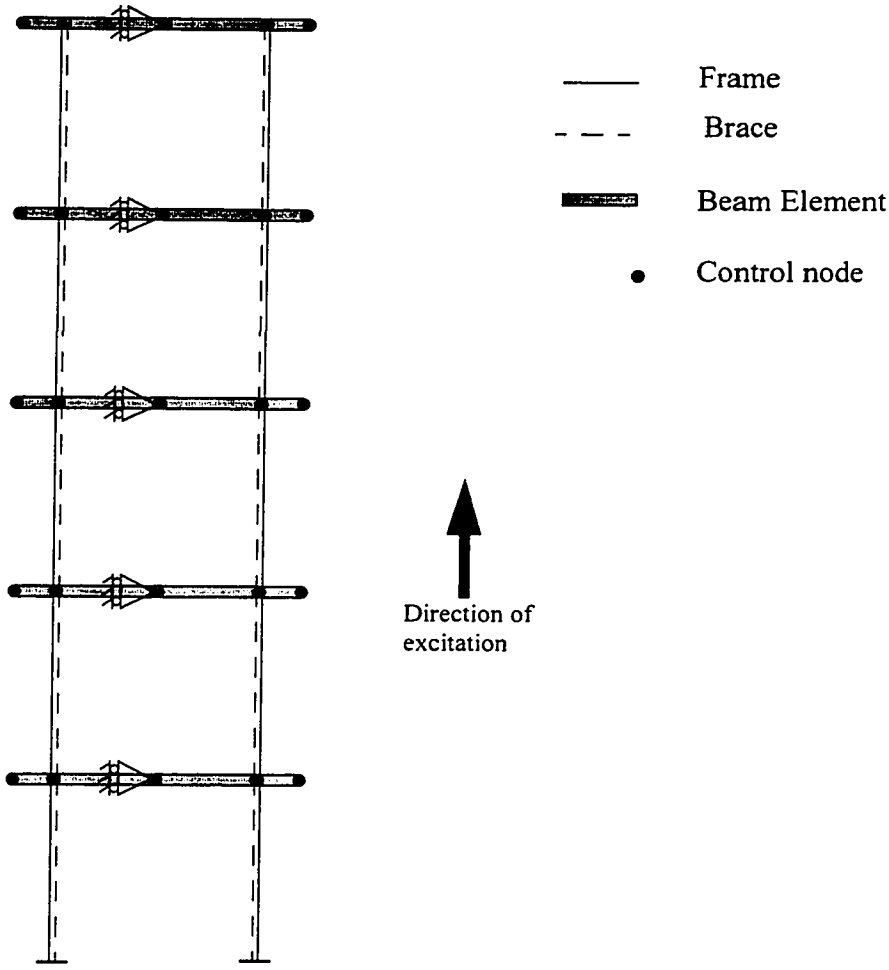

Figure 2.9 The idealized multi-storey model with two FDBF in the direction of excitation.

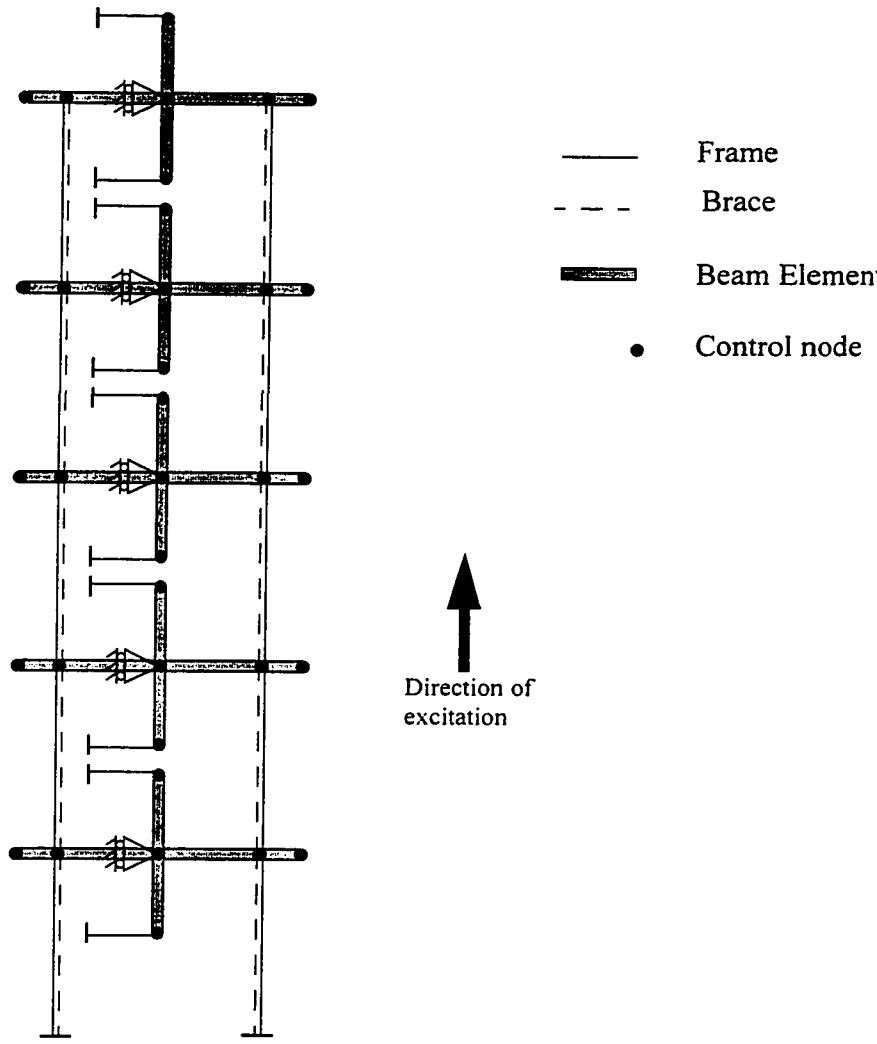

Figure 2.10 The idealized multi-storey model with two FDBF in the direction of excitation and two elastic elements in the orthogonal direction

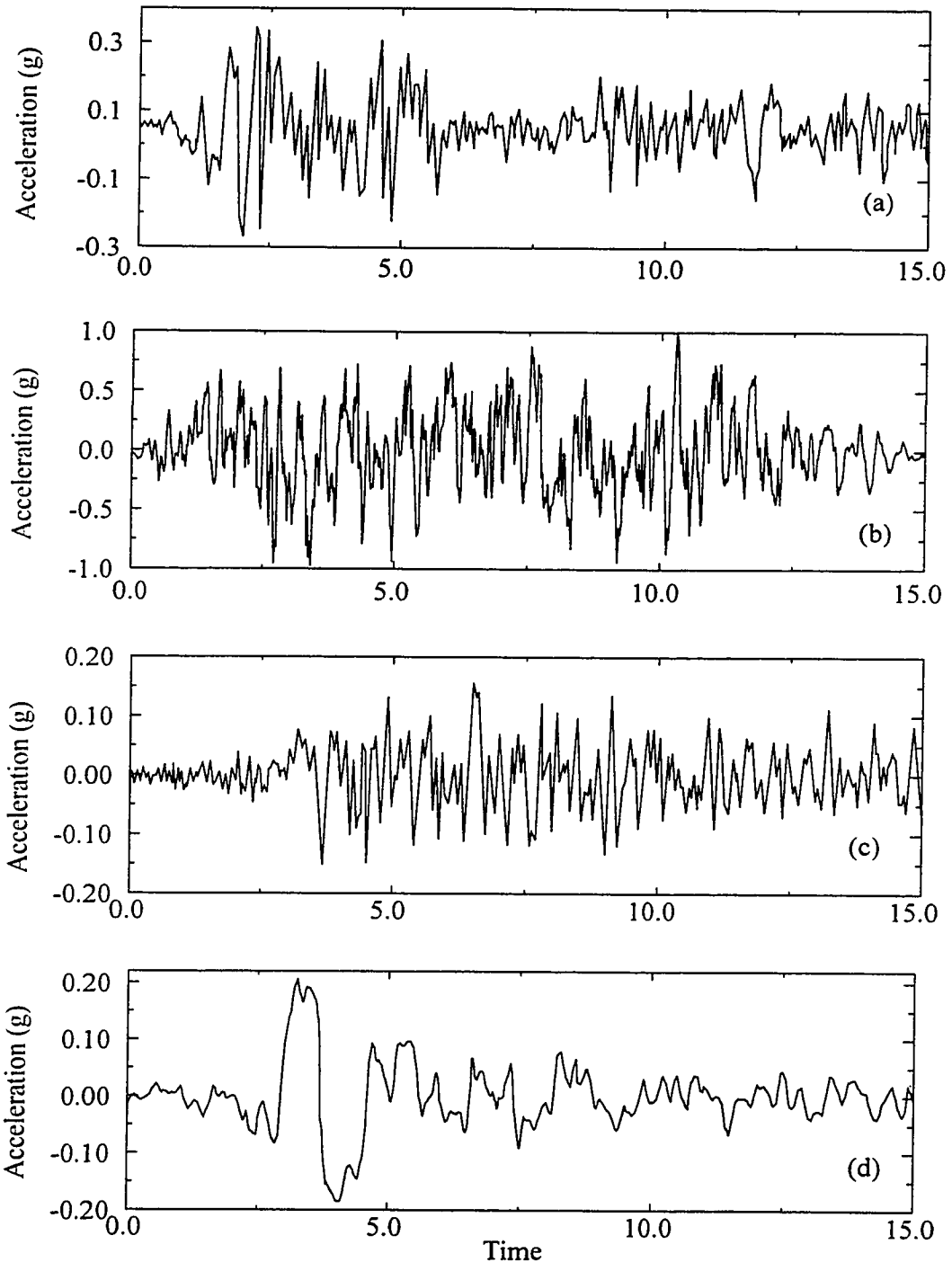

Figure 2.11 Acceleration time histories for earthquake ensemble: (a) 1940 El CentroNS; (b) Newmark-Blume Kapur artificial excitation; (c)1952 Taft S69E; (d) 1977 Romania N-S

CHAPTER 3

ANALYSIS AND RESULTS OF THE 2-D MULTI-STOREY MODELS SUBJECTED TO CHANGE IN SLIP LOAD DISTRIBUTION

3.1 INTRODUCTION

This chapter deals with the distribution of the slip load of friction damped braces in multi-storey structures. The optimum ratio of the slip load to frame strength, RB/RF, was determined by Baktash [3] to be equal to unity. The slip load and stiffness distribution of the single-storey structures was the subject studied by Martin [6]. The results obtained by Martin are the basis of this chapter. He obtained that the optimum slip load distribution for a single-storey model occurs when the slip load eccentricity equals to the stiffness eccentricity, but in the other direction. Martin and Pekau [7] later showed that the ratio of the brace stiffness to frame stiffness KB/KF = 3 is satisfactory.

The research herein aims to determine how the limits established by Baktash, Martin and Pekau can be utilized to minimize the response of the multi-storey models chosen (five and ten storey models).

3.2 OPTIMIZATION OF THE STRENGTH DISTRIBUTION

The ratio of the slip load (brace strength) to frame strength RB/RF was set to unity, and the ratio of the brace stiffness to frame stiffness KB/KF was chosen to be three.

The structural parameters allowed to vary were the normalized stiffness eccentricity $e_s^*=e_s/\rho$, and the slip load eccentricity of the friction damped braces $e_{pb}^*=e_{pb}/\rho$. The stiffness eccentricity e_s^* was allowed to vary from 0 to 1.2 which provides results for structures with no eccentricity to structures with eccentricity equal to 40 percent of the plan dimension. The slip load eccentricity was allowed to vary from $-e_s^*$ to e_s^* (from -1.2 to 1.2). The distribution of the frame strength also was allowed to vary from 0 to 1.2 and it is set to be equal to the normalized stiffness eccentricity ($e_{pf}^* = e_s^*$).

The stiffness of the brace to the stiffness of frame KB/KF=3 means that the stiffness of each brace was equal to three times that of the frame in which it was located. The braced system had the same stiffness eccentricity as the unbraced system.

For each storey of the multi-storey models, the total slip load required for the brace was calculated to be equal to the sum of all the strengths of the frames in which the braces were to be placed. The total required stiffness was determined as the sum of all the stiffnesses of the frames in which the brace were to be placed multiplied by the KB/KF ratio of three.

The stiffness eccentricity was introduced by increasing the stiffness on one side of each floor level (the stiff side) and decreasing the stiffness on the other side (the flexible side). Three values of the slip load eccentricity were introduced. The first one when $e_{pb}^*=e_s^*$ where the center of the slip load (the center of strength of the friction damped braces) CR_B coincides with the center of stiffness CS. This case is introduced by increasing the slip load on the stiff side and decreasing the slip load in the flexible side in each floor level while keeping the ratio of RB/RF equal to unity. The second value was

when $e_{pb}^* = 0$ where CR_B coincides with CM. In this case the total slip load was distributed equally on the two resisting elements. The last value of the slip load was $e_{pb}^* = -e_s^*$ in which the slip load increased in the flexible side of each floor level of the structure and decreased in the stiff side, while keeping the ratio of RB / RF equal to unity.

The response of the multi-storey models with five percent viscous damping and time step $\Delta t = 0.01$sec. was obtained using DRAIN-2D for six eccentricities ($e_s^* = 0$, 0.3, 0.5, 0.75, 0.9, 1.2) and four earthquakes (1940 EL Centro N-S, the Newmark-Blume-Kapur, artificial excitation, 1952 Taft S69-E, 1977 Romania N90-W) were processed. Normalized response is plotted verses normalized stiffness eccentricity for the three different values of the normalized slip load eccentricity.

The response was normalized by taking the maximum edge response of the structure and dividing it by the corresponding maximum edge response of the unbraced symmetric structure. A period of vibration of T = 1.0 sec. and the uncoupled torsional to translational frequency ratio $\Omega_0 = 0.9$ are specified.

3.3 RESULTS OF THE STRENGTH ANALYSIS

Described in this section is the analysis of the single, five and ten-storey models with two resisting element in the direction of excitation and no orthogonal resisting elements. The uncoupled torsional to lateral frequency ratio $\Omega_0 = 0.9$ is specified for the three models described in this section.

The study done by Martin [6] for single-storey model with four FDBF (two in direction of excitation and two in the orthogonal direction) and $\Omega_0 = 1.0$, has been

repeated here for the model with no resisting element in the orthogonal direction and uncoupled torsional to translational frequency $\Omega_0 = 0.9$ to be consistent with the multi-storey models chosen.

The results of the single storey model were identical with the results obtained by Martin in which showed a reduction in the maximum edge displacement and ductility demand as the slip load eccentricity moved from the stiff side to the flexible side of the structure. For large eccentricity ($e_s^* = 1.2$), the maximum edge displacement when $e_{pb}^* = -e_s^*$ was reduced by 70 percent of the maximum edge displacement when $e_{pb}^* = e_s^*$ (Figures 3.1 & 3.2)

Both multi-storey models showed also reduction in the maximum edge displacement as the slip load eccentricity moved from the stiff side to the flexible side of the structure. Figure 3.3 shows the normalized maximum edge displacement of the five storey model. As can seen for large eccentricity ($e_s^* = 1.2$) the response decreased from the case of $e_{pb}^* = e_s^*$ to that of $e_{pb}^* = -e_s^*$ by 50 percent. For the ten-storey model shown in Figure 3.8 the reduction was 53 percent.

For all models the case of $e_{pb}^* = -e_s^*$ keeps the normalized maximum edge displacement of all eccentricities less than one, i.e. less than the maximum edge displacement of the symmetric unbraced case.

The symmetric case ($e_s^* = 0$) of single, five and ten-storey models experiences a maximum edge displacement of one third that of the symmetric unbraced case [Y_{max} (e = 0 & KB/KF=0)]. This may be due to the fact that adding bracing is equivalent to increase the stiffness and yield strength of the frame, i.e. providing frames with higher stiffness and yield strength will decrease the maximum edge displacement. Consequently, it is

expected that the optimum response will be achieved if the slip load of the brace reduces the strength eccentricity represented in the unbraced system.

In general the minimum displacement occurs when the normalized slip load eccentricity e_{pb}* equals -e_s*; therefore, the minimum normalized response $Y_{max.}$/ $Y_{max.}$(e=0 & KB/KF=0) occurs when the eccentricity of the slip load equal to the stiffness of the structure but on the opposite side.

Most modern codes, including the national building code of Canada, involves the concept of ductility. Ductility is defined as the capacity of the members to safely absorb energy during earthquake while undergoing large inelastic deformation. The ductility demand of an element is the ratio of maximum displacement to yield displacement. Figures 3.5 to 3.7 and 3.10 to 3.12 show the ductility demand of the flexible edge for the five storey and ten storey models respectively.

The ductility demand of the first storey of the five and ten storey models are shown in Figures 3.4 and 3.9, respectively. As can seen, the ductility demand increases with increase in e_s*. More importantly, the ductility demand with variation of slip load distribution shows that the best results are obtained when e_{pb}* = -e_s*. Also the case of e_{pb}* = 0 keeps the ductility demand below e_{pb}* = e_s*.

If one stops to consider how ductility demand affect the multi-storey structure. one will realize that, in the symmetric case (e_s* = 0), few storeys were ductile (two storeys in the five storey model and three storeys in the ten storey model). While for large eccentricity (e_s* = 1.2), in the five storey model of Figure 3.7 three storeys were ductile when e_{pb}* = e_s*, four storeys when e_{pb}* = 0 and five storeys when e_{pb}* = -e_s*. The ten storey model with large eccentricity (e_s* = 1.2) of Figure 3.12 shows that six storeys were

ductile when $e_{pb}^* = e_s^*$, eight storeys when $e_{pb}^* = 0$ and nine storeys when $e_{pb}^* = -e_s^*$. This phenomenon means that, as the center of slip load moves from the stiff side to the flexible side, more storeys will participate in dissipating energy and the ductility demand will decrease.

3.4 CONCLUDING REMARKS

The analysis of the friction damped brace strength distribution of the multi-storey models has indicated to the following:

- Minimum response of multi-storey buildings were obtained when the slip load of the friction braces has been distributed so that the normalized slip load eccentricity equals the stiffness eccentricity but in the opposite side of the structure, i.e. $e_{pb}^* = -e_s^*$.

- For practicality, good results were obtained when the slip load of the brace has been distributed so that $e_{pb}^* = 0$, which places the center of the braces strength CR_B coincident with the center of mass CM.

- At the optimum distribution of the slip load ($e_{pb}^* = -e_s^*$), more storey levels will participate in dissipating energy.

All results were obtained using four earthquake records (1940 EL Centro N-S, the Newmark-Blume-Kapur, artificial excitation, 1952 Taft S69-E, 1977 Romania N90-W).

All model have only two FDBF in the direction of excitation.

3.5 EFFECT OF THE CHANGE OF THE TORSIONAL TO LATERAL FRE-

QUENCY RATIO ON THE RESPONSE

This part studied the effect of torsional rigidity of the structure on the maximum edge displacement and ductility demand of the multi-storey buildings with various slip load distribution.

The ten-storey model with the same parameters and limits indicated earlier except the torsional to lateral frequency ratio Ω_0 has been chosen in this part of the study.

Two cases of torsional rigidity have been considered: the first case is the torsionally flexible structure, in this case the torsional to translational frequency ratio chosen to be equal to 0.7 ($\Omega_0^2 = 0.5$); the second is the torsionally rigid case, in this case the torsional to translational frequency ratio chosen to be equal to 1.7 ($\Omega_0^2 = 3$). For the plan dimension chosen with two resisting elements in the direction of excitation, Ω_0 cannot exceed 0.9. Therefore, one has to introduce elements in the orthogonal direction to adjust Ω_0 to be equal to 1.7. These two elements are placed at distance "d" on either side of the center of mass CM in the y-direction. Most important is that the elements in the orthogonal direction are assumed to remain elastic, so that they do not contribute to the energy dissipation. The structure will still have two FDBF in the direction of excitation.

The rest of the parameters are kept as before (RB / RF = 1, KB / KF = 3 and T = 1sec.).

The analysis was performed using DRAIN-2D program with five percent viscous damping and integration time step Δt=0.01. The system was excited by the same four earthquake records (1940 EL Centro N-S, the Newmark-Blume-Kapur, artificial excitation, 1952 Taft S69-E, 1977 Romania N90-W).

3.6 RESULTS OF THE STRENGTH ANALYSIS

The results for the torsionally flexible model ($\Omega_0 = 0.7$) are shown in Figures 3.13 to 3.17. As expected the maximum edge displacement shows a reduction as the slip load eccentricity moves from the stiff side to the flexible side of the structure (Figure 3.13). The reduction is smaller than the reduction when $\Omega_0 = 0.9$; for example, for the large eccentricity (e_s*=1.2) of the torsionally flexible model ($\Omega_0 = 0.7$), the maximum normalized edge displacement is reduced from the case of $e_{pb}^* = e_s^*$ to that of $e_{pb}^* = -e_s^*$ by 35 while it was 53 percent when $\Omega_0 = 0.9$. Moreover, the maximum edge displacement in the case of $e_{pb}^* = -e_s^*$ for normalized stiffness eccentricity as large as 0.9 and 1.2 exceed $Y_{max.}$(e=0 & KB/KF=0), i.e. exceed the maximum edge displacement of the symmetric unbraced case.

The ductility demand in the first storey of the ten-storey torsionally flexible model (Figure 3.14) shows that the best performance occurs when $e_{pb}^* = -e_s^*$. Also more storeys will be ductile as the slip load eccentricity moves from the stiff side to the flexible side of the structure (Figures 3.15 to 3.17).

Correspondingly, the ten-storey torsionally rigid model ($\Omega_0 = 1.7$) showed that the best behavior occurs when $e_{pb}^* = -e_s^*$. Similarly, more storeys are ductile as the slip load eccentricity moves from the stiff side to the flexible side of the structure (Figure 3.18). The maximum edge displacement for all slip load distribution cases with different eccentricities is below that of the symmetric unbraced case. For large eccentricity (e_s*=1.2), the maximum edge displacement in the case of $e_{pb}^* = e_s^*$ is 0.58 $Y_{max.}$(e=0 & KB/KF=0). However, the maximum edge displacement is reduced from the case of e_{pb}^*

$= e_s^*$ to that of $e_{pb}^* = -e_s^*$ by 40 percent.

The ductility demand curves (Figures 3.19 to 3.22) show that the general trend still applies for $\Omega_0 = 1.7$, as can be seen that more storeys participate in dissipating energy as the slip load moves from the stiff side to the flexible side of the structure. It is obvious that the total number of storeys that have ductility for each eccentricity are less than the case of $\Omega_0 = 0.9$. For example, in large eccentricity (e_s^*=1.2), four storeys are ductile in the case of $e_{pb}^* = e_s^*$, five in the case of $e_{pb}^* = 0$ and seven in the case of $e_{pb}^* = -e_s^*$, while six storeys are ductile in the case of $e_{pb}^* = e_s^*$, eight in the case of $e_{pb}^* = 0$ and nine in the case of $e_{pb}^* = -e_s^*$when $\Omega_0 = 0.9$.

3.7 CONCLUDING REMARKS

The analysis of the possible variation in strength distribution between friction damped braces with changes in the uncoupled torsional to translational frequency ratio has revealed the following:

- As torsional rigidity of the structure increases, the maximum edge displacement decreases.

- The reduction from the case of $e_{pb}^* = e_s^*$ to that of $e_{pb}^* = -e_s^*$ decrease as the uncoupled torsional to translational frequency Ω_0 become smaller or greater than the critical value ($\Omega_0 = 0.9$), i.e the idea of having slip load eccentricity equal to the stiffness eccentricity but on the other side of the structure is most beneficial for structures that

have uncoupled torsional to translational frequency near one.

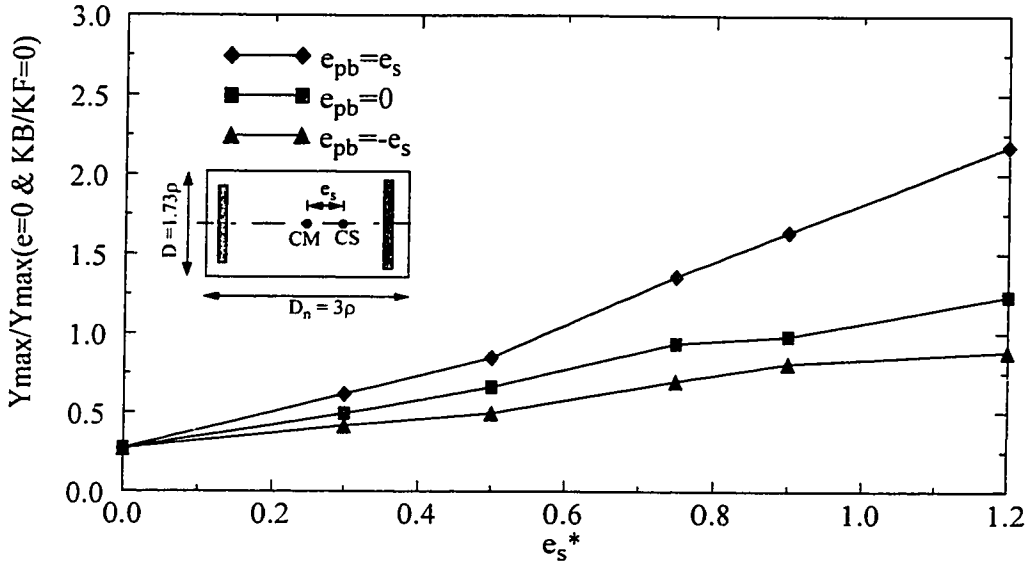

Figure 3.1 Displacement performance for single -storey model
(average of 4 earthquakes, Ω_0=0.9 & T=1)

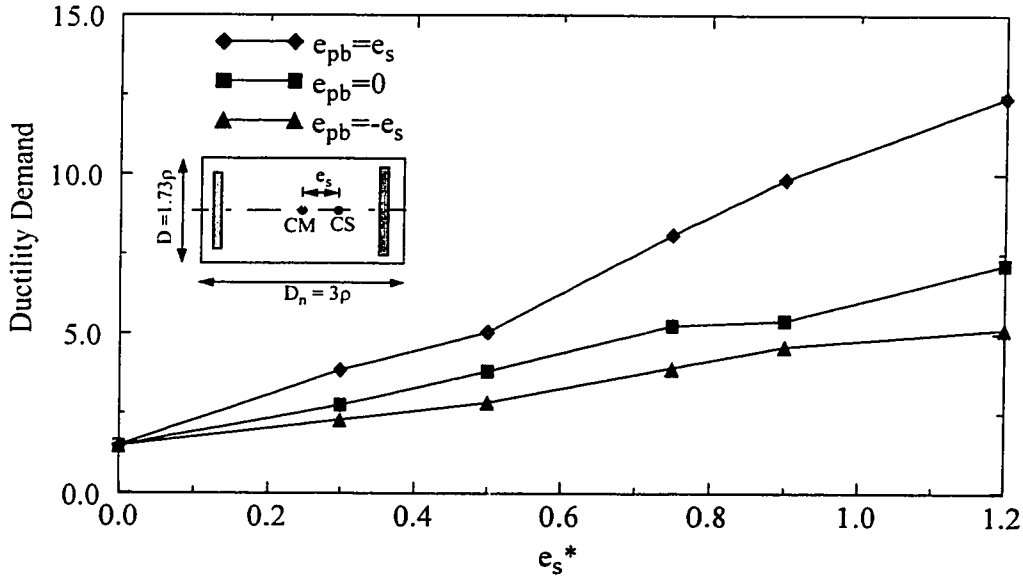

Figure 3.2 Ductility demand for single-storey model
(average of 4 earthquakes, Ω_0=0.9 & T=1)

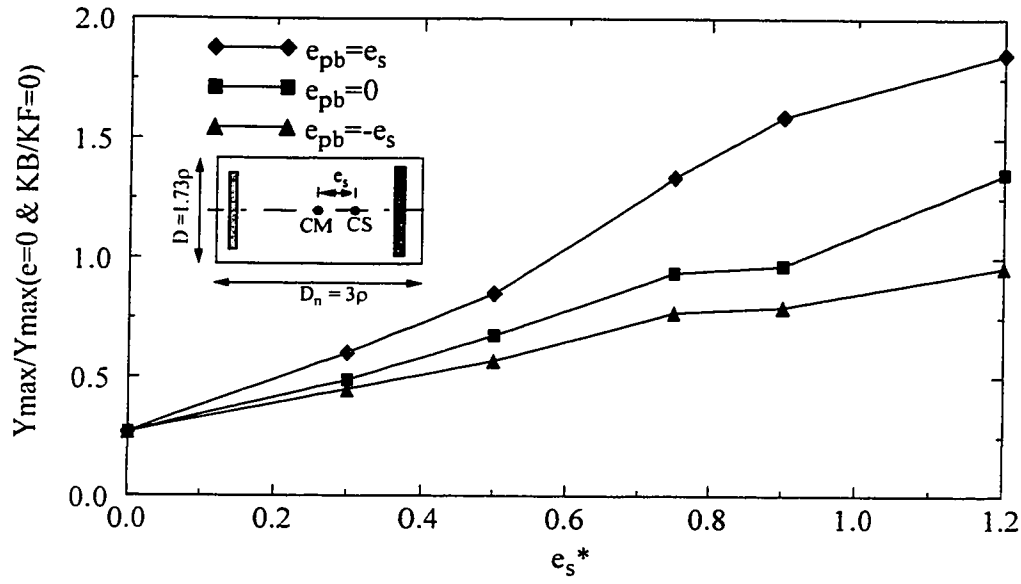

Figure 3.3 Maximum edge displacement of the five-storey model
(average of 4 earthquakes, Ω_0=0.9 & T=1)

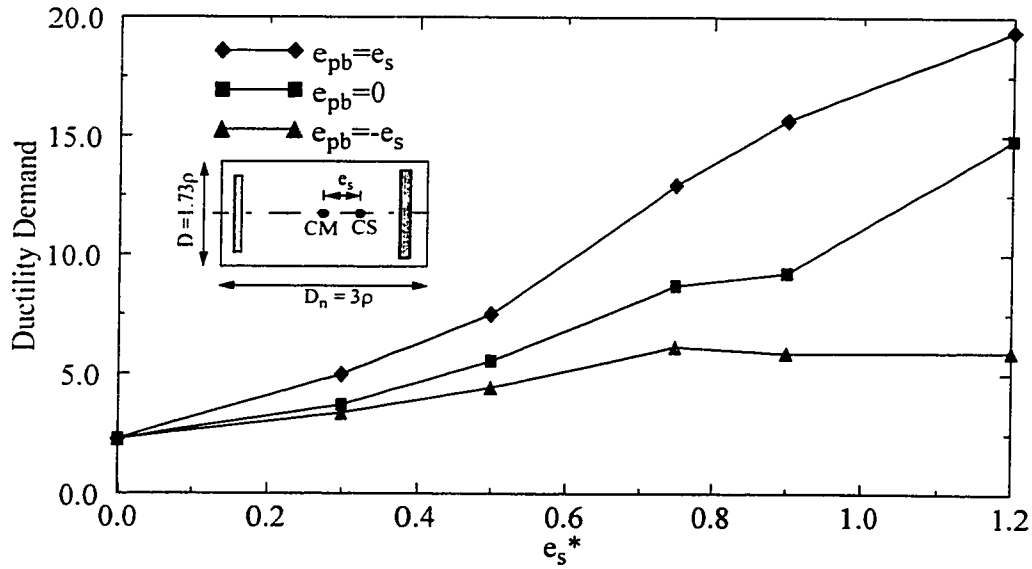

Figure 3.4 Ductility demand for the first storey of the five-storey model
(average of 4 earthquakes, Ω_0=0.9 & T=1)

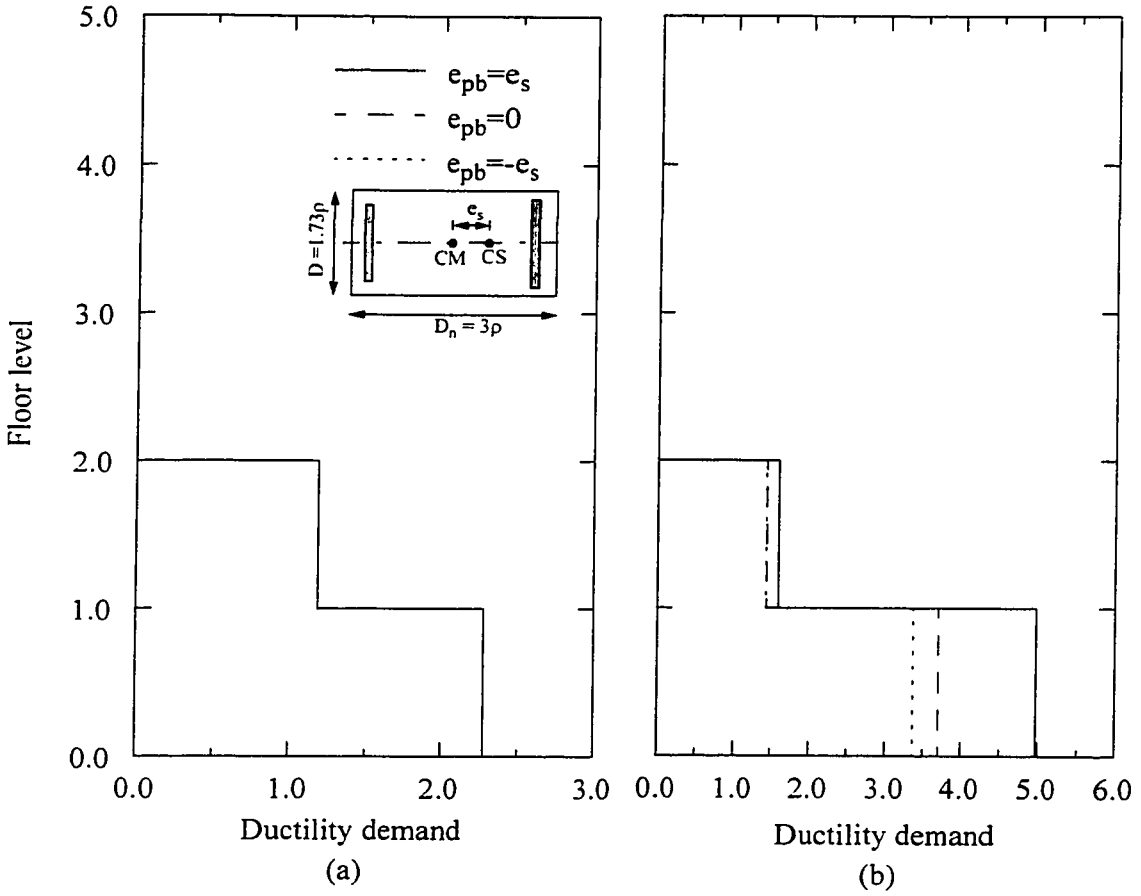

Figure 3.5 Ductility demand of the five-storey model
(average of 4 earthquakes, Ω_0=0.9 & T=1)
(a) e_s= 0 (b) e_s=0.3

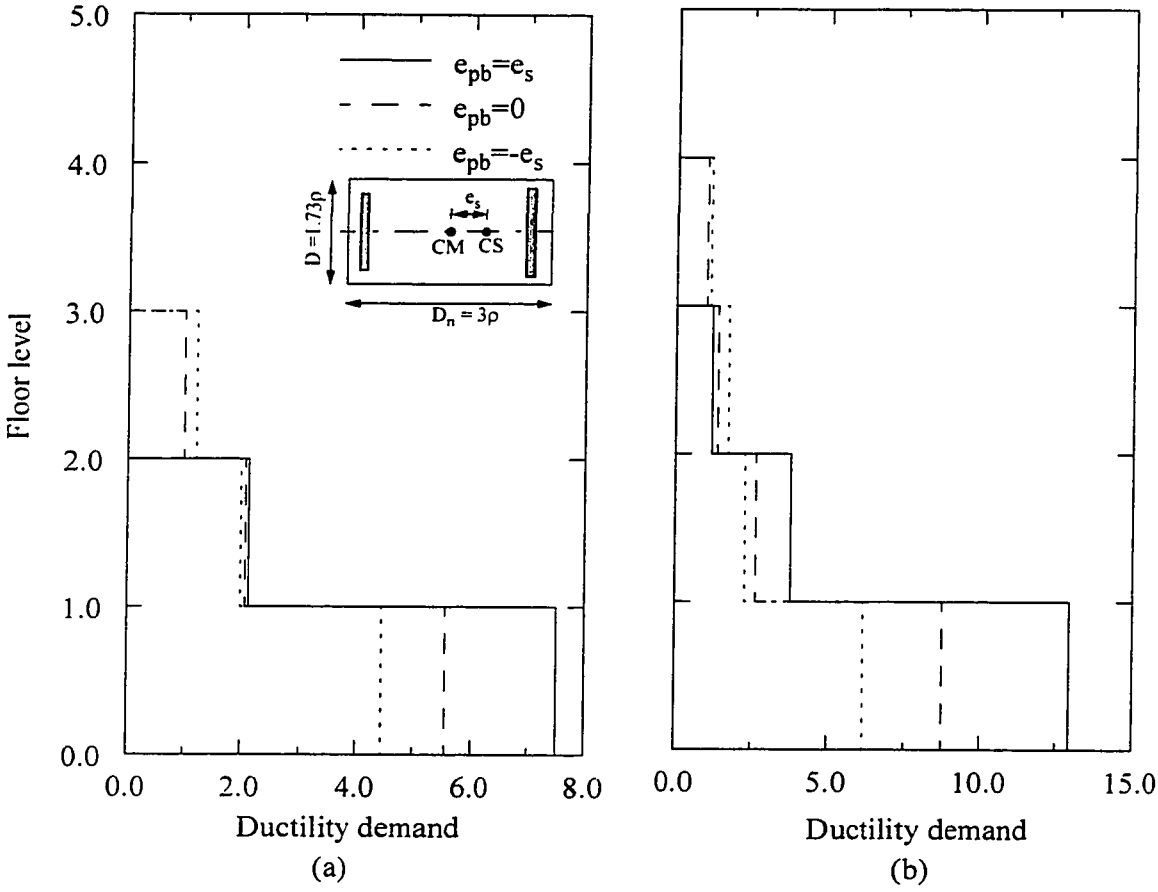

Figure 3.6 Ductility demand of the five-storey model
(average of 4 earthquakes, Ω_0=0.9 & T=1)
(a) e_s= 0.5 (b) e_s=0.75

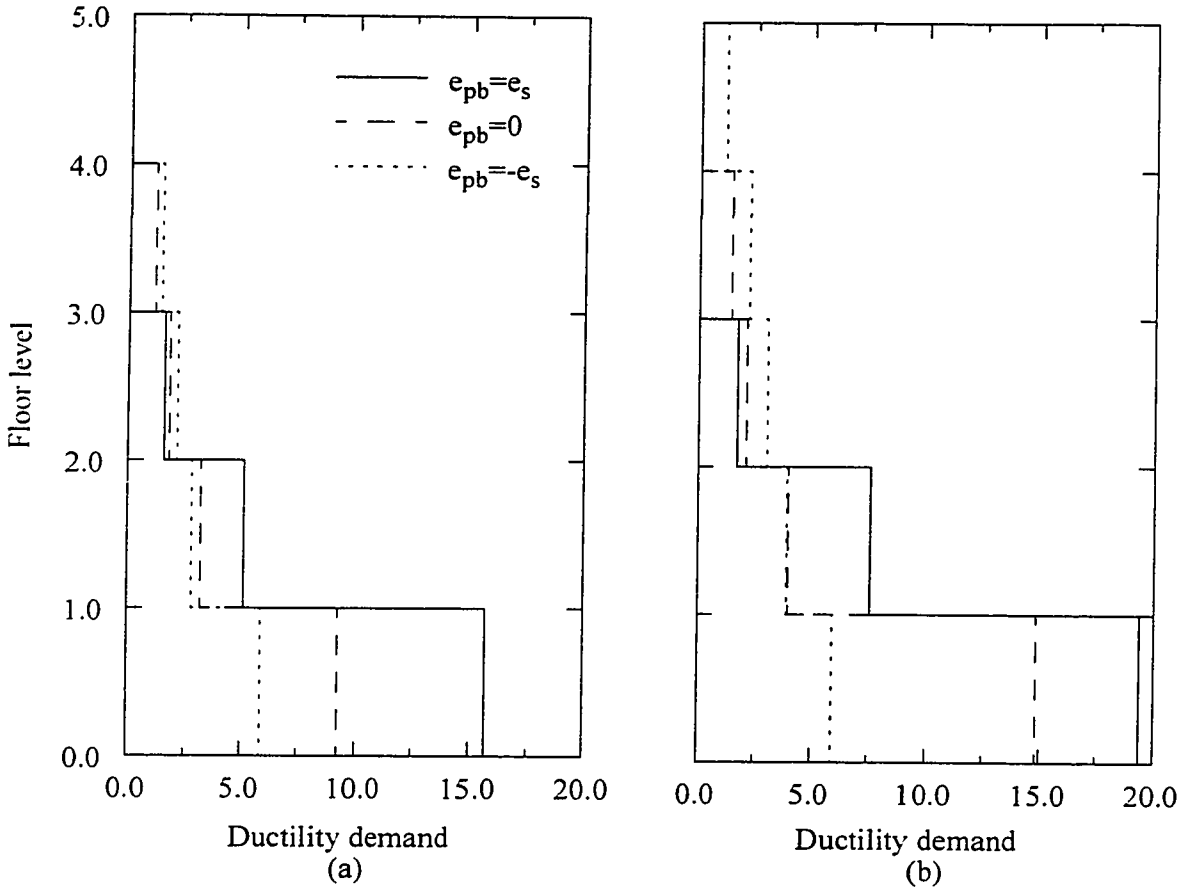

Figure 3.7 Ductility demand of the five-storey model
(average of 4 earthquakes, Ω_0=0.9 & T=1)
(a) e_s= 0.9 (b) e_s=1.2

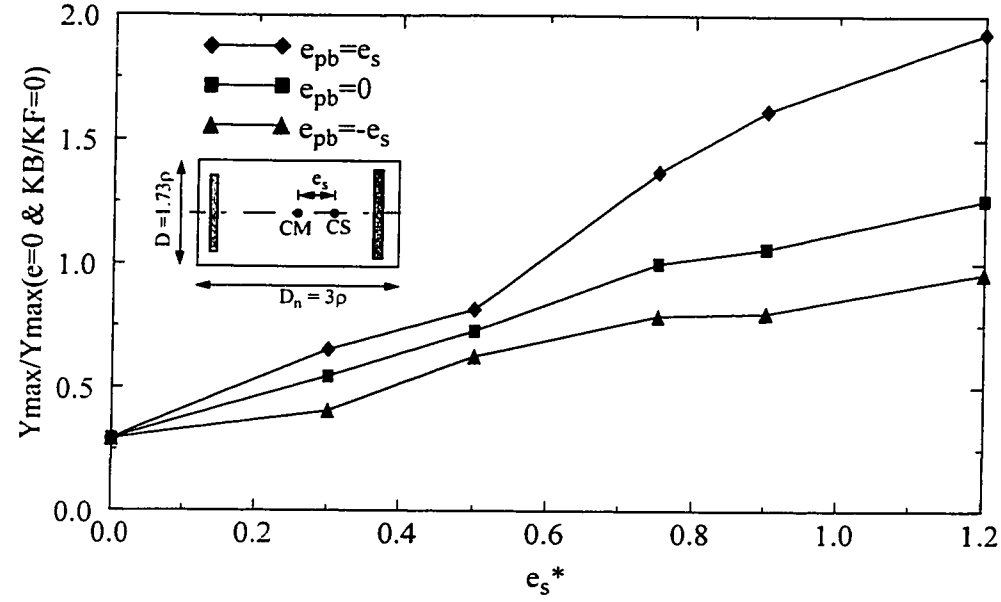

Figure 3.8 Maximum edge displacement of the ten-storey model
(average of 4 earthquakes, Ω_0=0.9 & T=1)

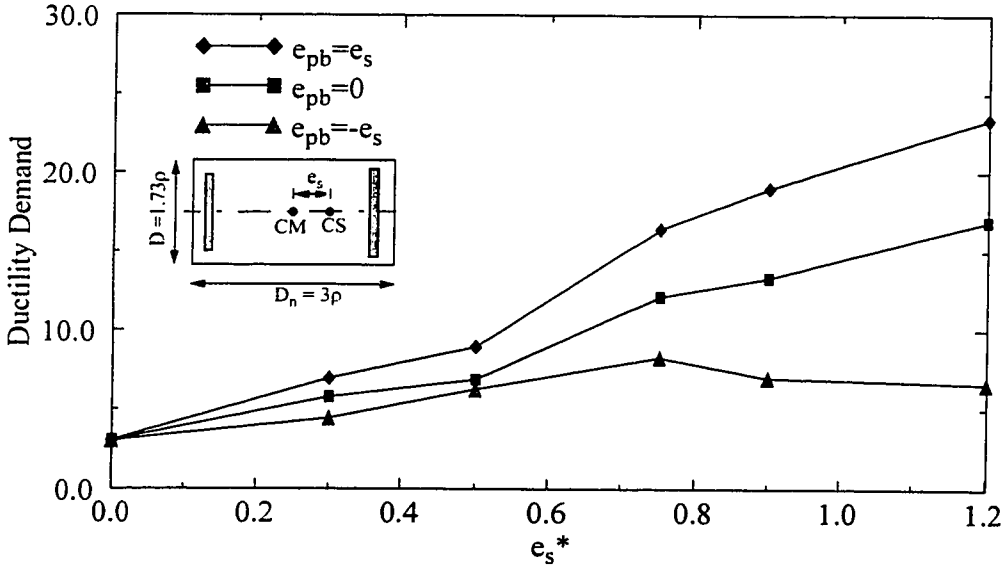

Figure 3.9 Ductility demand for the first storey the ten-storey model
(average of 4 earthquakes, Ω_0=0.9 & T=1)

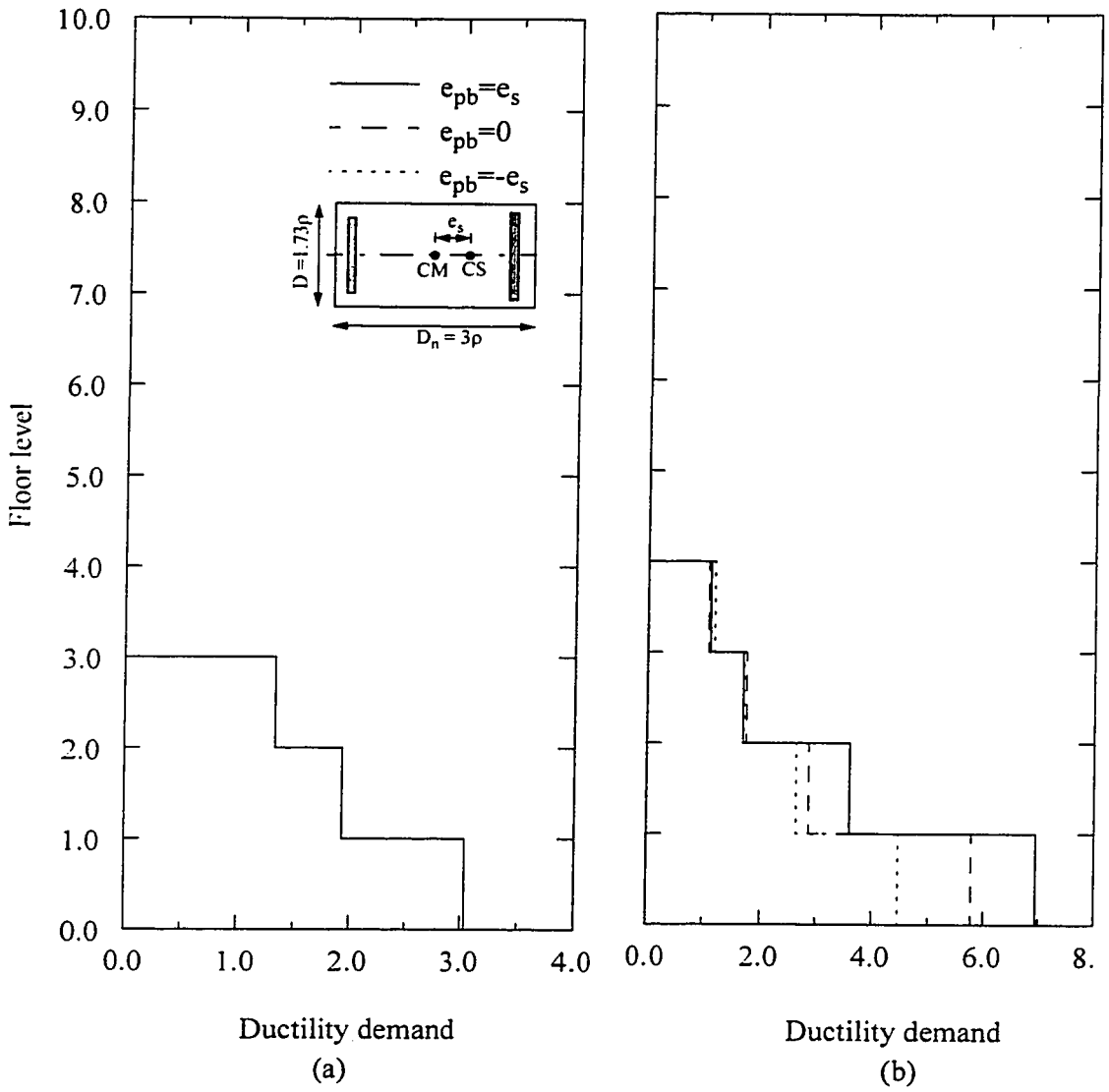

Figure 3.10 Ductility demand of the ten-storey model
(average of 4 earthquakes, Ω_0=0.9 & T=1)
(a) e_s= 0. (b) e_s=0.3

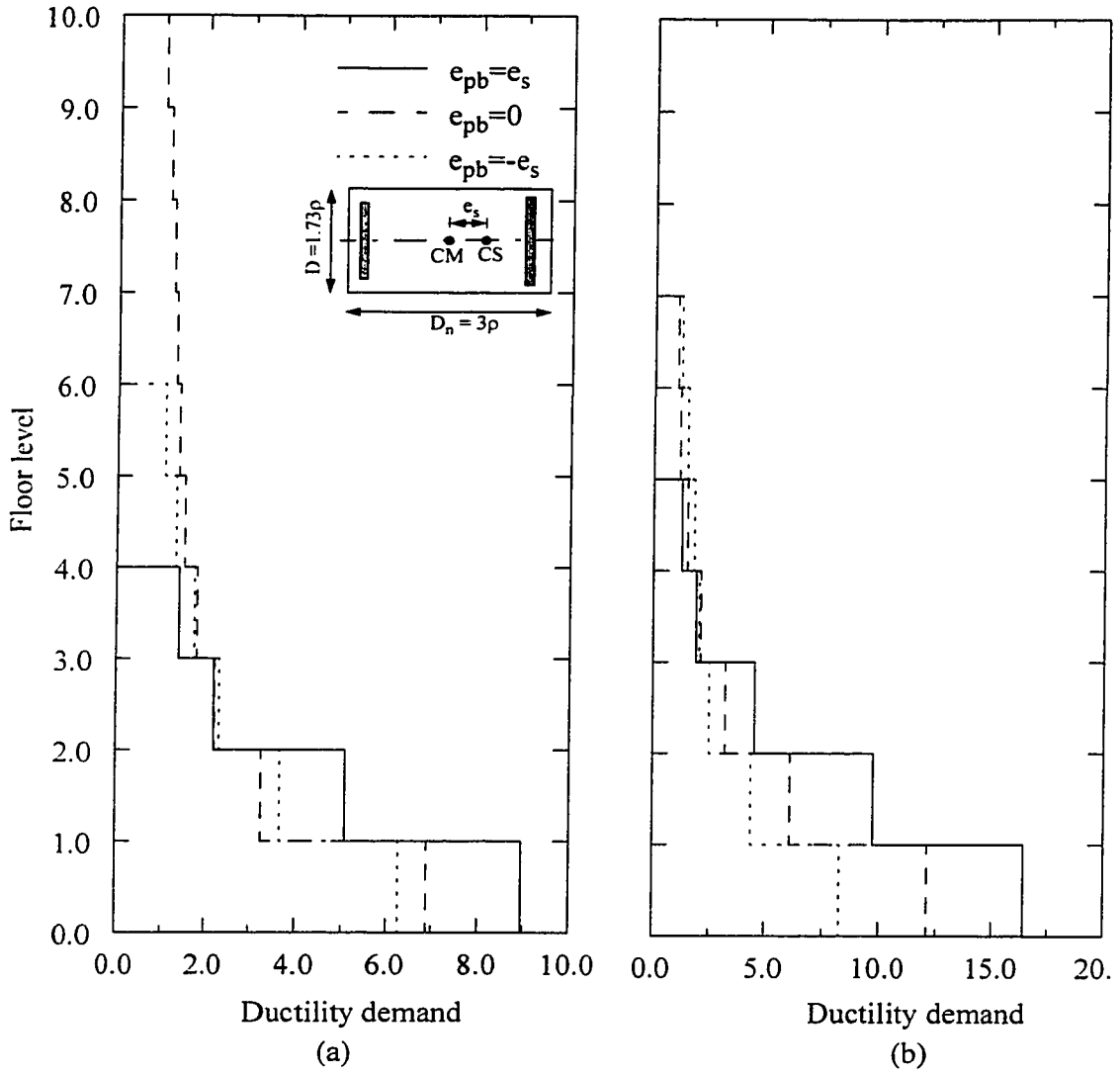

Figure 3.11 Ductility demand of the ten-storey model
(average of 4 earthquakes, Ω_0=0.9 & T=1)
(a) e_s= 0.5 (b) e_s=0.75

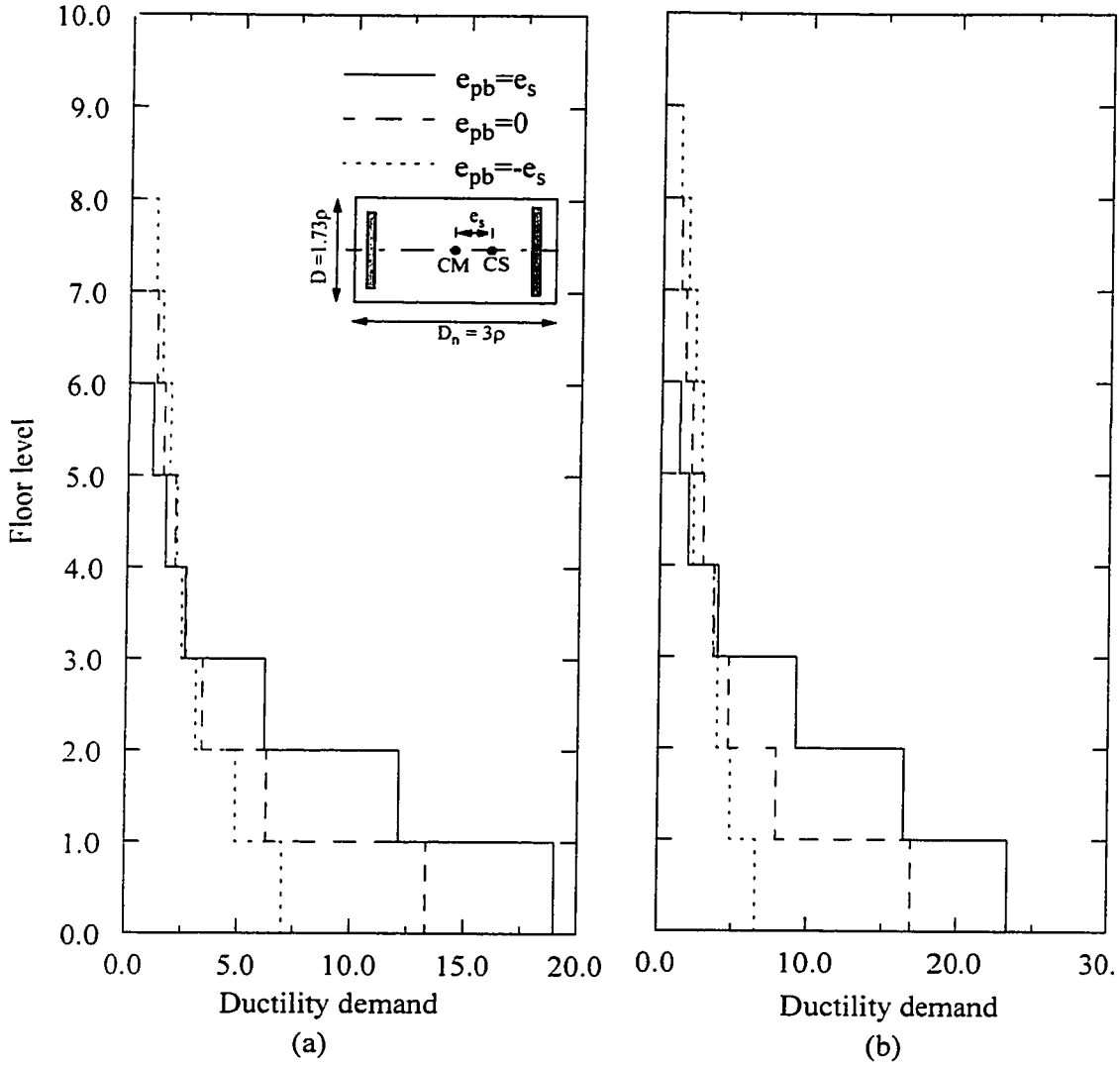

Figure 3.12 Ductility demand of the ten-storey model
(average of 4 earthquakes, Ω_0=0.9 & T=1)
(a) e_s= 0.9 (b) e_s=1.2

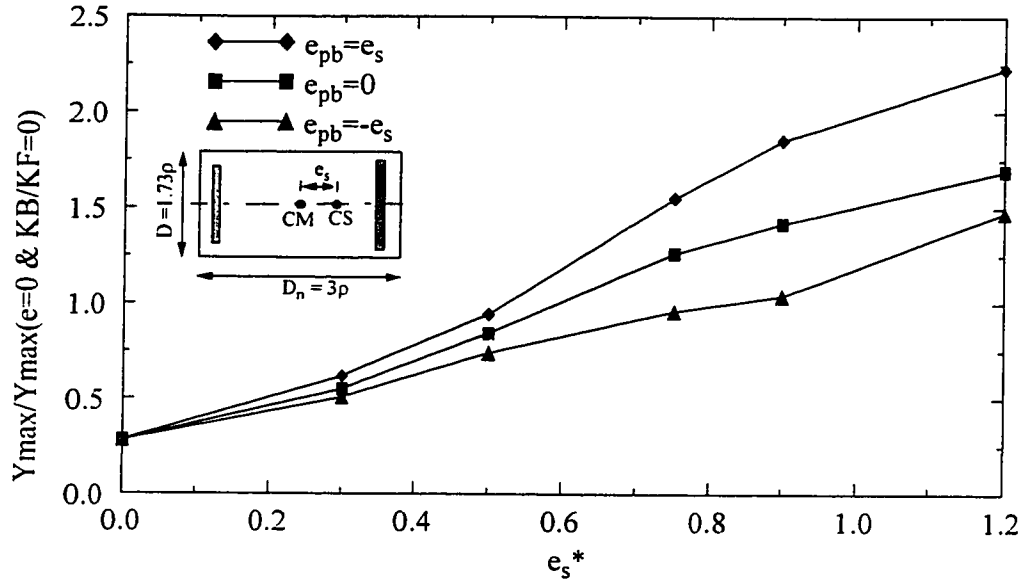

Figure 3.13 Maximum edge displacement of the torsionally flexible ten-storey model (average of 4 earthquakes, Ω_0=0.7 & T=1)

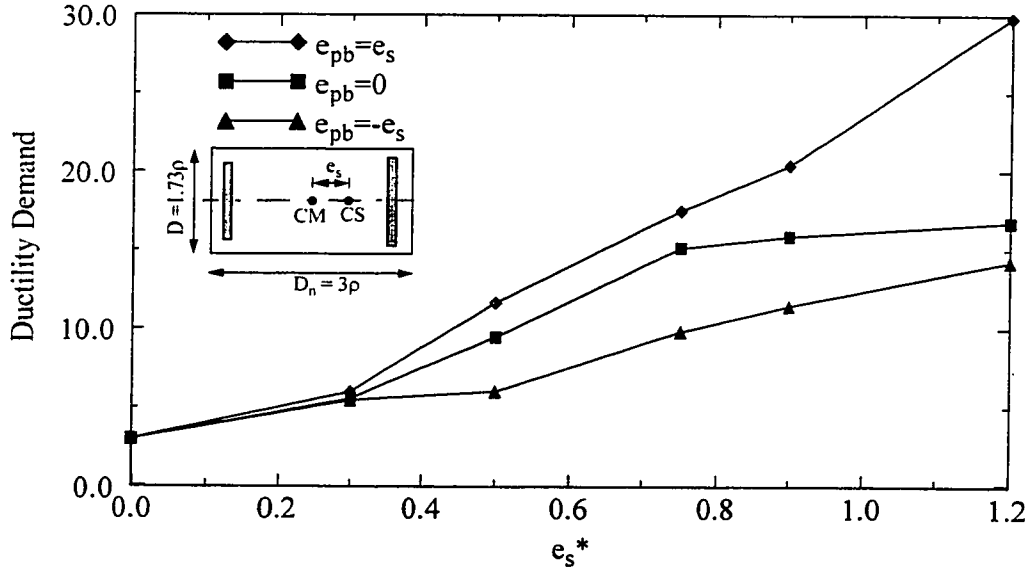

Figure 3.14 Ductility demand for the first storey of the torsionally flexible ten-storey model (average of 4 earthquakes, Ω_0=0.7 & T=1)

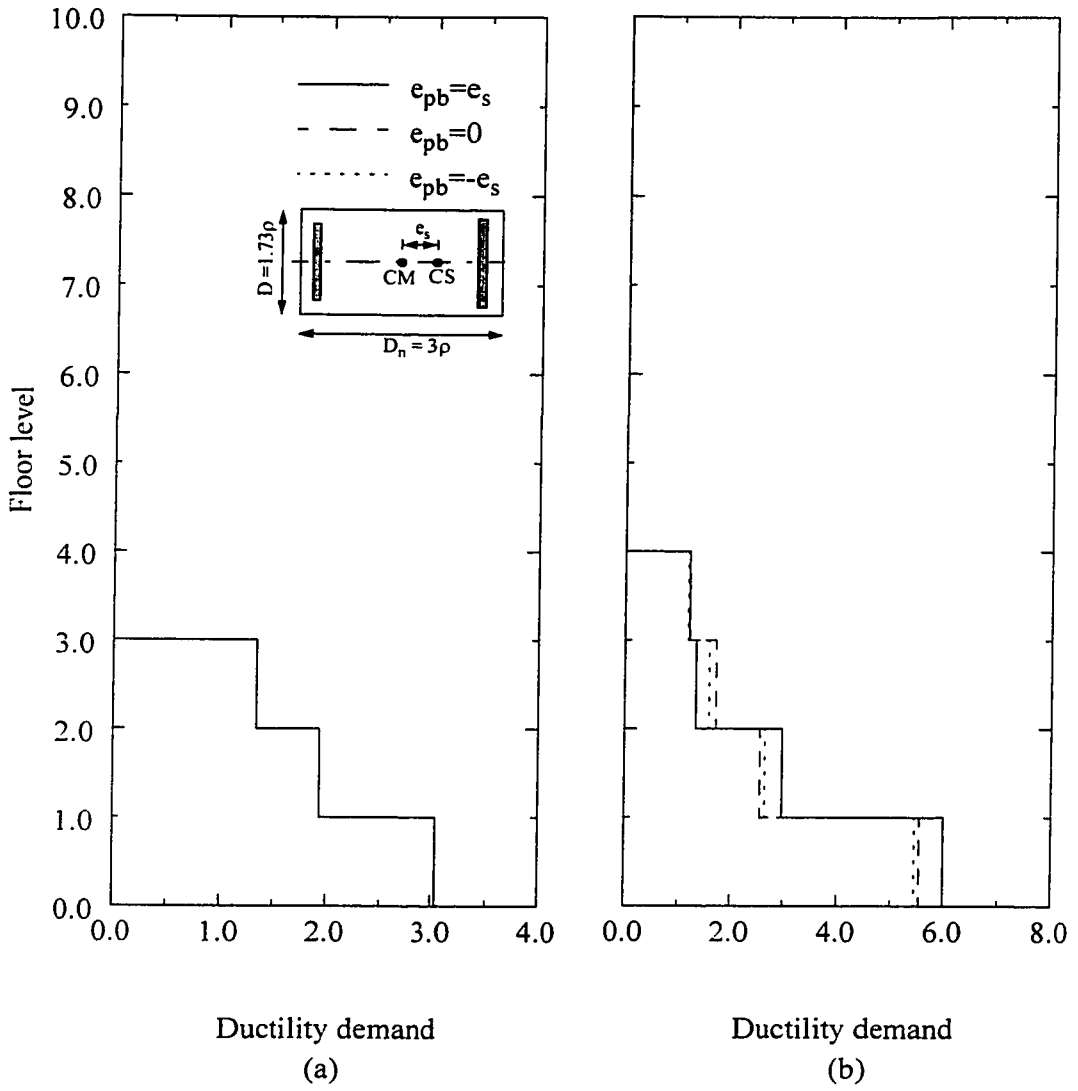

Figure 3.15 Ductility demand of the torsionally flexible ten-storey model (average of 4 earthquakes, Ω_0=0.7 & T=1)
(a) e_s= 0. (b) e_s=0.3

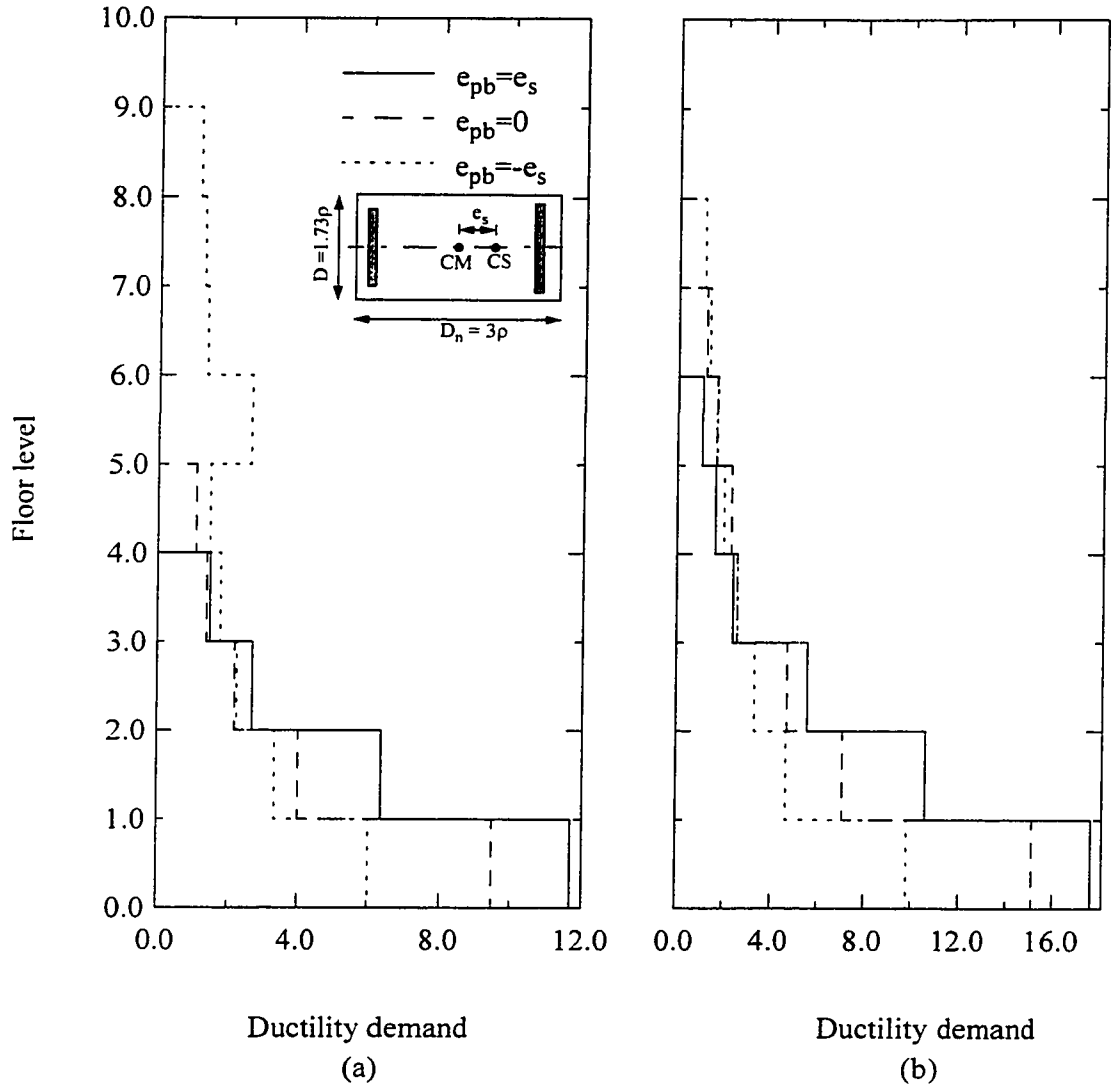

Figure 3.16 Ductility demand of the torsionally flexible ten-storey model (average of 4 earthquakes, Ω_0=0.7 & T=1)
(a) e_s= 0.5 (b) e_s=0.75

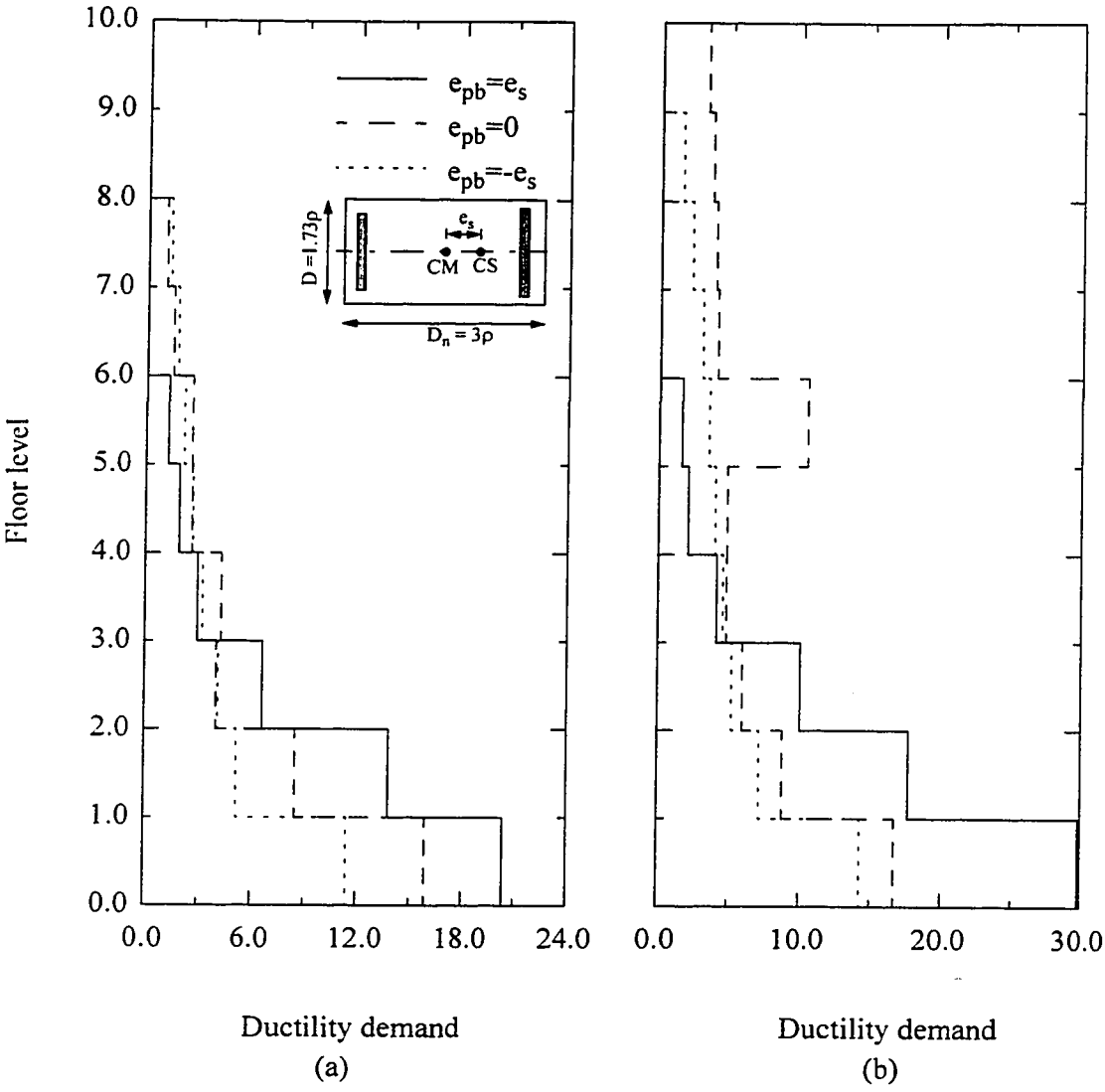

Figure 3.17 Ductility demand of the torsionally flexible ten-storey model
(average of 4 earthquakes, Ω_0=0.7 & T=1)
(a) e_s= 0.9 (b) e_s=1.2

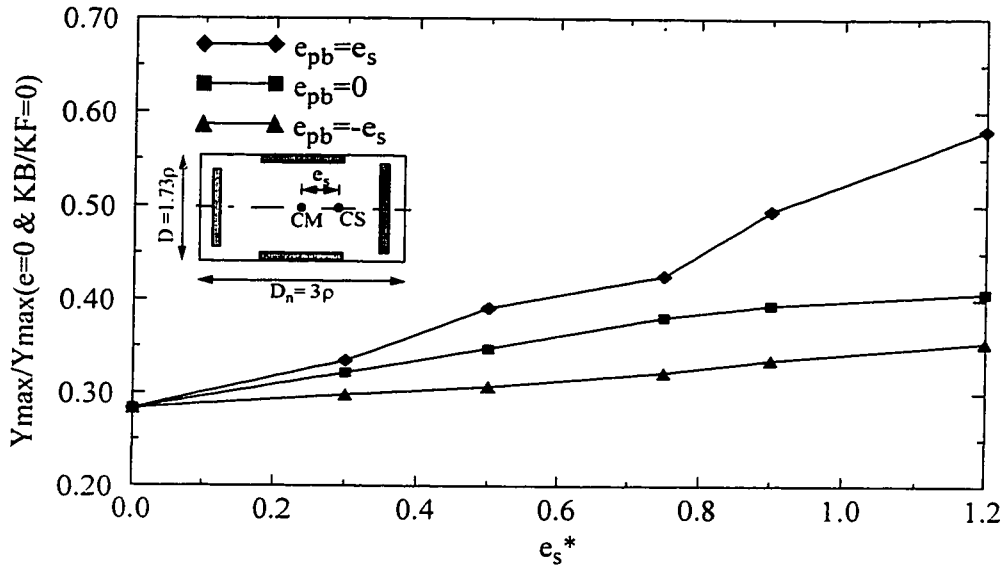

Figure 3.18 Maximum edge displacement of the torsionally rigid ten-storey model (average of 4 earthquakes, Ω_0=1.7 & T=1)

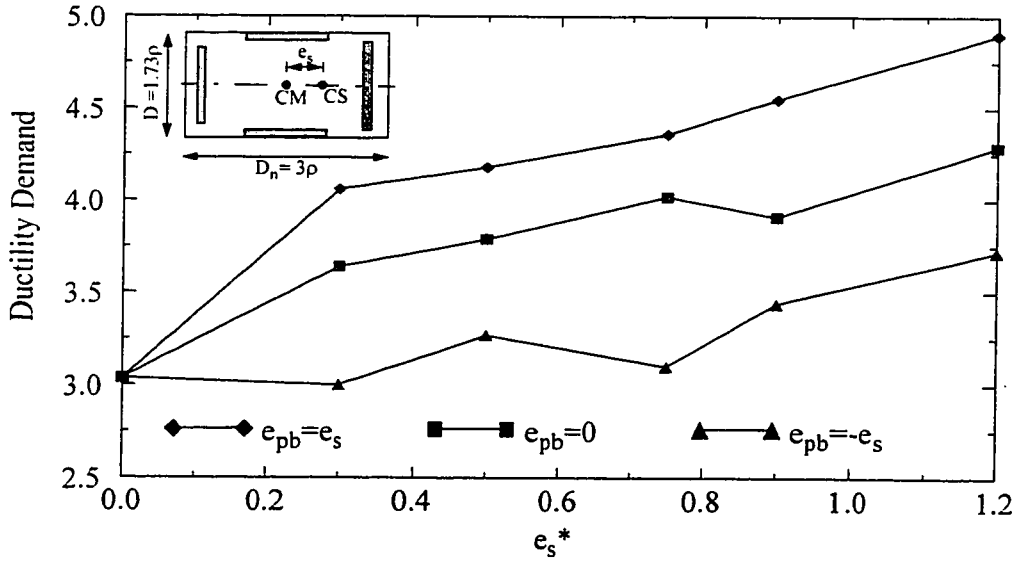

Figure 3.19 Ductility demand for the first storey of the torsionally rigid ten-storey model (average of 4 earthquakes, Ω_0=1.7 & T=1)

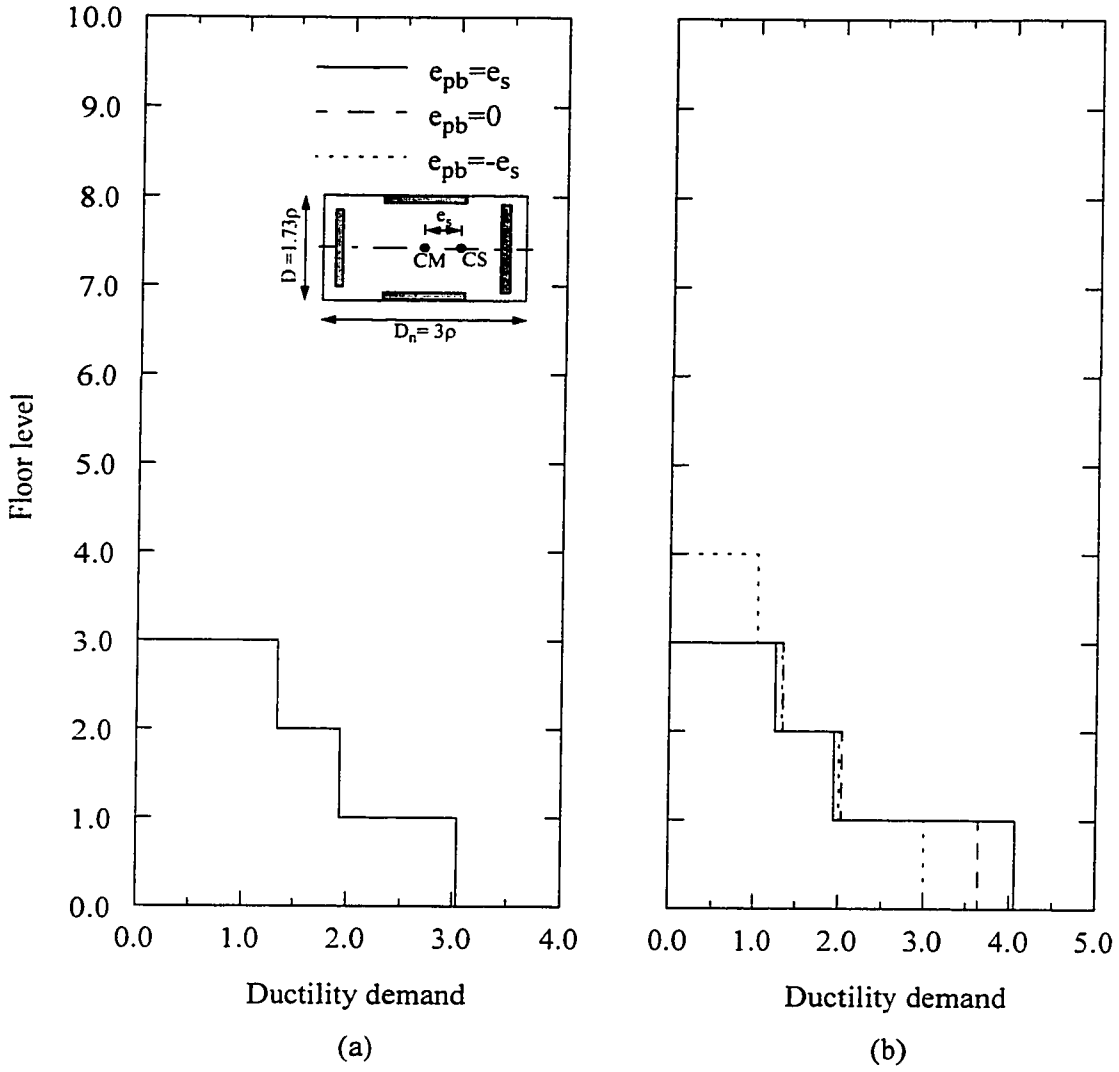

Figure 3.20 Ductility demand of the torsionally rigid ten-storey model
(average of 4 earthquakes, Ω_0=1.7 & T=1)
(a) e_s= 0 (b) e_s=0.3

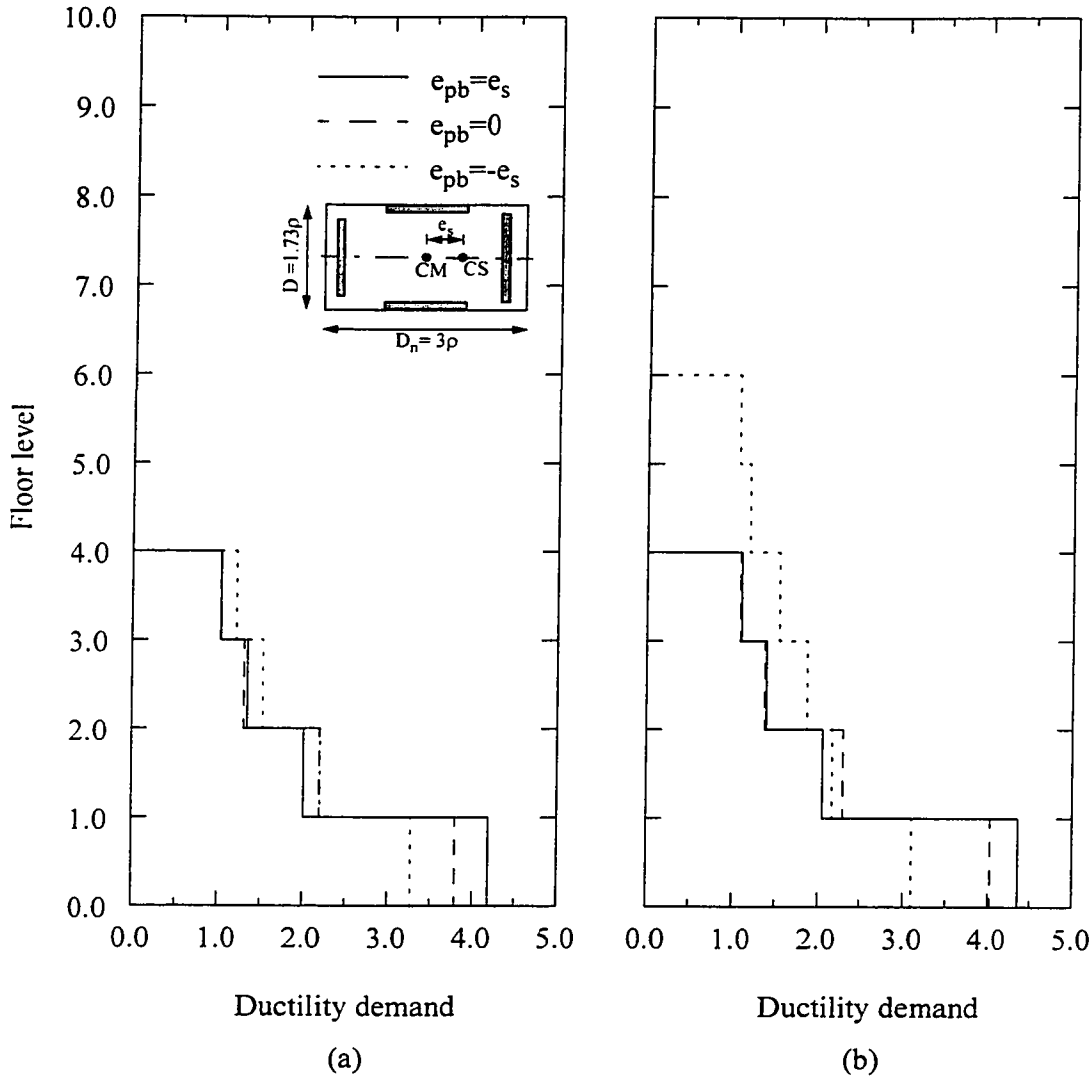

Figure 3.21 Ductility demand of the torsionally rigid ten-storey model (average of 4 earthquakes, Ω_0=1.7 & T=1)
(a) e_s= 0.5 (b) e_s=0.75

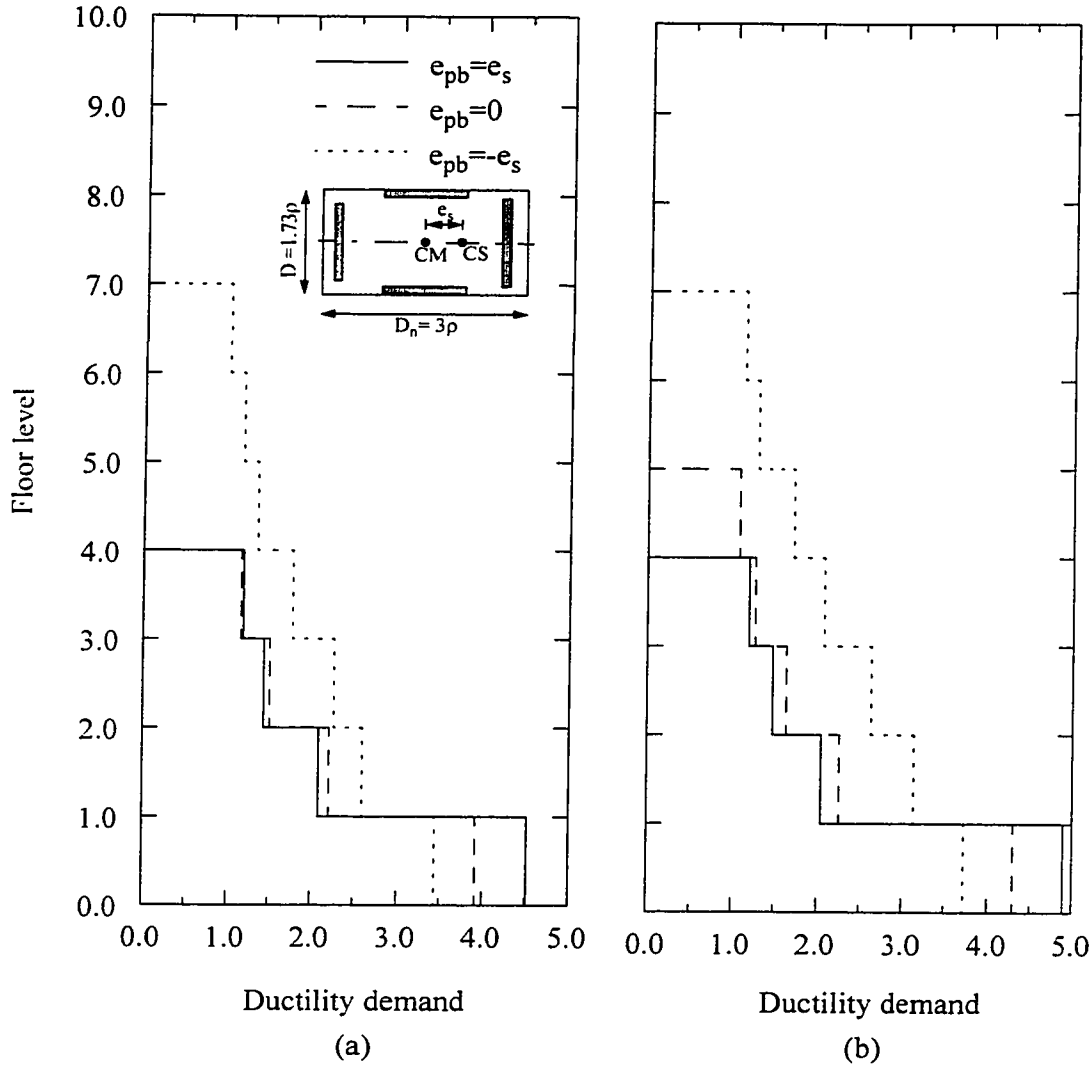

Figure 3.22 Ductility demand of the torsionally rigid ten-storey model (average of 4 earthquakes, Ω_0=1.7 & T=1)
(a) e_s= 0.9 (b) e_s=1.2

CHAPTER 4

EFFECT OF SLIP LOAD DISTRIBUTION ON THE BASE SHEAR AND TORQUE OF THE 2-D SINGLE-STOREY MODEL

4.1 INTRODUCTION:

Studied in this chapter is the effect of slip load distribution on the inelastic seismic behavior of asymmetric single-storey buildings using the histories of base shear and torque. The basis of this work is the research of De La Llera and Chopra [9 & 12]. They studied the inelastic seismic behavior of asymmetric-plan buildings and concluded that one can adjust the stiffness asymmetry and strength asymmetry to direct the inelastic behavior in any desired region of the base shear and torque (BST) surface. Independently varying the stiffness and strength may seem impractical for conventional steel and reinforced concrete buildings, but should be feasible for systems using friction damped braced frames.

The computer program DRAIN-2D was used to analyze the single-storey model described in chapter 2 having uncoupled torsional to lateral frequency ratio Ω_0=0.9 and fundamental period T=1 sec. The brace strength was set to be equal to the frame strength, i. e. RB / RF = 1, and the braces stiffness to frame stiffness KB/KF was set to be equal to three. The model was subjected to the N-S component of 1940 El Centro earthquake in the y-direction.

As before six normalized stiffness eccentricity were considered (e_s*=0, 0.3, 0.5, 0.75, 0.9 and 1.2). For each stiffness eccentricity three cases of slip load eccentricity were

considered ($e_{pb}^*=e_s^*$, $e_{pb}^*=0$ and $e_{pb}^*=-e_s^*$).

Examined in this chapter are the effects of the plan-wise distribution of the slip load by considering the base shear and torque response histories. These histories represented in the force plane spanned by base shear V_y and torque T_θ.

At each instant of the response, the base shear and torque define one point in this plane. The combination of the base shear and torque are bounded in this plane by a surface called the base shear and torque ultimate surface. The base shear and torque (BST) surface is defined by the set of base shear and torque combinations corresponding to the different collapse mechanisms that can be developed by the system [10].

4.2 THE BASE SHEAR AND TORQUE ULTIMATE SURFACE

The base shear and torque (BST) surface for the 2-D single-storey model spanned by the shear in the y-direction V_y and torque T_θ borders all combinations of the base shear and torque that when applied statically lead to collapse of the system. The BST surface is affected by the strength of the resisting elements and its distribution.

The single-storey model under consideration there is that of Figure 2.2, where only two friction damped braced frames are introduced in the direction of excitation (y-direction). The dimension of the rigid deck as well as the aspect ratio are described by equations 2-1 to 2-5, and the position of the CM are explained in chapter 2. Moreover the calculation of the stiffness, strength and slip load eccentricities as well as the properties of each resisting element are done through the use of equations 2.6 to 2.33.

The fundamental period was adjusted to be equal to one and the uncoupled torsional to translational frequency ratio Ω_0 of 0.9 is specified.

Figure 4.1 shows a symmetric single-storey system with two FDBF resisting elements in the direction of excitation (y-direction). Each one has identical lateral stiffness 2K (0.5K for the frame and 1.5K for the brace) and lateral strength R_y ($0.5R_y$ for the frame and $0.5R_y$ for the brace) and is subjected to a static base shear V_y and torque T_θ. It is obvious that the maximum lateral capacity of the system is $V_{y0}=2R_y$ and the maximum torque capacity of the system is $T_{\theta 0}=2R_y a$.

The BST surface of Figure 4.1.b can be constructed by representing the translational and rotational collapse mechanisms (Figure 4.2). For example the first quadrant of the BST surface in Figure 4.1.b can be determined as the following:

- Point (1): It corresponds to a translational mechanism in plan (Figure 4.2.a) and means that the resisting elements in the y-direction; must yield. At collapse (Figure 4.2.b) the system has translated from 0-0' to 1-1' producing simultaneous yielding of the two resisting elements in the y-direction, therefore, equilibrium of the system imposes that $V_y=2R_y$ and $T_\theta=0$.

- Point (2): This point corresponds to a rotational mechanism of the plan (Figure 4.2.c). It implies that the resisting elements in the y-direction must yield but in opposite directions. At collapse the system has rotated about the center of the deck and line 0-0' becomes 1-1' (Figure 4.2.d). Equilibrium of the system in the y-direction shows that $V_y=0$ and $T_\theta=2R_y a$.

Figure 4.1.c shows an asymmetric single-storey system with two resisting elements in the y-direction. Element (1) on the stiff side of the structure has lateral

stiffness K1 and lateral strength $R1_y$ while element (2) on the flexible side of the structure has lateral stiffness K2 and lateral strength $R2_y$. The total lateral stiffness of the system K1+K2=4K (1K lateral stiffness of the frame and 3K lateral stiffness of the braces) and the total strength of the system $R1_y+R2_y = 2R_y$ ($1R_y$ for the frame strength and $1R_y$ for the braces strength).

The construction the first quadrant of the base shear and torque surface shown in Figure 4.1.d can be done by representing the collapse mechanisms in Figures 4.2.e and g. One can determine points (1) and (2) as follows:

- Point (1): This point matches the mechanism shown in Figure 4.2.e. It implies that the two resisting elements must yield in the positive y-direction. The strengths of the two resisting elements are not identical; therefore, the base torque is exist. From the equilibrium of the system at mechanism 1-1'(Figure 4.2.f) one easily sees that the base shear $V_y = R1_y+R2_y=2R_y$ and the base torque $T_\theta=(R1_y-R2_y)a$.

- Point (2): Shown in Figure 4.2.g is the mechanism which associates with the this point. As can seen, the two resisting elements yield in opposite y-directions. The equilibrium of the system for mechanism 1-1' (Figure 4.2.h) gives the base shear $V_y = R1_y-R2_y$ and the base torque $T_\theta=2R_ya$.

The base torque $T_\theta = 2R_ya$ can be written as a function of eccentricities as follow:

$$R1_y = RB1_y + RF1_y \tag{4-1}$$

$$R2_y = RB2_y + RF2_y \tag{4-2}$$

Looking at Figures 4.2 d and h, the base torque can be defined as follow:

$$T_\theta = 2R_y.a = R1_y \cdot a + (-R2_y) \cdot (-a) = a \cdot (RB1_y + RF1_y + RB2_y + RF2_y) \tag{4-3}$$

Looking at Figures 4.2 b and f, the base torque can be define as follows:

$$T_\theta = (R1_y - R2_y) \cdot a = R1_y \cdot a + R2_y \cdot (-a) \tag{4-4}$$

$$T_\theta = a \cdot (RB1_y + RF1_y) + (-a) \cdot (RB2_y + RF2_y) \tag{4-5}$$

Equations 4.3 and 4.5 lead to the following equation:

$$T_\theta = \sum_i RF_{yi} \cdot a + \sum_i RB_{yi} \cdot a \tag{4-6}$$

Substitute in equation 4.6 using equations 2.26 and 2.28

$$T_\theta = e_{pf}^* \cdot \rho \cdot RF_y + e_{pb}^* \cdot \rho \cdot RB_y \tag{4-7}$$

$$T_\theta = e_{pf} \cdot RF_y + e_{pb} \cdot RB_y \tag{4-8}$$

In order to verify these equations one must follow the positive direction of V and T_θ as shown in Figures 4.1.a and c.

Moreover, it should be noted that the base shear has been normalized with respect to the maximum shear capacity of the system $V_y$max (point 1 in figures 4.1.b & d) and the base torque has been normalized with respect to the maximum torque capacity of the system $T_\theta$max (point 2 in figures 4.1.b & d).

4.3 ANALYSIS AND RESULTS

Regardless of the slip load eccentricity, the strength eccentricity of the frames increases with increase of the stiffness eccentricity, i.e the center of strength of the frames is coincident with the center of stiffness. When $e_{pb}^* = e_s^*$, the strength of the frames and the slip load are increased on the stiff side of the structure and decreased on the flexible side of the structure, while $e_{pb}^* = 0$ means that the center of the slip load coincides with

the center of mass, but the frames center of strength is identical to the center of stiffness. It can be concluded that the strength is eccentric in these two cases ($e_{pb}^* = e_s^*$ and $e_{pb}^* = 0$). This eccentricity in strength causes an asymmetry in the BST surface. The third case ($e_{pb}^* = -e_s^*$) means that the strength of the frames is increased on the stiff side of the structure and decreased on the flexible side, while the slip load (brace strength) is increased on the flexible side and decreased on the stiff side of the structure. The brace strength to the frame strength ratio (RB/RF=1) together with adjusting slip load eccentricity to be equal to stiffness eccentricity but on the other side of the structure, means that the total strength (frames and braces) on the stiff side of the structure equals to the total strength on the flexible side, i.e $e_{pb}^* = e_s^*$ causes a symmetry in strength, therefore the BST surface has to be symmetric in this case.

Looking at cases (a) and (b) in Figures 4.4 to 4.8, it can be recognized that as the strength eccentricity is increased from 0 to 1.2 the BST surface becomes skewed and stretched toward the first and third quadrants.

The results of the base shear and torque response histories are plotted in Figures 4.3 to 4.8 which each figure presenting three cases of slip load eccentricity ($e_{pb}^*=e_s^*$, $e_{pb}^*=0$, and $e_{pb}^* = -e_s^*$), for one case of stiffness eccentricity.

Figure 4.4 shows that the maximum normalized torque occurred is 0.65 in the case of $e_{pb}^*=e_s^*$, 0.59 in the case of $e_{pb}^*=0$ and 0.57 the case of $e_{pb}^*=-e_s^*$ which mean that, as the slip load moves from the stiff side to the flexible side of the structure the maximum torque that occurs will decrease.

Same comment can be made for Figure 4.5 where $e_s^*=0.5$; in addition, it starts to appear that the maximum base shear of the BST surface can be reached in the case of

e_{pb}*=0 and e_{pb}*=-e_s*,while it cannot be reached in the case of e_{pb}*=e_s*.

These two remarks become obvious as the stiffness eccentricity e_s* increase. The maximum decrease in base torque due to slip load distribution occurs when e_s* = 0.75 (Figure 4.6), as it can be seen that the maximum base torque when e_{pb}* = -e_s* is 50 percent less then its counterpart in the case of e_{pb}* = e_s*.

For all cases shown in Figures 4.4 to 4.8, none of the components reach the maximum base torque of the BST surface.

The case of e_{pb}* = -e_s* expresses the case of strength symmetry (strength eccentricity of the structure equal to zero), since the total strength on the flexible side matches the strength of the stiff side. Most important, however, is that the strength eccentricity of this case is constant with different stiffness eccentricity. Therefore this case is convenient in studying the effect of stiffness eccentricity on the base shear and torque. Case (c) of Figures 4.4 to 4.8 together with Figure 4.3 show that the behavior of base shear and torque inside the base shear and torque ultimate surface is modified as the stiffness eccentricity change.

4.4 CONCLUDING REMARKS

- Base shear and torque response history is a good way to reflect the behavior of asymmetric buildings.

-As the slip load eccentricity moves from the stiff side to the flexible side of the structure, the torque decreases and the shear increases inside the BST surface.

- The response history of the base shear and torque can reach the maximum value

of the shear in the BST surface when T_θ=0; on the other hand there is no evidence that it can reach the maximum value of torque in the BST surface when V_y=0.

- Strength eccentricity and stiffness eccentricity affect the behavior of base shear and torque inside the base shear and torque ultimate surface, while the strength eccentricity effect controls the shape of BST surface.

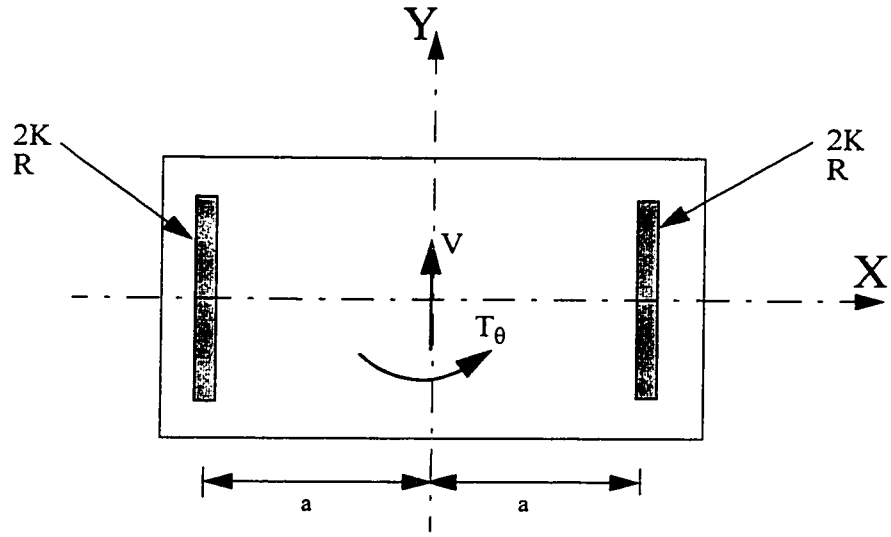

Figure 4.1.a Resistant element in the y-direction for symmetric case

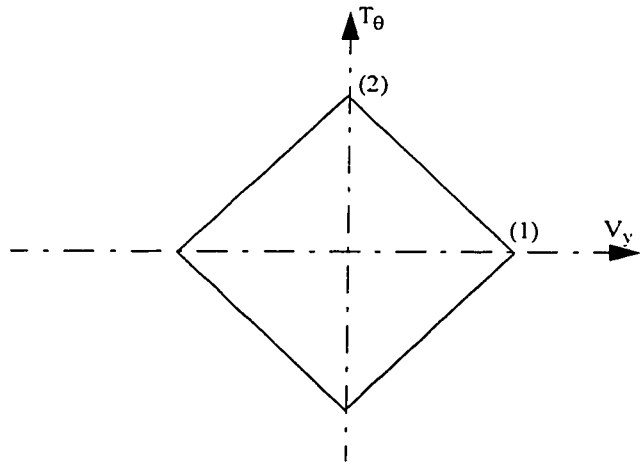

Figure 4.1.b Base shear and torque surface for symmetric case

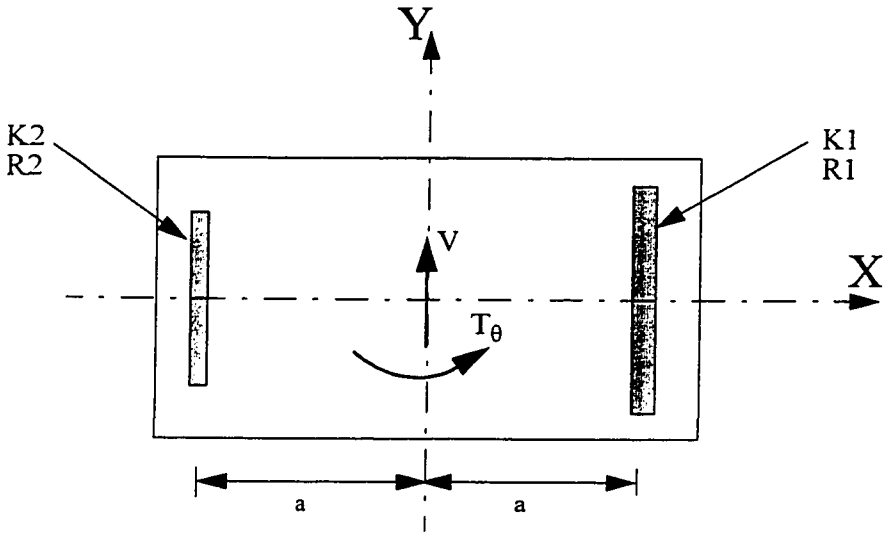

Figure 4.1.c Resistant element in the y-direction for asymmetric case

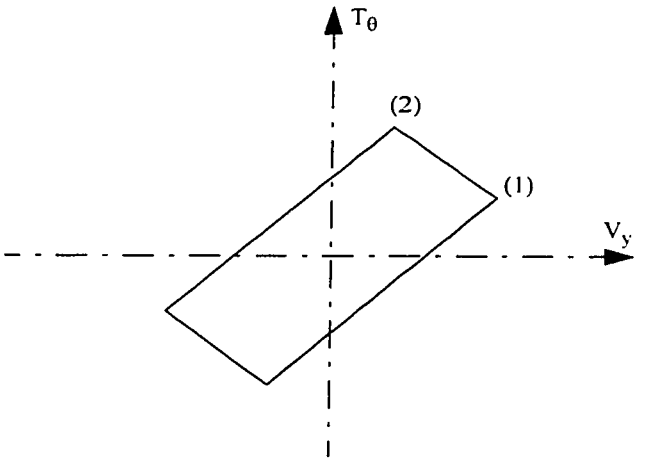

Figure 4.1.d Base shear and torque surface for asymmetric case

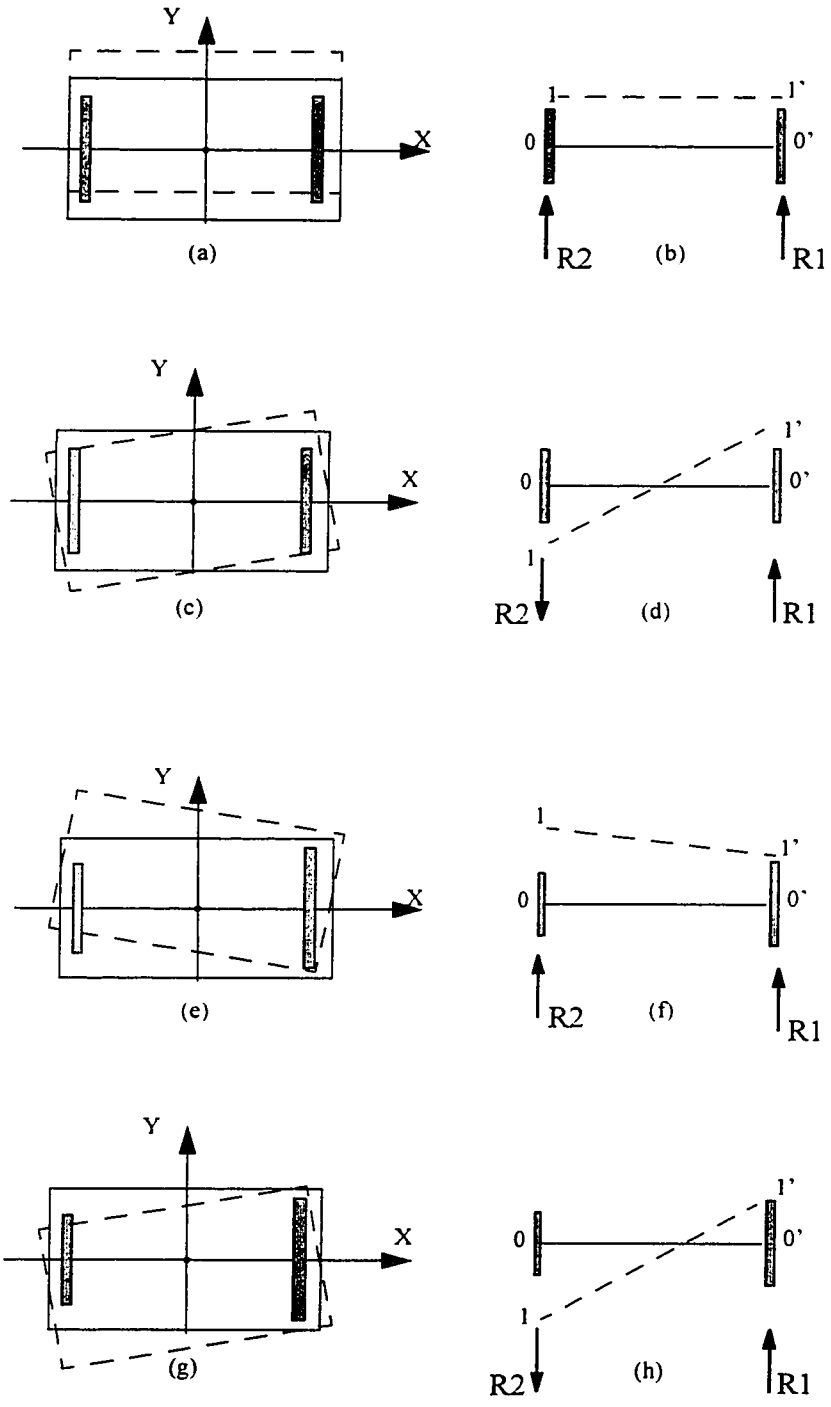

Figure 4.2 Construction of the base shear and torque surface

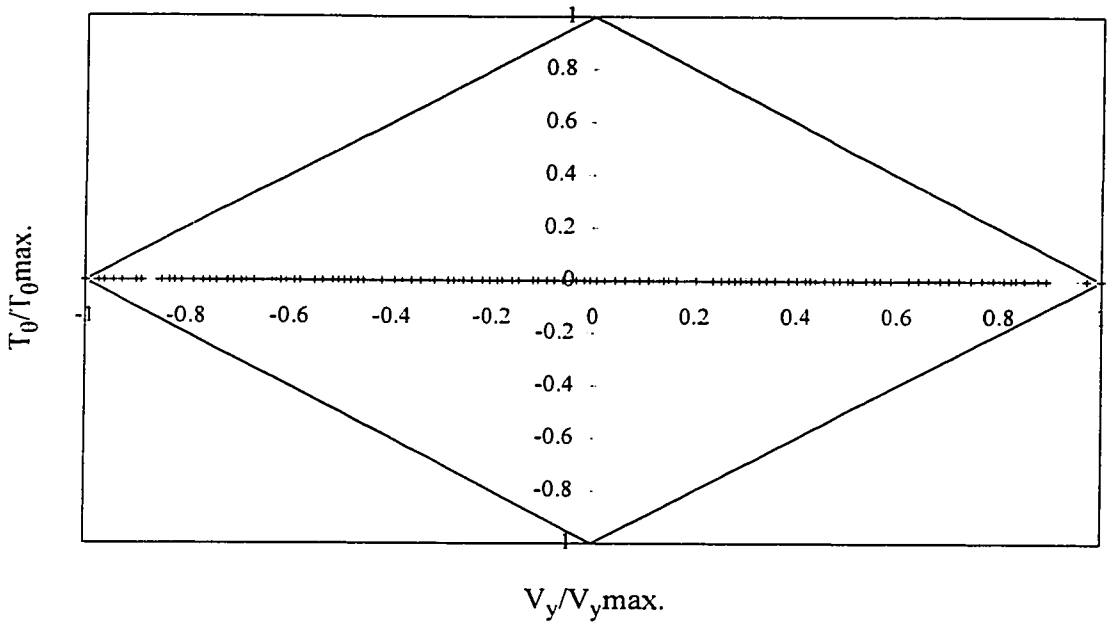

Figure 4.3 Effect of the slip load eccentricity on the seismic behavior of single-storey buildings (e_s*=0, 1940 El Centro N-S)

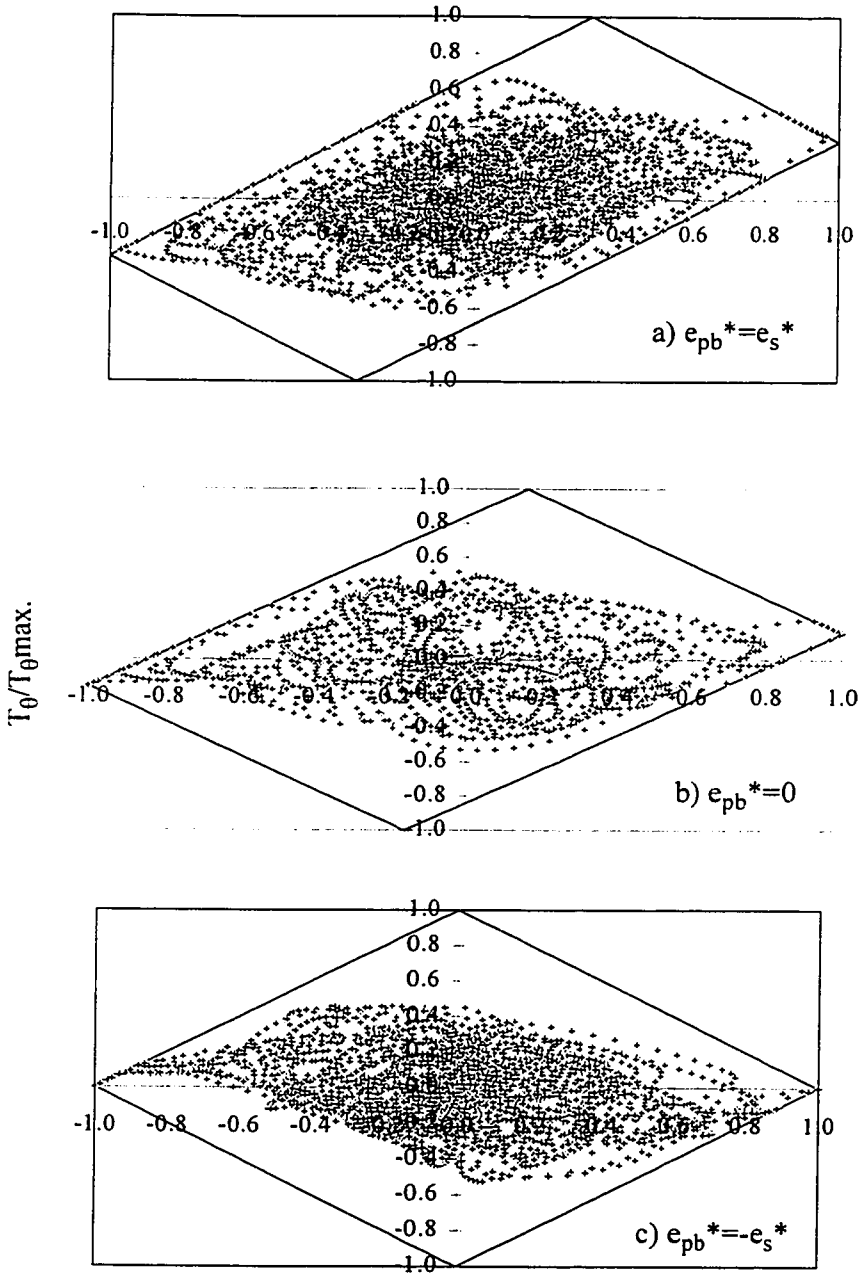

Figure 4.4 Effect of the slip load eccentricity on the seismic behavior of single-storey buildings (e_s*=0.3, 1940 El Centro N-S)

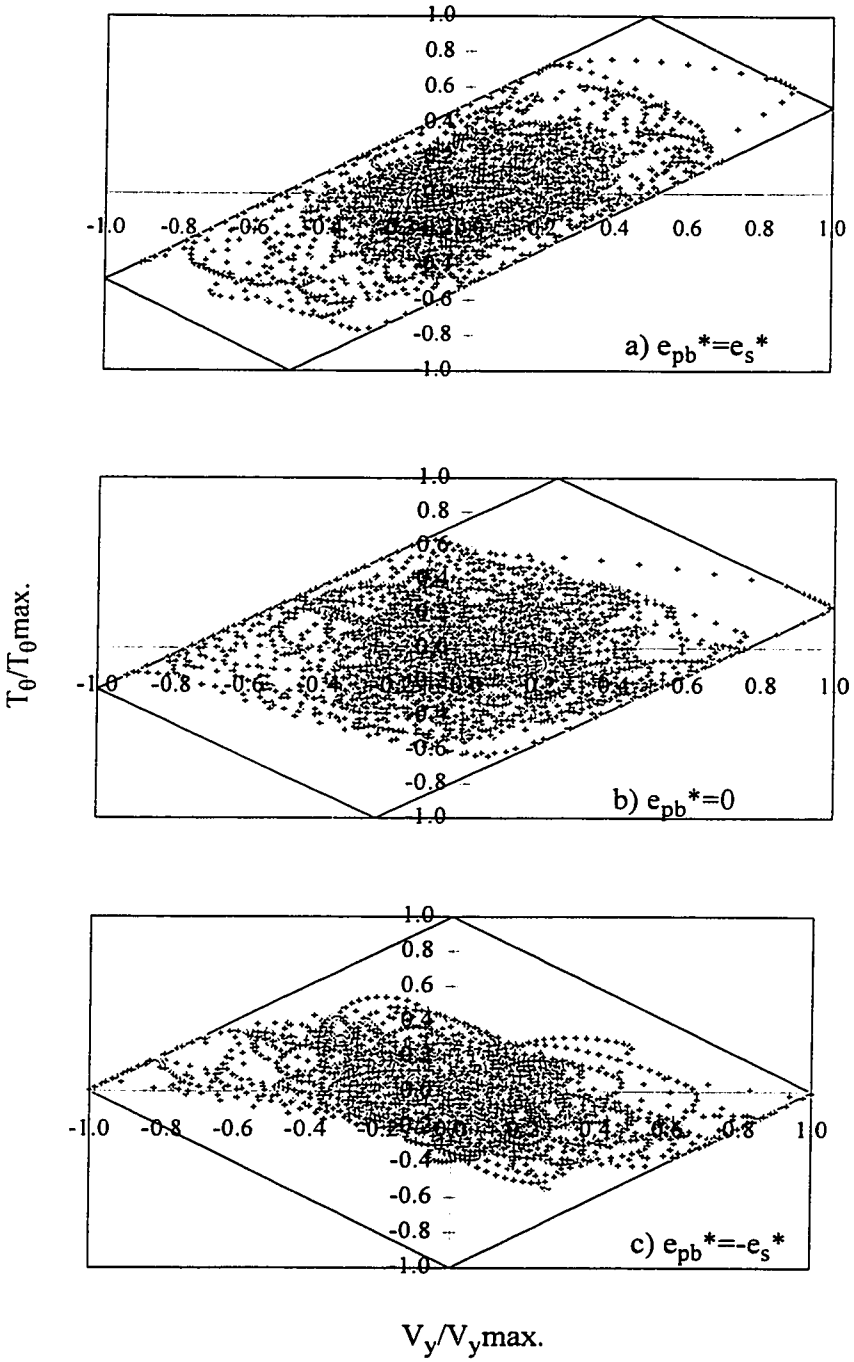

Figure 4.5 Effect of the slip load eccentricity on the seismic behavior of single-storey buildings (e_s*=0.5, 1940 El Centro N-S)

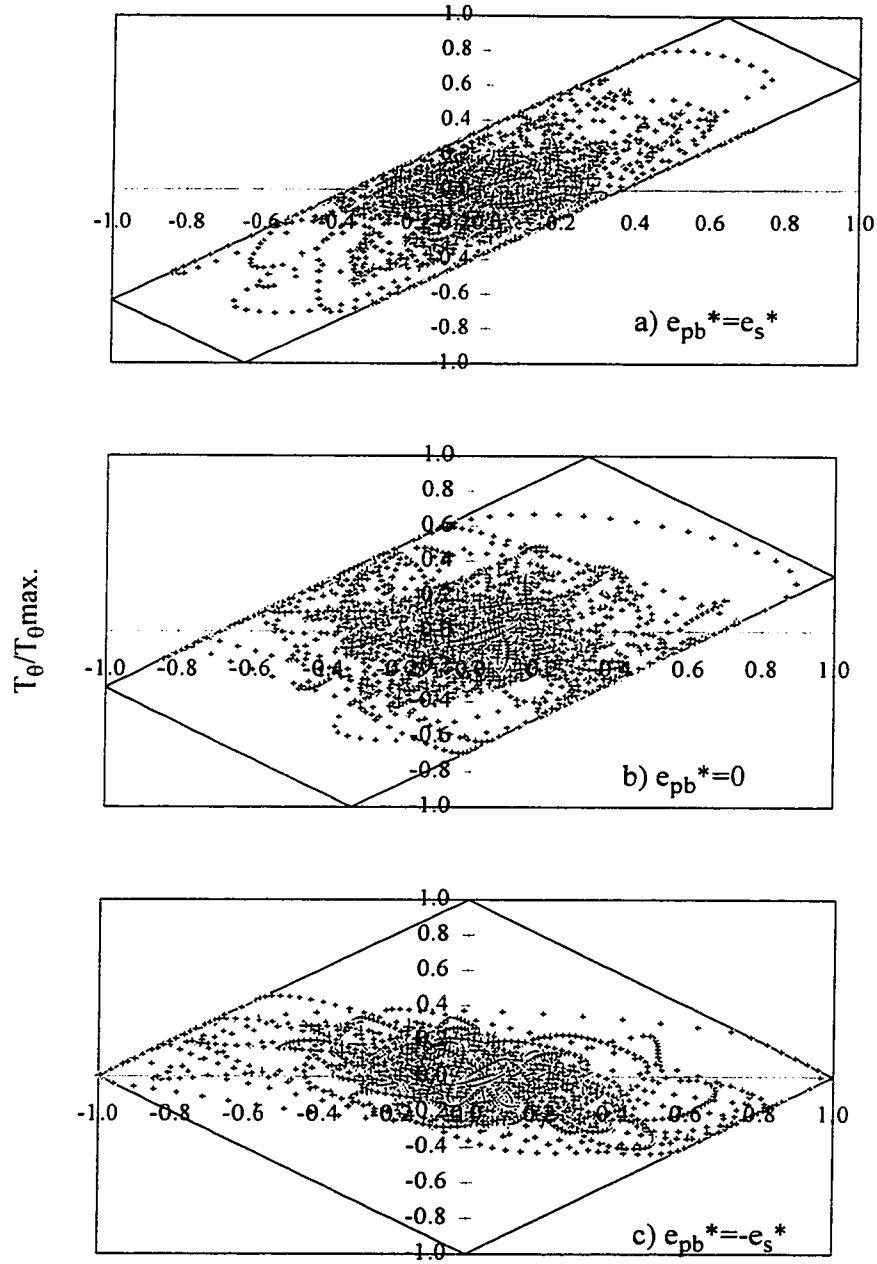

Figure 4.6 Effect of the slip load eccentricity on the seismic behavior of single-storey buildings (e_s*=0.75, 1940 El Centro N-S)

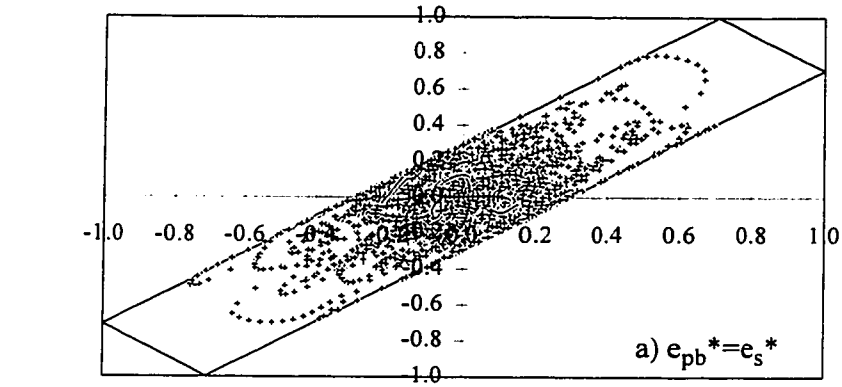

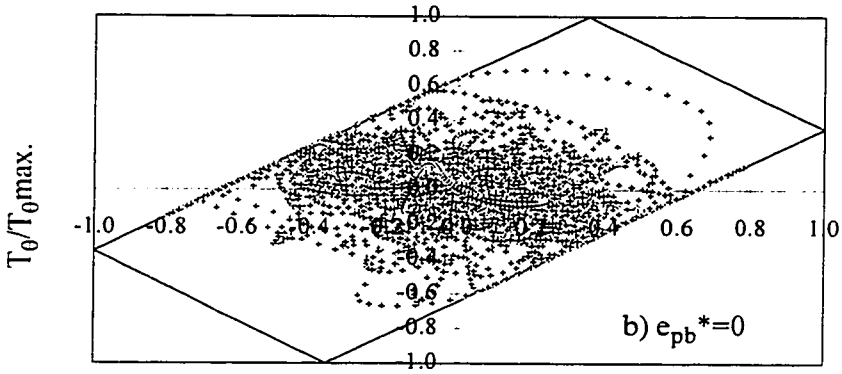

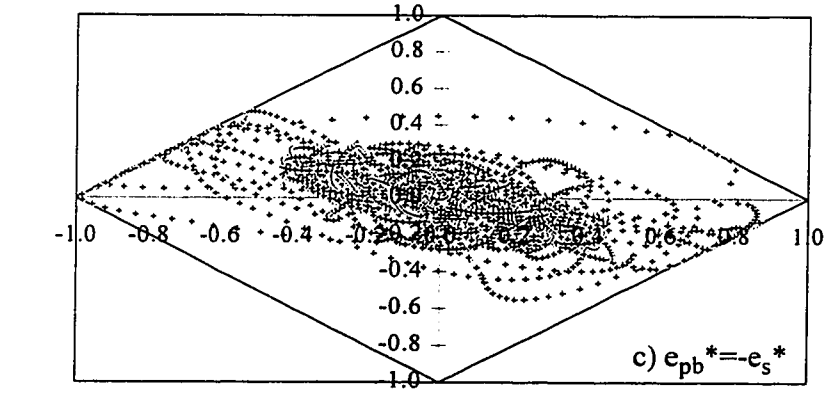

$T_0/T_0max.$

$V_y/V_ymax.$

Figure 4.7 Effect of the slip load eccentricity on the seismic behavior of single-storey buildings (e_s*=0.9, 1940 El Centro N-S)

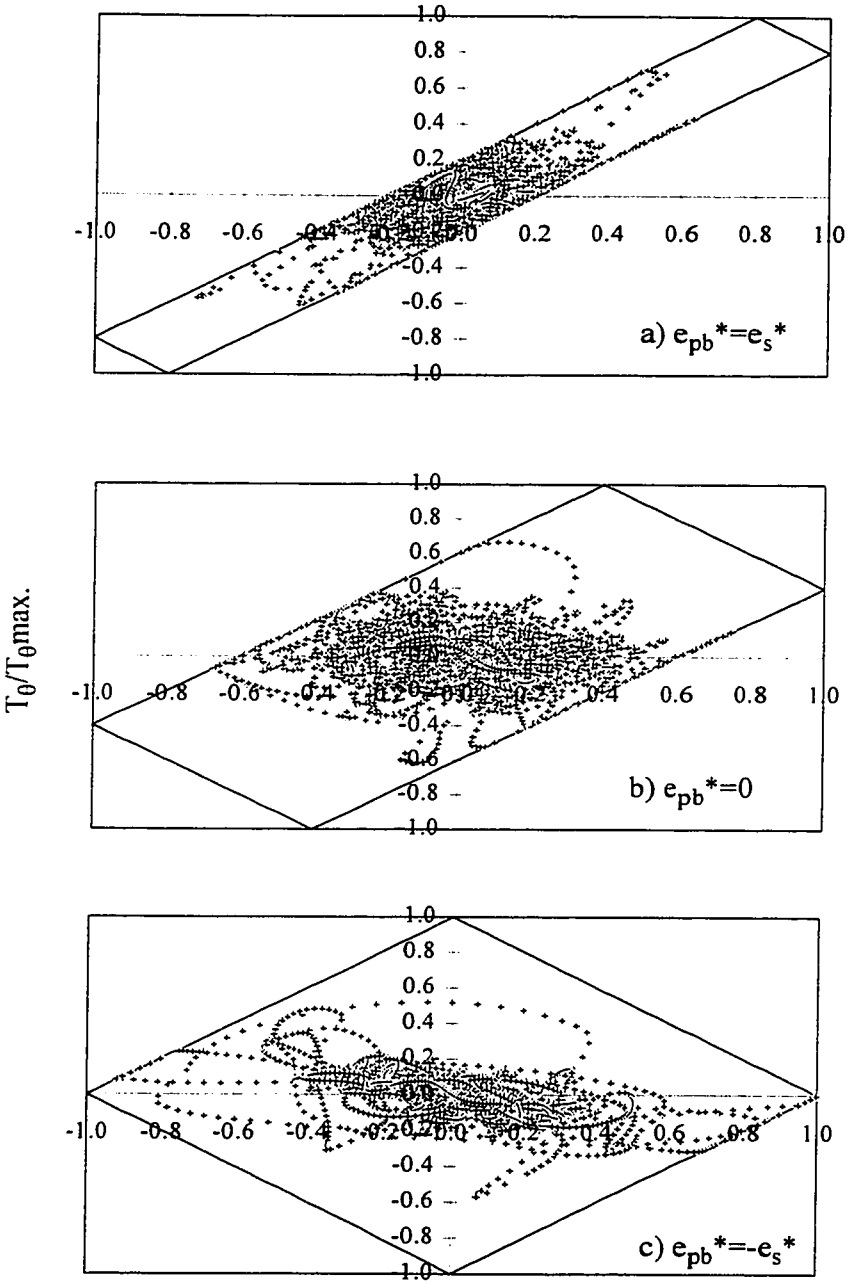

Figure 4.8 Effect of the slip load eccentricity on the seismic behavior of single-storey buildings (e_s*=1.2, 1940 El Centro N-S)

CHAPTER 5

ENERGY TERMS OF THE SINGLE-STOREY MODEL UNDER THE EFFECT OF THE SLIP LOAD DISTRIBUTION

5.1 INTRODUCTION:

The research carried out so far has dealt with the distribution of the slip load to minimize the response, ductility and base torque for the structures studied. This chapter studies the effect of the slip load distribution on the energy terms in order to determine the benefit of the new distribution on the energy dissipated by the structure, in particular the energy that will be dissipated by the friction braces.

The model used was the 2-D single-storey model described in chapter 2 (Figure 2.2) with uncoupled torsional to translational frequency ratio Ω_0=0.9 and fundamental period T=1 sec. The resisting elements are two FDBF in the direction of excitation. The brace stiffness chosen was three times the frame stiffness (KB/KF=3) and the brace strength was set to be equal to the frame strength (RB/RF=1). The model was subjected to 1977 Romania N90E earthquake in the y-direction.

The response data was generated using DRAIN-2D for five percent viscous damping and time step Δt=0.01 sec. Using the results obtained from DRAIN-2D, a separate program was used to calculate the different energy terms.

5.2 ENERGY EQUATIONS FOR SDOF SYSTEMS:

Two methods can be employed to calculate the energy terms imparted to a

structure by a seismic excitation, the absolute energy method and the relative energy method [19 & 21]. The difference between these two methods can be explained in the SDOF systems of Figure 5.1. Given the viscously damped SDOF system of Figure 5.1.a subjected to a horizontal earthquake ground motion, the equation of motion can be written as:

$$m\ddot{y}_t + c\dot{y} + f_s = 0 \tag{5-1}$$

where m is the mass of the system, c is the viscous damping coefficient and f_s is the restoring force. The absolute displacement of the mass is $y_t = y + y_g$ where y is the relative displacement of the mass to the ground and y_g is the ground displacement due to seismic excitation.

By letting $\ddot{y}_t = \ddot{y} + \ddot{y}_g$ the equation of motion can be written as:

$$m\ddot{y} + c\dot{y} + f_s = -m\ddot{y}_g \tag{5-2}$$

Therefore the system in the Figure 5.1.a which includes ground displacement in addition to relative mass to ground displacement can be treated conveniently as the equivalent fixed base system of Figure 1.5.b subjected to a horizontal dynamic force of magnitude $-m\ddot{y}_g$ and the relative displacement is employed. Analysis of the system of Figure 5.1.b thus employs the relative energy method. This latter concept was the one used in this study.

Depending upon the relative energy concept, integration of equation 5-2 with respect to y gives:

$$\int m\ddot{y}dy + \int c\dot{y}dy + \int f_s dy = -\int m\ddot{y}_g dy \tag{5-3}$$

The first term on the left-hand-side of equation 5-3 represents the relative kinetic energy

or the energy stored by the mass of the structure calculated at the end of each time step. The second term is the energy dissipated in viscous damping as it increases during the duration of motion. The third term represents the recoverable elastic strain energy and the energy absorbed by the system in the form of irrecoverable hysteretic energy (energy dissipated by the frame yield and by brace slippage), calculated at end of each time step. The right-hand-side term of the equation 5-3 thus defines the input energy of the system. The relative energy equation can be written as follows [20]:

$$E_t = E_k + E_\xi + E_s \tag{5-4}$$

where

$$E_t = -\int m\ddot{y}_g dy \tag{5-5}$$

$$E_k = \int m\ddot{y}dy = \frac{m\dot{y}^2}{2} \tag{5-6}$$

$$E_\xi = \int c\dot{y}dy \tag{5-7}$$

$$E_s = \int f_s dy \tag{5-8}$$

5.3 ENERGY EQUATIONS FOR THE TWO DOF SYSTEM USED IN THIS STUDY:

Expanding the same approach of the SDOF systems, the equation of motion of the two DOF system shown in Figure 5.2 can be written as:

$$\begin{bmatrix} m & 0 \\ 0 & m\rho^2 \end{bmatrix} \begin{bmatrix} \ddot{y} \\ \ddot{\theta} \end{bmatrix} + [C] \begin{bmatrix} \dot{y} \\ \dot{\theta} \end{bmatrix} + [F] = -\begin{bmatrix} m\ddot{y}_g \\ 0 \end{bmatrix} \tag{5-9}$$

Integrating the above equation with respect to y gives the energy terms of equation 5-4 for the two DOF system used in current study as follows:

$$\int\{\ddot{y}(t)\}^T \cdot [M] \cdot \{dy(t)\} + \int\{\dot{y}(t)\}^T \cdot [C] \cdot \{dy(t)\} + \int[F] \cdot \{dy(t)\}$$

$$= -\int\{dy\}^T \cdot [M] \cdot \begin{bmatrix} \ddot{y}_g(t) \\ 0 \end{bmatrix} \tag{5-10}$$

and $\{\dot{y}(t)\}$ is the vector of mass velocity defined as:

$$\{\dot{y}(t)\} = \begin{bmatrix} \dot{y}(t) \\ \dot{\theta}(t) \end{bmatrix} \tag{5-11}$$

where $\{\ddot{y}(t)\}$ is the vector of mass acceleration defined as:

$$\{\ddot{y}(t)\} = \begin{bmatrix} \ddot{y}(t) \\ \ddot{\theta}(t) \end{bmatrix} \tag{5-12}$$

The first term of equation (5-10) leads to the kinetic energy of the system, the second term leads to the damping energy of the system and the third term gives the stored elastic and irrecoverable plastic energy. The right hand side of equation 5-10 gives the input energy. Explained next is the calculation of the different energy terms at the end of each time step.

5.3.1 Input Energy

The input energy can be defined as:

$$E_t(t) = -\int \{dy(t)\}^T \cdot [M] \cdot \begin{bmatrix} \ddot{y}_g(t) \\ 0 \end{bmatrix} \qquad (5\text{-}13)$$

It has been calculated at the end of each time step as follow:

$$E_t(t) = E_t(t-\Delta t) + \frac{1}{2}\{y(t) + y(t-\Delta t)\}^T \cdot [M] \cdot \begin{bmatrix} \ddot{y}_g(t) - \ddot{y}_g(t-\Delta t) \\ 0 \end{bmatrix} \qquad (5\text{-}14)$$

5.3.2 Kinetic Energy:

The first term of the left hand side of equation 5.10 leads to the kinetic energy which can be defined as follow:

$$E_k = \int \{\ddot{y}(t)\}^T \cdot [M] \cdot \{dy(t)\} = \frac{1}{2}(\{\dot{y}(t)\}^T \cdot [M] \cdot \{\dot{y}(t)\}) \qquad (5\text{-}15)$$

Substitute in 5-15 using equation 5-11, kinetic energy can be written as:

$$E_k = \frac{m}{2} \cdot \{[\dot{y}(t)]^2 + \rho^2[\dot{\theta}(t)]^2\} \qquad (5\text{-}16)$$

5.3.3 Energy Dissipated In Viscous Damping:

The energy dissipated by viscous damping can be written as:

$$E_\xi(t) = \int \{\dot{y}(t)\}^T \cdot [C] \cdot \{dy(t)\} \qquad (5\text{-}17)$$

At each time step the energy dissipated by viscous damping may be calculated from the following equation:

$$E_\xi(t) = E_\xi(t-\Delta t) + \frac{1}{2}\{\dot{y}(t-\Delta t) + \dot{y}(t)\} \cdot [C] \cdot \{y(t) - y(t-\Delta t)\} \qquad (5\text{-}18)$$

where $\{y(t)\}$ is the vector of mass displacement defined as:

$$\{y(t)\} = \begin{bmatrix} y(t) \\ \theta(t) \end{bmatrix} \tag{5-19}$$

and the damping matrix [C] defined as follow:

$$[C] = \begin{bmatrix} 2\xi\omega_y & 0 \\ 0 & 2\xi\omega_{\theta 0} \end{bmatrix} \tag{5-20}$$

Substitute in equation 5-18 using equations 5-11, 5-19 and 5-20 the energy dissipated in viscous damping at the end of each time step can be written as:

$$E_\xi(t) = E_\xi(t-\Delta t) + \frac{\xi}{2} \cdot \{\omega_y[\dot{y}(t-\Delta t) + \dot{y}(t)] + \omega_{\theta 0}[y(t) - y(t-\Delta t)]\} \tag{5-21}$$

5.3.4 The Stored Elastic (Strain Energy) And The Irrecoverable Energy:

The elastic strain energy stored by the system can be written as:

$$E_s = \frac{1}{2}(\{y(t)\}^T \cdot [K] \cdot \{y(t)\}) \tag{5-22}$$

Where [K] is the linear portion of the stiffness matrix and which may written as:

$$[K] = \begin{bmatrix} \sum_i k_i & \sum_i k_i x_i \\ \sum_i k_i x_i & \sum_i k_i x_i^2 \end{bmatrix} \tag{5-23}$$

Substitute in equation 5-22 using equations 5-21 and 5-23, the strain energy may calculated at the end of each time step as follow:

$$E_s(t) = \frac{1}{2} \cdot \left(\sum_i k_i [y_i(t)]^2 + \sum_i k_i x_i^2 [\theta(t)]^2\right) + \sum_i k_i x_i [\theta(t)][y_i(t)] \tag{5-24}$$

The energy dissipated by friction braces can be calculated directly at the end of

each time step as the product of the slip load and the total slip travel:

$$E_{brace} = \sum_i RB_i \cdot |\Delta_{slip}| \tag{5-25}$$

where RF_i represents the i^{th} slip load of the braces and Δ_{slip} is the accumulative (absolute) slip travel.

The energy dissipated by the frame yield can be also calculated at the end of each time step as the product of the frame strength by the ductility displacement:

$$E_{frame} = \sum_i RF_i \cdot |\Delta_i - \Delta_{iy}| \tag{5-26}$$

where RF_i is the i^{th} frame strength, Δ_i is the i^{th} frame maximum displacement and Δ_{iy} is the yield displacement of the i^{th} frame.

The input energy defined by equation 5-5 is calculated separately at the end of each time step. The energy terms of the right hand side of equation 5-4 are summed to produce the total energy mobilized by the system at the end of each time step. The accuracy of calculation is checked by computing the sum of energies mobilized with the input energy.

5.4 DISCUSSION OF RESULTS

The energy curves obtained for the various eccentricities are normalized with respect to the elastic input energy of the symmetric case (Figure 5.3). Thus, the energy curves presented in this chapter depict the effect of eccentricity increase on the energy imparted to the structure as well as the energy dissipated by the braces and by frame yield

according to the three cases considered of the slip load distribution ($e_{pb}^* = e_s^*$, $e_{pb}^* = 0$ and $e_{pb}^* = -e_s^*$).

Energy consumed through yielding of frames and slippage of braces are the irrecoverable hysteretic energy dissipated by the system. Figure 5.4 shows the energy terms for the case of $e_s^*=0$. As can seen, the energy dissipated by frame yield in this case is almost negligible compared with the energy dissipated by the brace slippage. Figures 5.5 to 5.9 show the energy terms for different stiffness eccentricities ($e_s^* = 0$, 0.3, 0.5, 0.75, 0.9 and 1.2), each figure showing three cases of slip load eccentricities ($e_{pb}^* = e_s^*$, $e_{pb}^* = 0$ and $e_{pb}^* = -e_s^*$). Case (a) in Figures 5.5 to 5.9 show the energy curves for $e_{pb}^* = e_s^*$, which indicates that the input energy E_t has no significant change in the small and moderate stiffness eccentricity ($e_s^* = 0.3$ to 0.75). However, E_t increases as the stiffness eccentricity increases in large eccentricity ($e_s^* = 0.9$ and 1.2). The energy dissipated by the braces and by frame yielding almost remain constant as e_s^* increases from 0.3 to 1.2. Cases (b) and (c) for $e_{pb}^* = 0$ and $e_{pb}^* = -e_s^*$, respectively (Figures 5.5 to 5.9) imply that, for both cases the input energy increases as the stiffness eccentricity increases, but it is obvious that the rate of increase when $e_{pb}^* = -e_s^*$ is more than the rate of increase in the case of $e_{pb}^* = 0$.

For small and moderate eccentricity ($e_s^* = 0.3$ to 0.75) it may be concluded from Figures 5.5 to 5.7 that the input and dissipated energies decrease as the slip load eccentricity moves from the stiff side to the flexible side of the structure. While for large eccentricity ($e_s^* = 1.2$) of Figure 5.9, the energy dissipated by the braces E_{brace} increases and the energy dissipated by the frame yield E_{frame} decreases as the slip load eccentricity

moves from the stiff side to the flexible side of the structure.

To study the energy dissipated by brace slippage and by the frame yield, the energy curves are summarized in Figures 5.10 to 5.12. In these charts, the results were obtained for 1977 Romania N90W excitation. For each eccentricity the peak input energy and the maximum dissipated energy by the frame yield and by the brace slippage were normalized with respect to the peak input energy of the symmetric unbraced case ($e_s = 0$ & KB/KF = 0). The three cases of slip load eccentricity ($e_{pb}^* = e_s^*$, $e_{pb}^* = 0$ and $e_{pb}^* = -e_s^*$) are plotted in Figures 5.10 to 9.12, respectively. Figure 5.10 shows the input and dissipated energies for the six different eccentricities ($e_s^* = 0$, 0.3, 0.5, 0.75, 0.9 and 1.2) in the case of $e_{pb}^* = e_s^*$. It can be seen that the input energy increases with increase of stiffness eccentricity. For the small stiffness eccentricity ($e_s^* = 0.3$) the input energy is two times the input energy of the symmetric case, while in the large stiffness eccentricity ($e_s^* = 1.2$) the input energy is 2.7 times the input energy of the symmetric case. For $e_s^* =$ 0.5 and 0.75 the rate of increase was zero, which means that the rate of increase in the input energy was high in large stiffness eccentricity (from 0.9 to 1.2) and in small eccentricity (from 0 to 0.3), while the rate of increase of the input energy was negligible in moderate eccentricity (from 0.3 to 0.75). Similarly behaves the curve of the energy dissipated by the frame yield. The energy dissipated by the brace slippage is constant for small and moderate eccentricity, while it is increased for large stiffness eccentricity. A phenomenon that manifests itself is that for symmetric friction damped braced frames most of the energy is dissipated through slippage of the friction device as can be clearly seen in Figure 5.10 where the energy dissipated by the frame yield in the case of $e_s^* = 0$ is almost zero.

The energy input and dissipated for the case of $e_{pb}^* = 0$ are presented in Figure 5.11. It shows that the input energy increases as the stiffness eccentricity increases. For small eccentricity $e_s^* = 0.3$ the input energy was 1.1 times the input energy of the symmetric case, while in the large eccentricity ($e_s^* = 1.2$) the input energy is 2.4 times the input energy of the symmetric case. The energy dissipated by the brace slippage (E_{brace}) also increases with increase of e_s^*. For large eccentricity ($e_s^* = 1.2$), (E_{brace}) is 1.65 times its counterpart for $e_{pb}^* = e_s^*$. The energy dissipated by the frame yield is 0.5 the input energy of the case when $e_s^*=0.5$ but it comes to $0.4E_t$ ($e_s^* = 0$) when $e_s^* = 0.9$ and 1.2.

Figure 5.12 shows the energy curves for the case of $e_{pb}^* = -e_s^*$. For large eccentricity ($e_s^* = 1.2$), the input energy for is three times E_t ($e_s^* = 0$). The energy dissipated by the braces slippage (E_{brace}) was two times its counterpart in the case of $e_{pb}^* = e_s^*$. The energy dissipated by the frame yield (E_{frame}) is $0.4E_t$ ($e_s^* = 0$) when $e_s^* = 0.75$ but it comes to $0.125\ E_t$ ($e_s^* = 0$) when $e_s^* = 1.2$.

The average results of the four earthquake records: 1940 El-Centro N-S; the Newmark-Blume-Kapur artificially generated ground motion; 1952 Taft; 1977 Romania N90W, are summarized in Figures 5.13 to 5.15. In these charts, for each eccentricity the peak input energy and the maximum dissipated energy by the frame yield and by the brace slippage was normalized with respect to the peak input energy of the symmetric case ($e_s = 0$). The three cases of slip load eccentricity ($e_{pb}^* = e_s^*$, $e_{pb}^* = 0$ and $e_{pb}^* = -e_s^*$) are plotted in Figures 5.13 to 5.15 respectively. Figure 5.13 shows the input and dissipated energies for the six different eccentricities ($e_s^* = 0$, 0.3, 0.5, 0.75, 0.9 and 1.2)

in the case of $e_{pb}^*=e_s^*$. It can seen that the input energy increases with increase of stiffness eccentricity. For the small stiffness eccentricity (e_s^* = 0.3 and 0.5) the input energy is equal to the input energy of the symmetric case, while in the large stiffness eccentricity (e_s^* = 1.2) the input energy is 2.4 times the input energy of the symmetric case, which mean that the rate of increase in the input energy is high for large stiffness eccentricity (from 0.9 to 1.2), while the rate of increase of the input energy was small in small and moderate eccentricity (from 0.3 to 0.75). Similarly behaves the curve of the energy dissipated by brace slippage. The energy dissipated by frame yield increases as the stiffness eccentricity increase (from 0.1 E_t at $e_s = 0$ to 0.4 E_t at $e_s = 1.2$).

The energy input and dissipated for the case of $e_{pb}^* = 0$ are presented in Figure 5.14. It shows that the input energy increases as the stiffness eccentricity increases. For small eccentricity e_s^* = 0.3 the input energy is 1.1 times the input energy of the symmetric case, while in the large eccentricity (e_s^* = 1.2) the input energy was 1.7 times the input energy of the symmetric case. The energy dissipated by brace slippage (E_{brace}) also increases with increase of e_s^*. For large eccentricity (e_s^* = 1.2), E_{brace} is equal to its counterpart for $e_{pb}^* = e_s^*$. The energy dissipated by frame yield is 0.3 times the input energy of the symmetric case when e_s^*=0.75 but it comes to $0.25E_t$ ($e_s^* = 0$) when e_s^* = 0.9 and $0.22E_t$ ($e_s^* = 0$) when $e_s^* = 1.2$.

Figure 5.15 shows the energy curves for the case of $e_{pb}^* = -e_s^*$. For large eccentricity (e_s^* = 1.2), the input energy is two times E_t ($e_s^* = 0$). The energy dissipated by the brace slippage (E_{brace}) is equal to its counterpart in the case of $e_{pb}^* = e_s^*$. The energy dissipated by the frame yield (E_{frame}) is $0.24E_t$ ($e_s^* = 0$) when e_s^* = 0.5 & 0.9 but

it comes to 0.125 E_t ($e_s^* = 0$) when $e_s^* = 1.2$.

5.5 CONCLUDING REMARKS

- The energy dissipated by brace slippage increases as the slip load eccentricity moves from the stiff side to the flexible side of the structure.

- For $e_s^* > 0.3$, the energy dissipated by the braces slippage and by frame yield are almost constant for $e_{pb}^* = e_s^*$.

- For $e_s^* > 0.5$, as the slip load eccentricity moves from the stiff side to the flexible side of the structure, the energy dissipated by braces slippage (E_{brace}) increases and the energy dissipated by frame yield (E_{frame}) decreases for $e_{pb}^* = 0$ and $e_{pb}^* = -e_s^*$

- For $e_s^* = 0.5$, the energy dissipated by the frame yield (E_{frame}) are approximately equal for $e_{pb}^* = e_s^*$ and e_{pb}^*

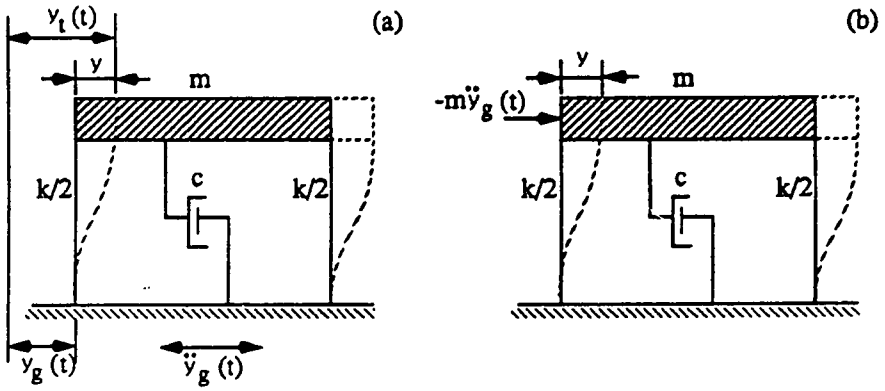

Figure 5.1 Idealized SDOF systems subjected to earthquake ground motion

(a) Absolute motion (b) Equivalent relative displacement

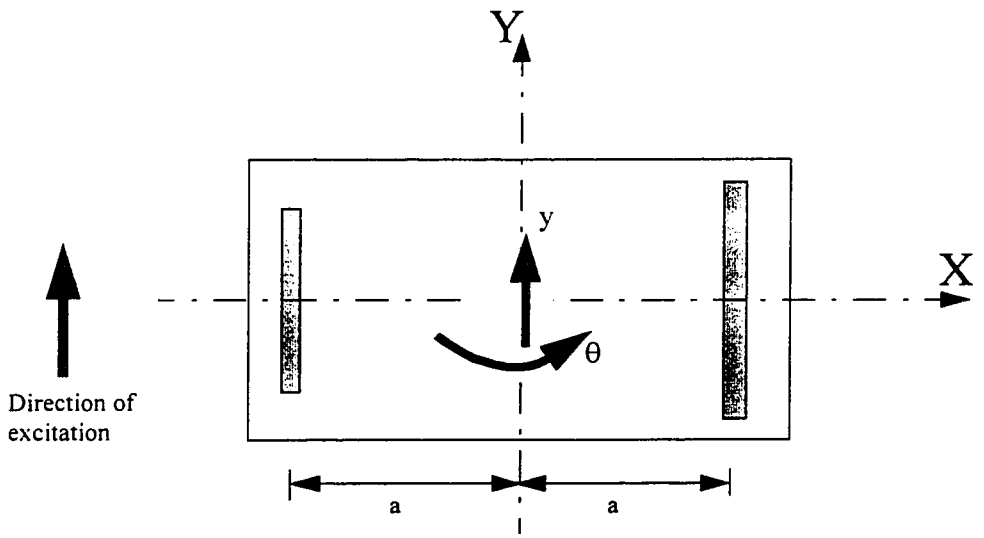

Figure 5.2 Idealized 2-DOF model used in current study

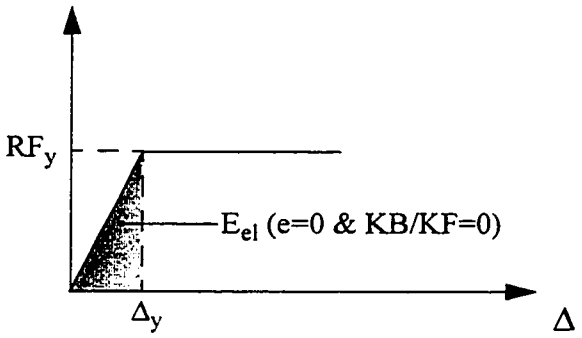

Figure 5.3 Elastic energy for symmetric unbraced case

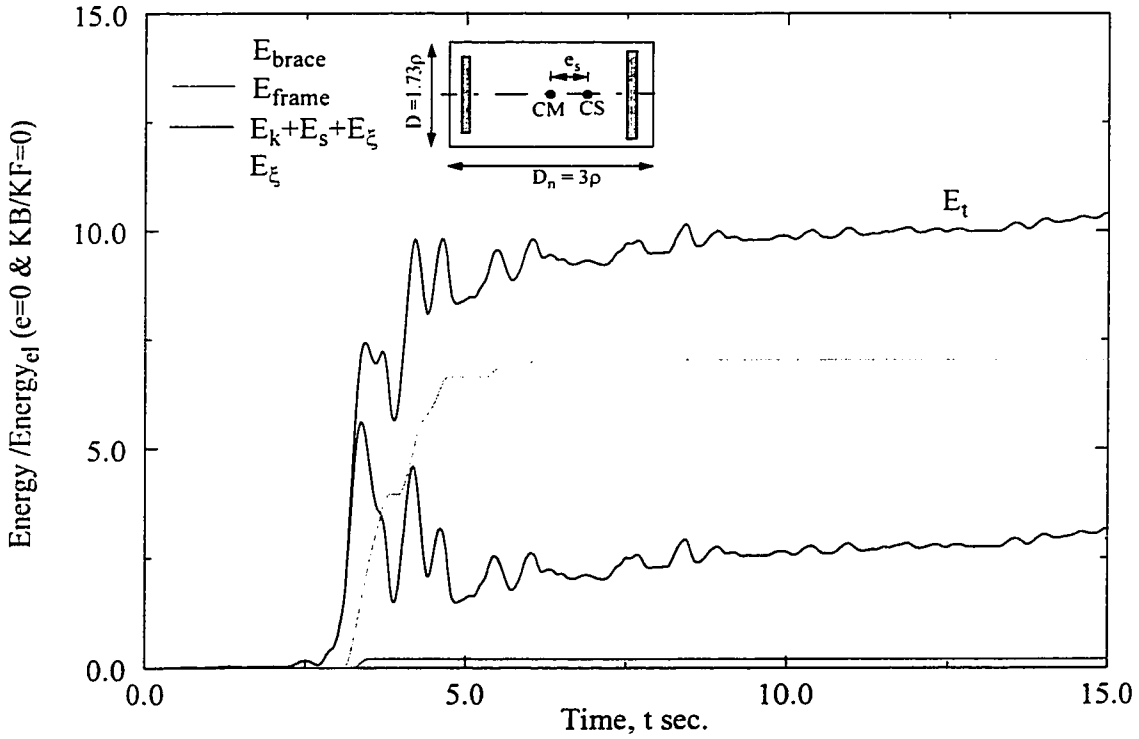

Figure 5.4 Energy terms time-history for e_s*=0
(1977 Romania N90W)

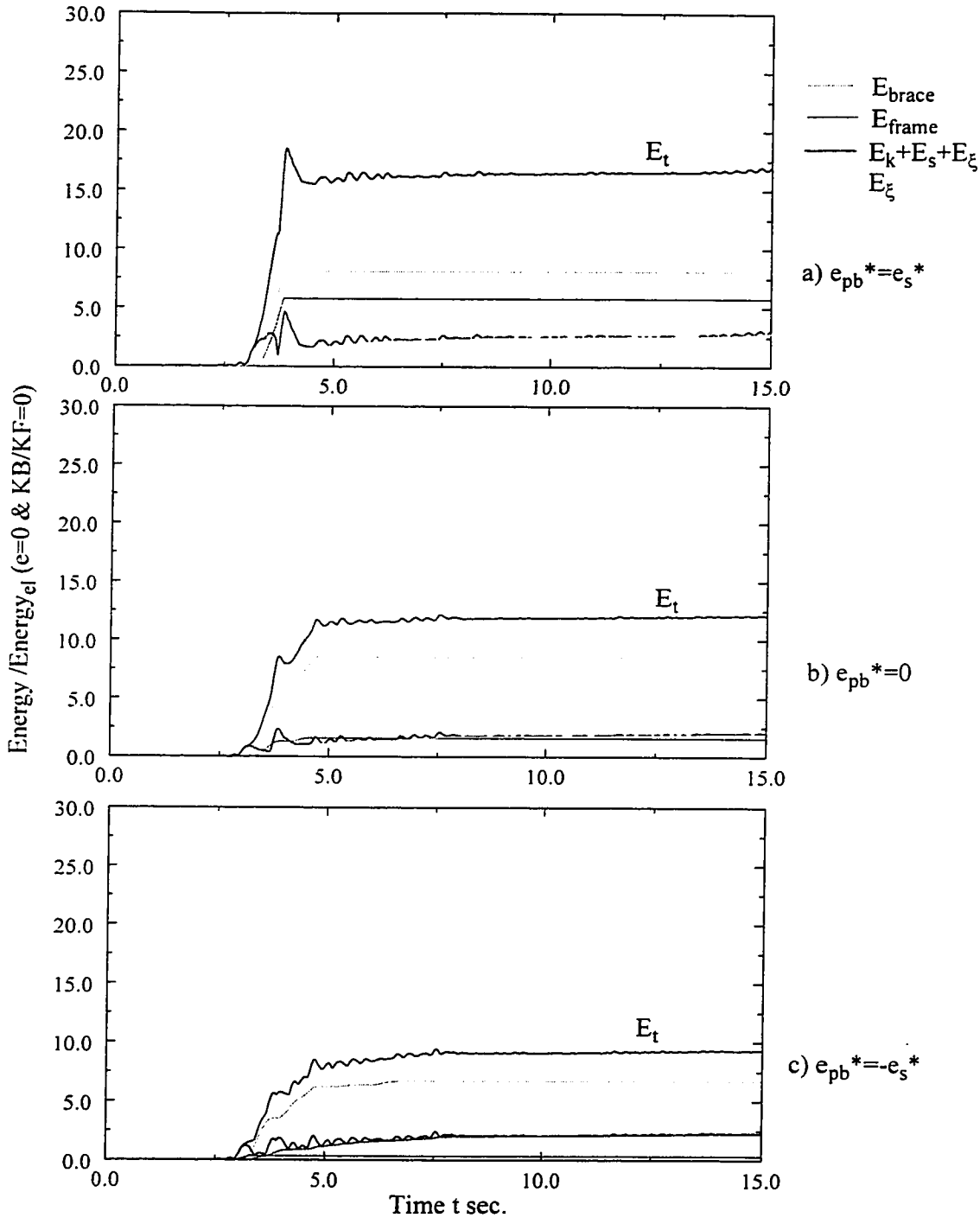

Figure 5.5 Energy terms time-history for $e_s^*=0.3$
(1977 Romania N90W)

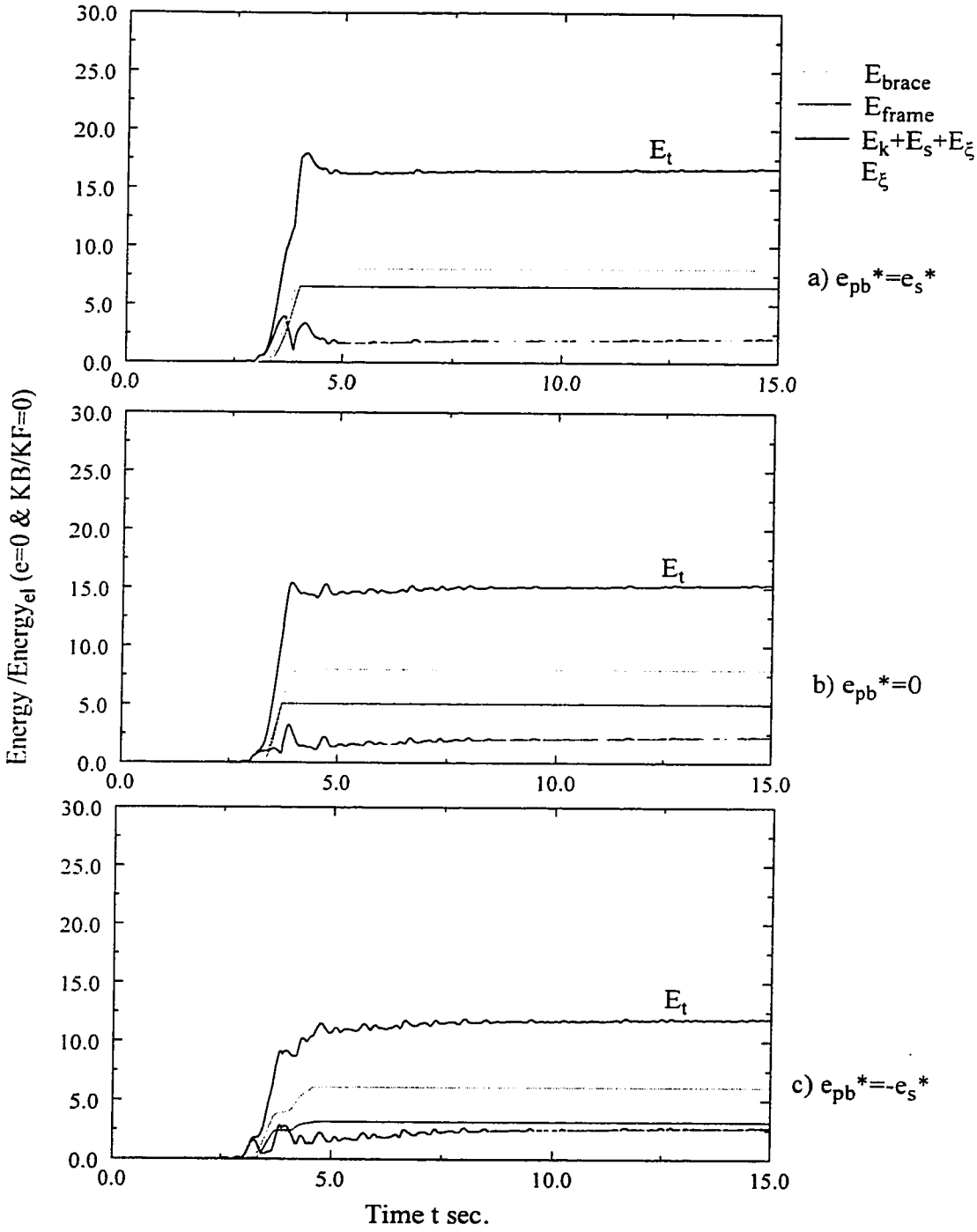

Figure 5.6. Energy terms time-history for $e_s*=0.5$
(1977 Romania N90W)

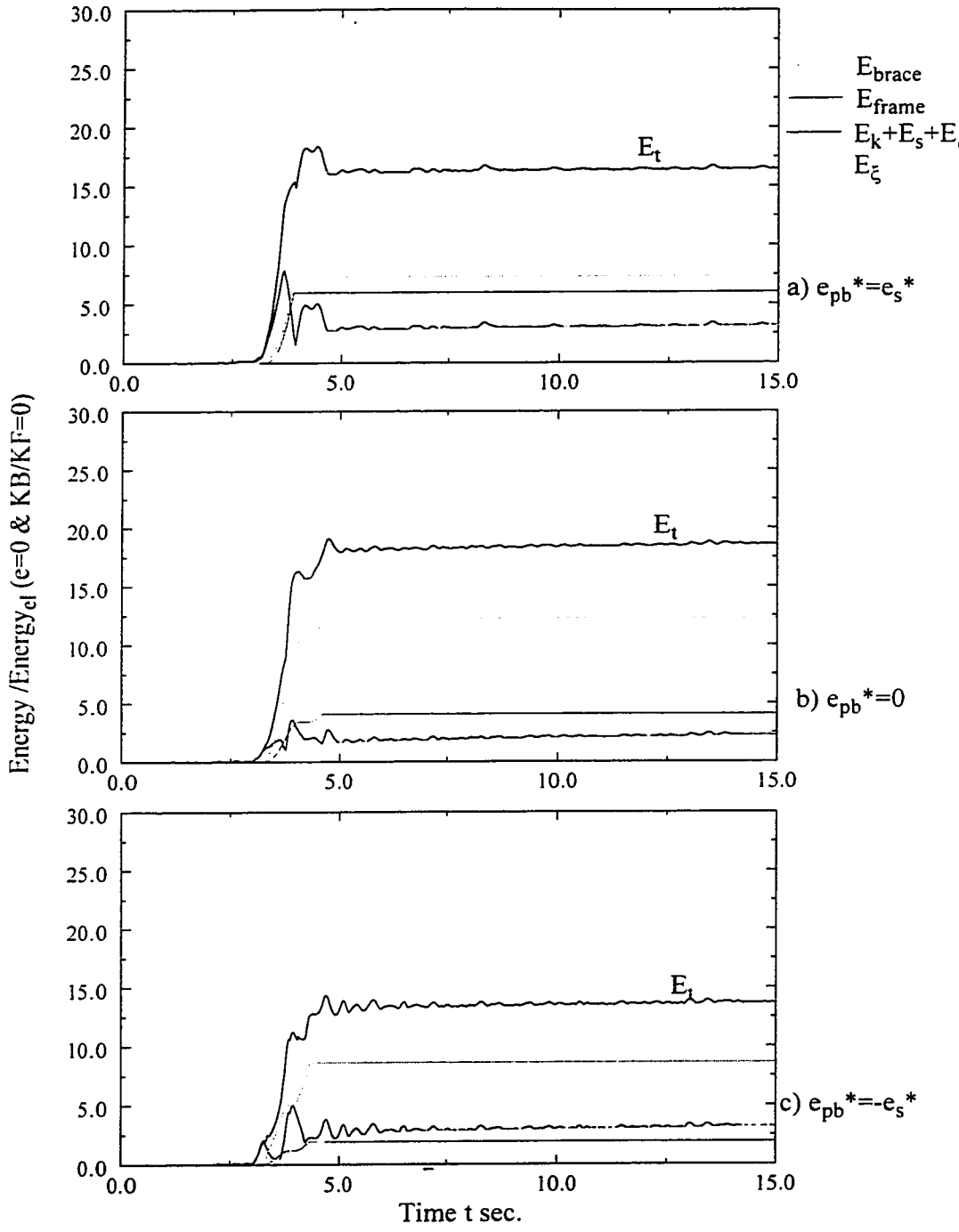

Figure 5.7 Energy terms time-history for $e_s^*=0.75$
(1977 Romania N90W)

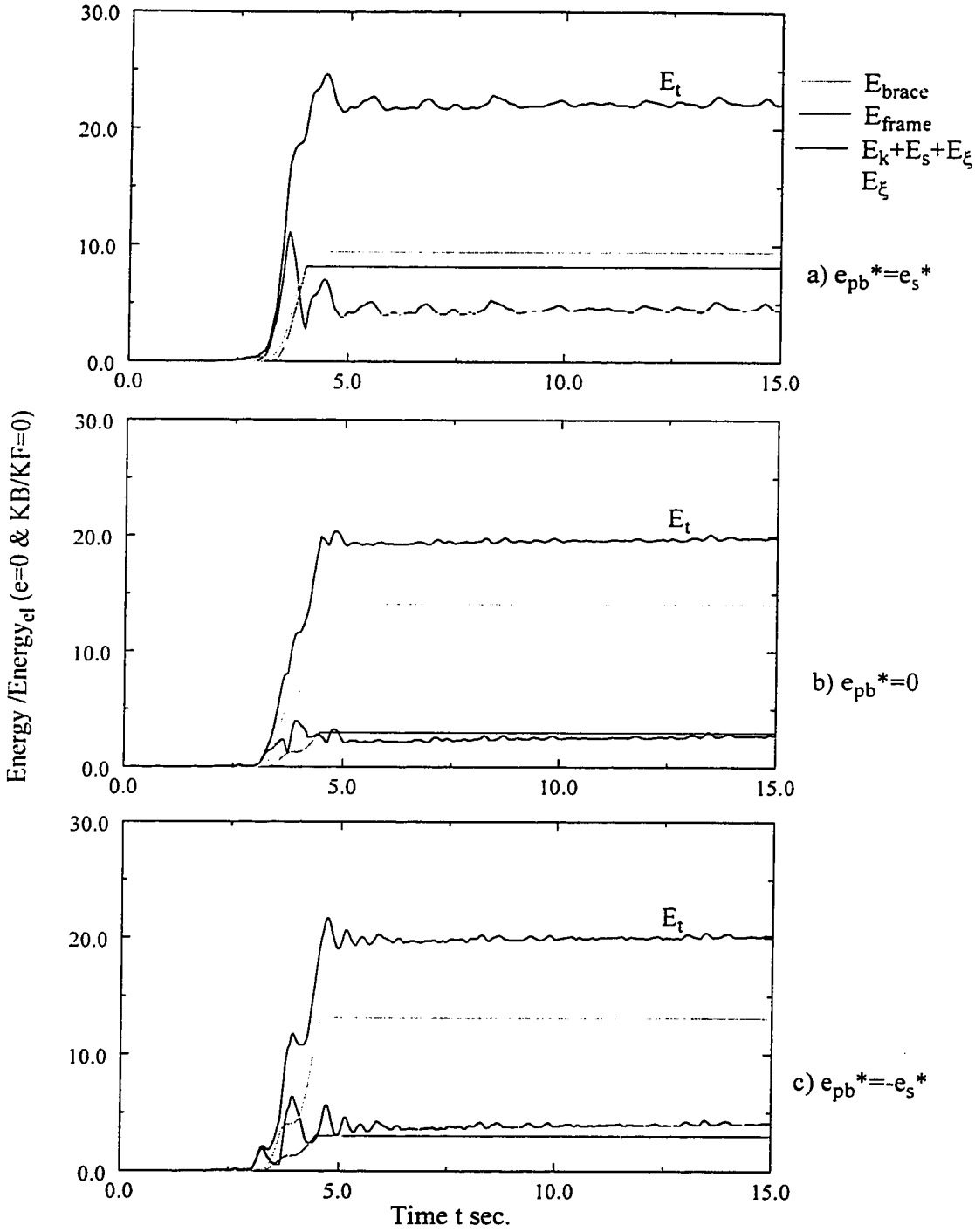

Figure 5.8 Energy terms time-history y for $e_s*=0.9$
(1977 Romania N90W)

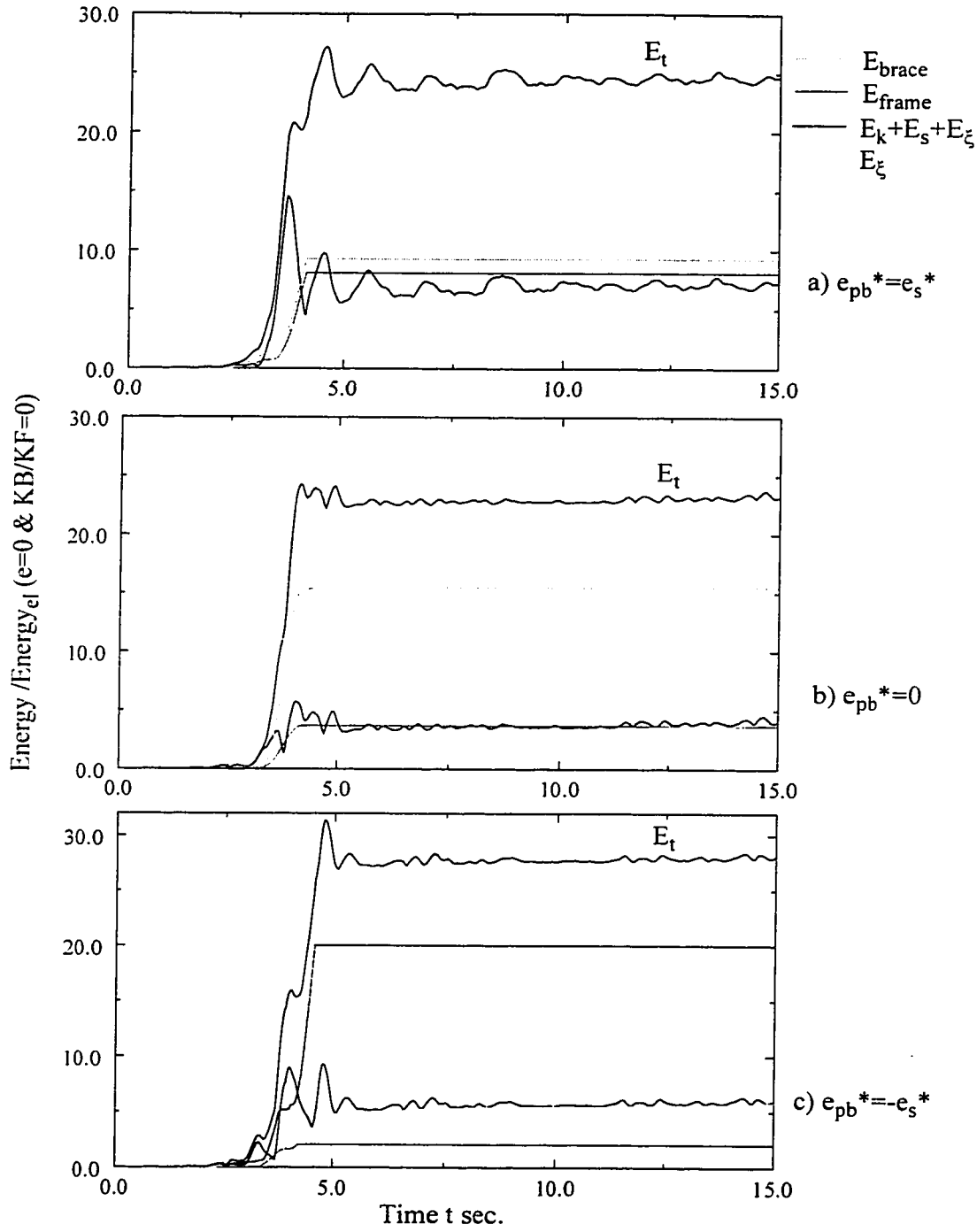

Figure 5.9. Energy terms time-history for $e_s^*=1.2$
(1977 Romania N90W)

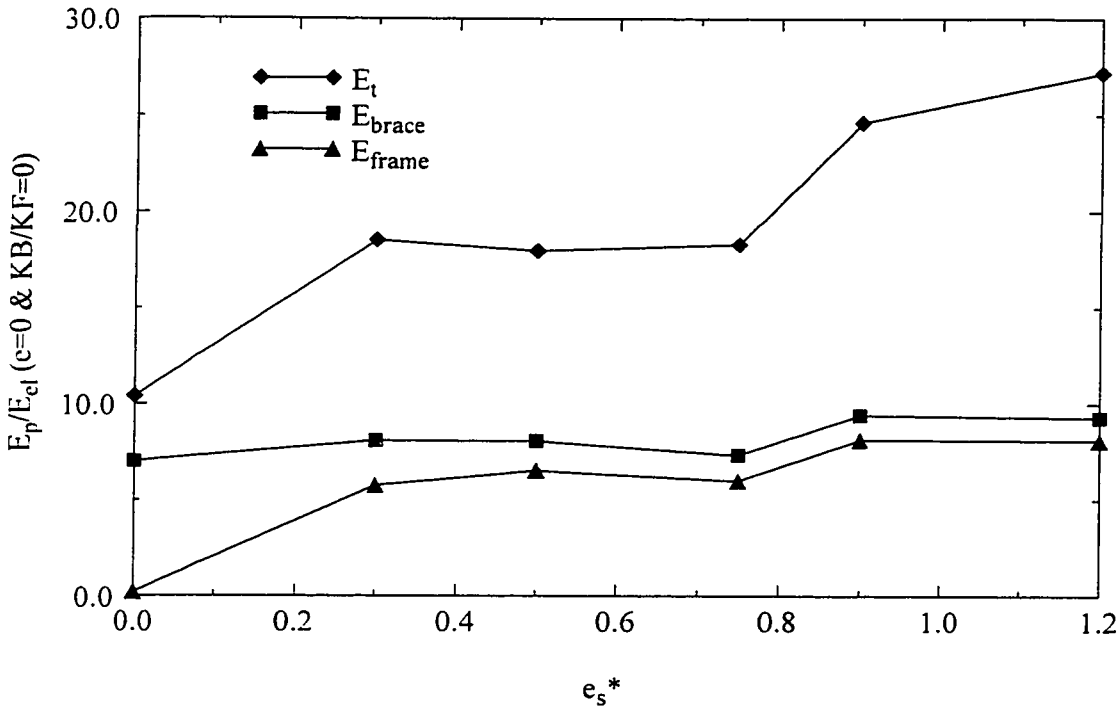

Figure 5.10 Normalized input and dissipated energy for $e_{pb} = e_s$
(1977 Romania N90W)

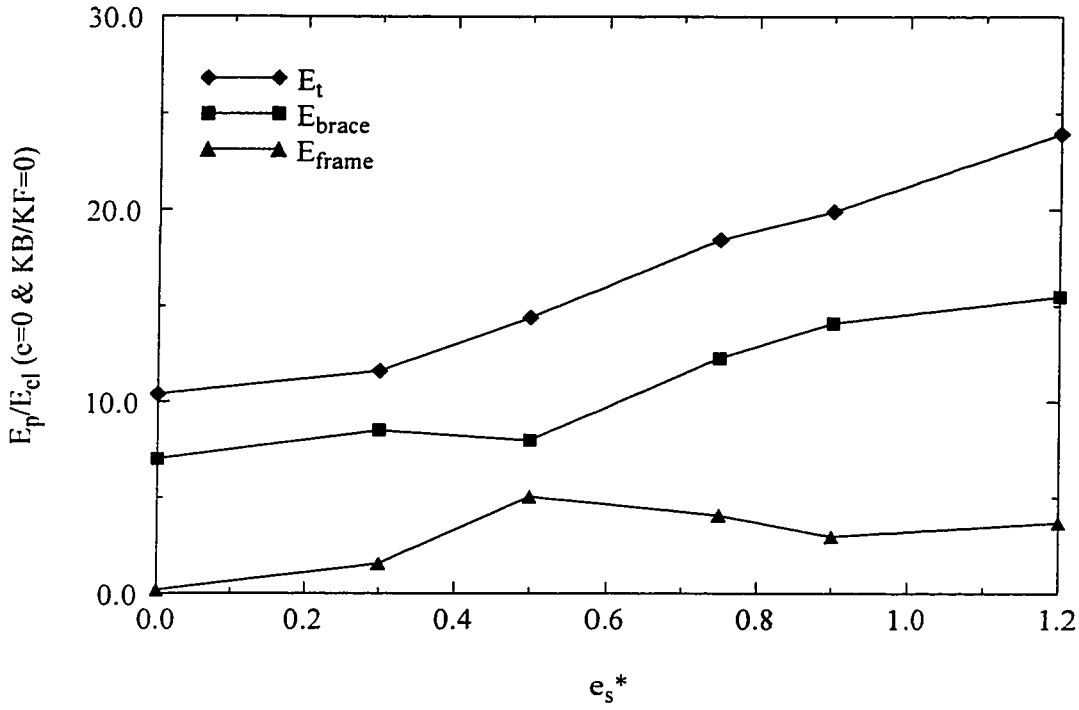

Figure 5.11 Normalized input and dissipated energy for $e_{pb} = 0$
(1977 Romania N90W)

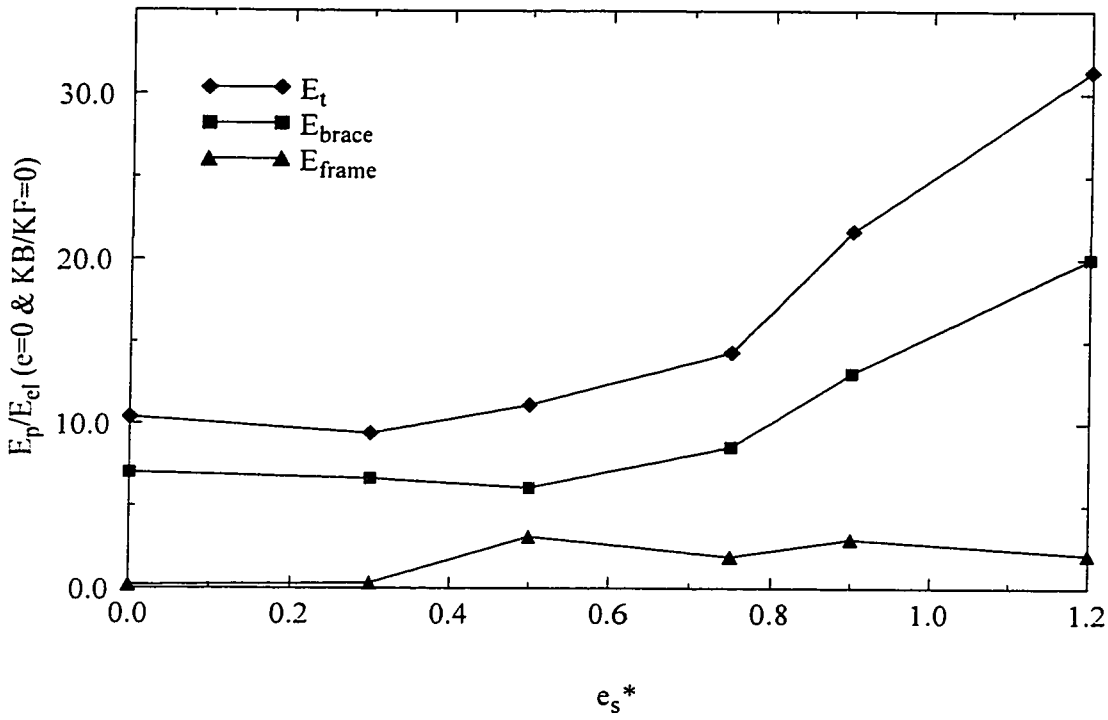

Figure 5.12 Normalized input and dissipated energy for $e_{pb} = -e_s$
(1977 Romania N90W)

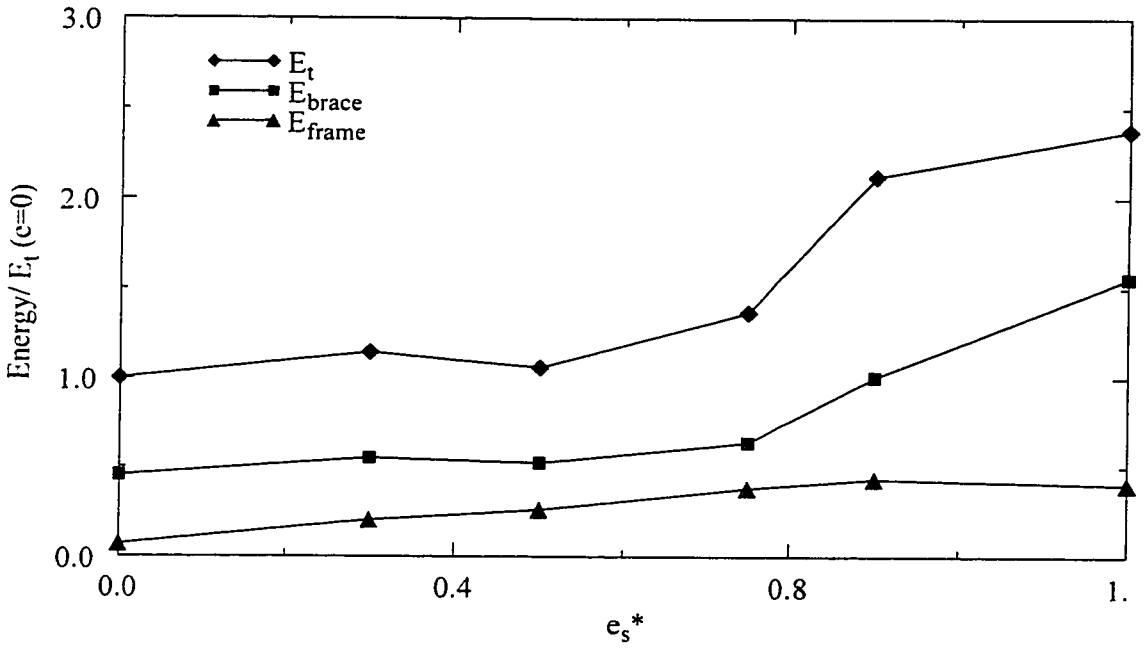

Figure 5.13 Summary of normalized input and dissipated energy terms for $e_{pb} = e_s$ (Average of the four earthquake records:1940 El-Centro N-S; the Newmark-Blume-Kapur artificially generated ground motion; 1952 Taft; 1977 Romania N90W).

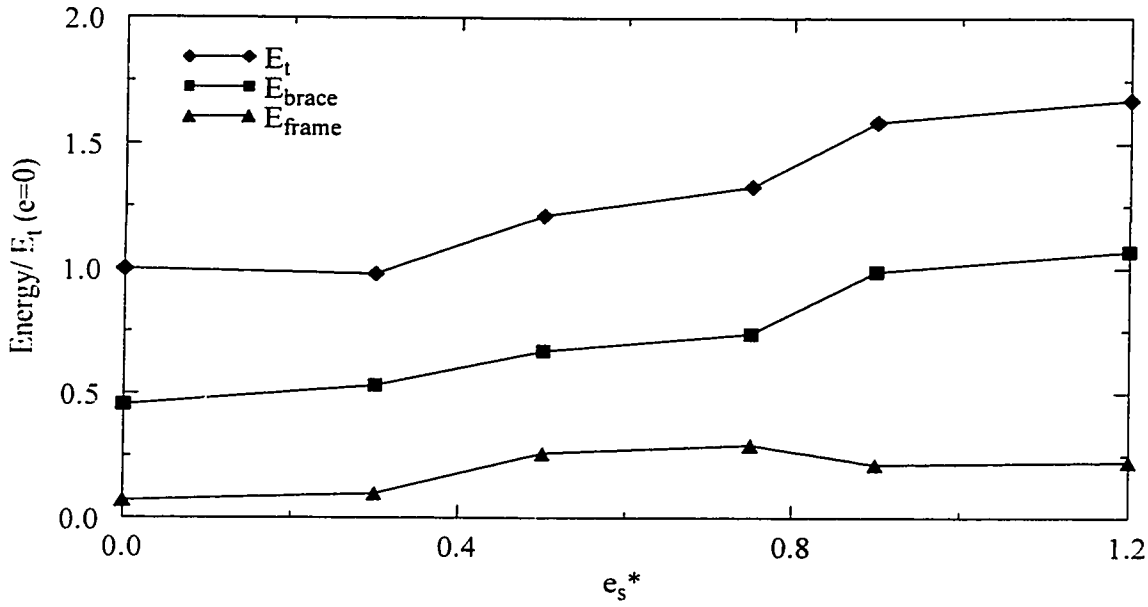

Figure 5.14 Summary of normalized input and dissipated energy terms for $e_{pb} = 0$ (Average of the four earthquake records:1940 El-Centro N-S; the Newmark-Blume-Kapur artificially generated ground motion; 1952 Taft; 1977 Romania N90W).

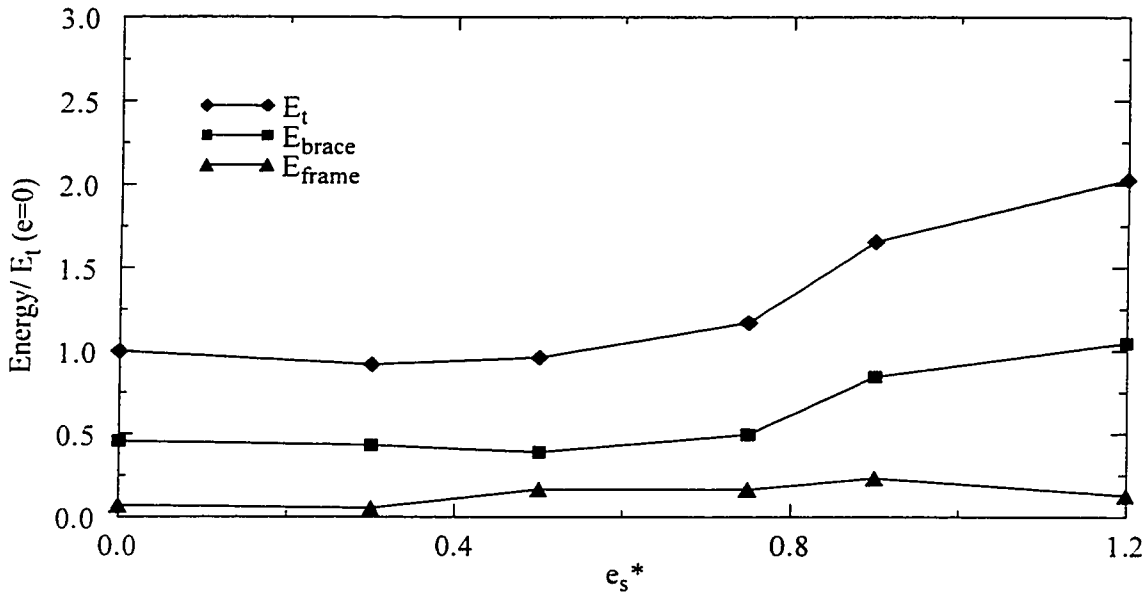

Figure 5.15 Summary of normalized input and dissipated energy terms for $e_{pb} = -e_s$ (Average of the four earthquake records:1940 El-Centro N-S; the Newmark-Blume-Kapur artificially generated ground motion; 1952 Taft; 1977 Romania N90W).

CHAPTER 6

CONCLUSION

This research examined the performance improvement of FDBF due to slip load redistribution. The study consists of three parts; the first part was a study of the two dimensional multi-storey models with FDBF conducted using DRAIN-2D program to determine the slip load distribution that gives the optimum response and minimum ductility demand; the second part was a study of the effect slip load redistribution on the inelastic behavior of two dimensional single-storey model using the history of base shear and torque in order to determine the optimum slip load distribution that gives the minimum base torque. The analysis was made through the use of DRAIN-2D program; the third and final part was a study of the energy imparted and dissipated by the system in order to examine the effect of slip load redistribution on the amount of energy dissipation by the brace slippage. In this part, after analyzing the single storey model, a separate program was run to calculate the energy terms.

In chapter 2, the description of the single and multi-storey models was presented along with the equations that control the placement of the resisting frames and braces as well as the distribution of slip load, strength and stiffness.

In chapter 3, the parametric study of the multi-storey models over the range chosen of stiffness eccentricity (e_s from 0 to 1.2) with various slip load distributions showed that optimum responses are obtained when the slip load eccentricity is opposite the stiffness eccentricity (i.e. $e_{pb} = -e_s$). It was demonstrated that as the slip load eccentricity move to the flexible side of the structure, more storeys will participate in dissipating energy and the ductility demand will reduced.

Chapter 4 dealt with the effect of slip load distribution on the inelastic behavior of a single storey model. The results showed that the minimum base torque was obtained when the slip load eccentricity equals the stiffness eccentricity put in the opposite side of the structure ($e_{pb} = -e_s$).

In chapter 5, the study of the energy imparted and dissipated by the system demonstrated that the amount of energy dissipated by the brace slippage increase as the slip load eccentricity moves from the stiff side to the flexible side of the structure.

It is concluded from this study that the slip load distribution must be considered in the design of FDBF, as well as the optimum strength ratio RB / RF and the optimum stiffness ratio KB / KF.

For future research, more investigation of inelastic behavior using history of base shear and torque is require. It is suggested to use the strength eccentricity to reshape the BST ultimate surface in order to minimize the base torque.

Also the study of the storey shear and torque for multi-storey structures require more investigation using the concept of slip load redistribution.

REFERENCES

1. A. S. Pall and C. Marsh, 'Response of friction damped braced frames', *J. struct. div.ASCE.* vol. 108, 1313-1323 (1982).

2. P. Baktash, 'Friction damped braced frames', *Ph.D. Thesis,* Concordia University, Montreal, Quebec, (1989).

3. C. Pasquin, A. Pall and R. Pall, 'Friction-dampers For Seismic Rehabilitation Of Casino De Montreal', *7th Canadian conference of Earthquake Engineering.* Montreal, 943-949, (1992)

4. O. A. Pekau and R. Guimond, 'Controlling Seismic Response of Eccentric Structures by Friction Dampers', *Earthquake Engineering and Structural Dynamics,* vol. 20, 505-521 (1991).

5. R. K. Goel and A. K. Chopra, 'Inelastic seismic response of one-storey, asymmetric plan systems', *Report No. EERC 90-14,* Earthquake Engineering Research Center, University of California, Berkeley, CA, (1990).

6. Luciano Martin 'Parametric study of a Tuning Scheme for the Design of friction Damped Braced Frames', *M.A.Sc. Thesis*, Concordia University, Montreal, Quebec, (1995).

7. L. Martin and O. A. Pekau, 'Improved Performance Of Friction Damped Asymmetric Structures', *7th Canadian conference of Earthquake Engineering.* Montreal, 927-934, (1995)

8. W. K. Tso and H. Ying, 'Additional seismic inelastic deformation caused by structural asymmetry', *Earthquake eng. struct. dyn.* vol. 19, 243-258 (1990).

9. Juan C. De La Llera and Anil K. Chopra, 'Understanding The Inelastic Seismic Behavior Of Asymmetric-plan Buildings', *Earthquake eng. struct. dyn.* vol. 24, 549-572 (1995).

10. Juan C. De La Llera and Anil K. Chopra, 'A Simplified Model For Analysis And Design Of Asymmetric Plan-buildings', *Earthquake eng. struct. dyn.* vol. 24, 5739-594 (1995).

11. R. Guimond, 'Accidental Eccentricity and Limiting the Effects of Design Eccentricity for

Seismic Response of Buildings', *M. ENG. Thesis,* Concordia University, Montreal, Quebec, (1989)

12. Juan C. De La Llera and Anil K. Chopra, 'Accidental And Natural Torsion In Earthquake Response And Design Of Buildings', *Report No. EERC 94/07,* University of California, Berkley, CA, (1990).

13. J. L. Humar, 'Design for Seismic Torsional Forces', *Canadian Journal of Civil Engineering,* vol. 11, 150- 163 (1984).

14. A. E. Kannan and G. M. Powell, 'Drain-2D, A General Purpose Computer Program for Dynamic Analysis of Inelastic Plane Structures', *Report No. EERC* 73-6, Earthquake Engineering Research Center, University of California, Berkeley, CA, (1973).

15. W. K. Tso, 'A Proposal to Improve the Static Torsional Provisions for the National Building Code of Canada', *Canadian Journal of Civil Engineering,* vol. 10, 561565 (1983).

16. Associate Committee on the National Building Code, 'NBCC 1990', National Research Council of Canada, Ottawa 1990.

17. A. Rutenberg and O. A. Pekau, 'Earthquake Response of Asymmetric Buildings: A Parametric Study', *Fourth Canadian Conference on Earthquake Engineering Proceedings,* 271-281(1983).

18. A. Filiatrault and S. Cherry, 'Seismic Tests of Friction Damped Steel Frames', *Dynamic Response of Structures,* Proceedings of the Third Conference Organized by the Engineering Mechanics Division of the ASCE, UCLA, 138-145 (1986).

19. A. Filiatrault and S. Cherry, 'Comparative Performance of Friction Damped Systems and Base Isolation Systems for Earthquake Retrofit and Aseismic Design', *Earthquake Engineering and Structural Dynamics,* vol. 16, 389-416 (1988).

20. C. Uang and V. V. Bertero, 'Evaluation of seismic energy in structures', *Earthquake eng.*

struct. dyn. vol. 19, 77-90 (1990).

21. A. W. Sadek and W. K. Tso, 'Inelastic seismic response of simple eccentric structures', *Earthquake eng. struct. dyn.* vol 13, 255-269 (1985).

22. Haluk Sucuoglu and Alphan Nurtug, 'Earthquake ground motion Characteristics and seismic Energy Dissipation', *Earthquake eng. struct. dyn.* vol 24, 1195-1213 (1995).

23. Masayoshi Nakashima, Kazuhiro Saburi and Bunzo Tsuji, 'Energy Input And Dissipation Behavior Of Structures With Hysteretic Dampers', *Earthquake eng. struct. dyn.* vol 25, 483-496 (1996).

24. V. W.-T. Cheung and W. K. Tso, 'Eccentricity in Irregular Multistorey Buildings'. *Canadian Journal of Civil Engineering,* vol. 13, pp. 46-52 (1986).

25. A. Rutenberg and M. Eisenberger, 'Laterally loaded Asymmetric Shear Buildings: Planar Analysis'. *Advances in Tall Buildings, Council on Tall Buildings and Urban Habitat.* Van Nostrand Oeinhold Company, New York. (1986)

APPENDIX A

NUMERICAL INPUT VALUES

A.1 SINGLE-STOREY MODEL

The following are the numerical input values for DRAIN-2D program:

T=1.0 sec., Ω_0= 0.9, ξ=0.05, Δt = 0.01 sec., m=1, and ρ=100.

[All units are SI units, N and mm]

Table 1: Elements Properties $e_s = 0$

ELEMENT	ELEMENT TYPE	YOUNG'S MODULUS	AREA	YIELD STRENGTH
1	Frame	0.394784	5000	Table 3
	Brace	0.394784	15000	Table 4, 5 & 6
2	Frame	0.394784	5000	Table 3
	Brace	0.394784	15000	Table 4, 5 & 6

- Young's modulus remains constant.
- Stiffness eccentricity introduced by changing the area of elements 1& 2.
- Slip load eccentricity introduced by changing the yield strength of elements 1 & 2.

Table 2: Different Areas of Elements for Different Eccentricities

		0.3	0.5	0.75	0.9	1.2
1	Frame	6581.1	7428.2	8200.9	8535.5	9000
	Brace	19743.3	22284.6	24602.7	25606.5	27000
2	Frame	3418.9	2571.8	1799.1	1464.5	1000
	Brace	10256.7	7715.4	5397.3	4393.5	3000

Table 3: Frame Yield Strength for Different Earthquake Records

	El Centro	N-B-K	Taft	Romania
Frame 1 &2	0.11802	0.375	0.03262	0.12392

Table 4: Brace Yield Strength for Different Earthquake Records ($e_{pb} = e_s$)

	El Centro	N-B-K	Taft	Romania
Brace 1 & 2	0.03934	0.125	0.01087	0.04131

Table 5: Brace Yield Strength for Different Earthquake Records ($e_{pb} = 0$)

		El Centro	N-B-K	Taft	Romania
$e_s = 0.3$	Brace 1	0.02988	0.09497	0.00826	0.03138
	Brace 2	0.05753	0.18281	0.0159	0.06041
$e_s = 0.5$	Brace 1	0.02684	0.08414	0.00732	0.02781
	Brace 2	0.07648	0.24302	0.02114	0.08031
$e_s = 0.75$	Brace 1	0.02389	0.07621	0.00663	0.0.2518
	Brace 2	0.10933	0.34739	0.03022	0.11479
$e_s = 0.9$	Brace 1	0.02305	0.07322	0.00637	0.02419
	Brace 2	0.13431	0.42677	0.03712	0.14103
$e_s = 1.2$	Brace 1	0.02186	0.06944	0.00604	0.02295
	Brace 2	0.19670	0.62500	0.05437	0.20653

Table 6: Brace Yield Strength for Different Earthquake Records ($e_{pb} = -e_s$)

		El Centro	N-B-K	Taft	Romania
$e_s = 0.3$	Brace 1	0.02043	0.06494	0.00565	0.02146
	Brace 2	0.07573	0.24061	0.02093	0.07951
$e_s = 0.5$	Brace 1	0.01324	0.04207	0.00366	0.01390
	Brace 2	0.11485	0.36453	0.03171	0.12046
$e_s = 0.75$	Brace 1	0.00863	0.02742	0.00238	0.00906
	Brace 2	0.17932	0.56979	0.04956	0.18828
$e_s = 0.9$	Brace 1	0.00675	0.02145	0.00187	0.00709
	Brace 2	0.22928	0.72853	0.6337	0.24075
$e_s = 1.2$	Brace 1	0.00437	0.01388	0.00121	0.00459
	Brace 2	0.35406	1.12500	0.09786	0.37176

Table 7: Distance Between The Resisting Elements and CM.

e_s	0.0	0.3	0.5	0.75	0.9	1.2
a	90	95	103	117	127	150

A.2 FIVE-STOREY MODEL

The following are the numerical input values of the five-storey model for DRAIN-2D program:

T=1.0 sec., Ω_0= 0.9, ξ=0.05, Δt = 0.01 sec., m=1, and ρ=100.
[All units are SI units, N and mm]

Table 8: Elements Properties $e_s = 0$

ELEMENT	ELEMENT TYPE	YOUNG'S MODULUS	AREA	YIELD STRENGTH
1	Frame	0.406087	60000	Table 10
	Brace	0.406087	180000	Table 11, 12 & 13
2	Frame	0.406087	60000	Table 10
	Brace	0.406087	180000	Table 11, 12 & 13

- Young's modulus remains constant.
- Stiffness eccentricity introduced by changing the area of elements 1& 2.
- Slip load eccentricity introduced by changing the yield strength of elements 1 & 2.

Table 9: Different Areas of Elements for Different Eccentricities

		0.3	0.5	0.75	0.9	1.2
1	Frame	78947.37	89126.21	98461.54	102519.69	108000
	Brace	236842.11	267378.64	295384.62	307559.06	324000
2	Frame	41052.63	30873.79	21538.46	17480.31	12000
	Brace	123157.89	92621.36	64615.38	52440.94	36000

Table 10: Frame Yield Strength for Different Earthquake Records

	El Centro	N-B-K	Taft	Romania
Frame 1 &2	0.04535	0.14554	0.01491	0.04825

Table 11: Brace Yield Strength for Different Earthquake Records ($e_{pb} = e_s$)

	El Centro	N-B-K	Taft	Romania
Brace 1 & 2	0.01512	0.04851	0.00497	0.01608

Table 12: Brace Yield Strength for Different Earthquake Records ($e_{pb} = 0$)

		El Centro	N-B-K	Taft	Romania
$e_s = 0.3$	Brace 1	0.01149	0.03687	0.00378	0.01222
	Brace 2	0.02209	0.0709	0.00726	0.02351
$e_s = 0.5$	Brace 1	0.01146	0.03266	0.00335	0.0183
	Brace 2	0.02938	0.09429	0.00939	0.03126
$e_s = 0.75$	Brace 1	0.00921	0.02933	0.00303	0.00980
	Brace 2	0.04211	0.13514	0.01385	0.04481
$e_s = 0.9$	Brace 1	0.00885	0.02839	0.002911	0.00941
	Brace 2	0.05189	0.16652	0.01706	0.05520
$e_s = 1.2$	Brace 1	0.00840	0.02695	0.00276	0.00894
	Brace 2	0.07558	0.24257	0.02485	0.08042

Table 13: Brace Yield Strength for Different Earthquake Records ($e_{pb} = -e_s$)

		El Centro	N-B-K	Taft	Romania
$e_s = 0.3$	Brace 1	0.00786	0.02523	0.00258	0.00836
	Brace 2	0.02907	0.09329	0.00956	0.03093
$e_s = 0.5$	Brace 1	0.00525	0.01681	0.00172	0.005571
	Brace 2	0.04364	0.14005	0.01435	0.04643
$e_s = 0.75$	Brace 1	0.003306	0.01061	0.00109	0.00352
	Brace 2	0.06910	0.22178	0.02272	0.07352
$e_s = 0.9$	Brace 1	0.00258	0.00823	0.00085	0.00274
	Brace 2	0.08866	0.28452	0.02915	0.09433
$e_s = 1.2$	Brace 1	0.00168	0.00054	0.00055	0.00179
	Brace 2	0.13605	0.43662	0.04474	0.14475

Distance (a) between the resisting element as table "7".

A.3 TEN-STOREY MODEL

A.3.1 Ten-storey Model With The Critical Value Of Ω_0.

The following are the numerical input values of the ten-storey model for DRAIN-2D program:

T=1.0 sec., Ω_0= 0.9, ξ=0.05, Δt = 0.01 sec., m=1, and ρ=100.
[All units are SI units, N and mm]

Table 14: Elements Properties $e_s = 0$

ELEMENT	ELEMENT TYPE	YOUNG'S MODULUS	AREA	YIELD STRENGTH
1	Frame	0.883648	100000	Table 16
	Brace	0.883648	300000	Table 17, 18, & 19
2	Frame	0.883648	100000	Table 16
	Brace	0.883648	300000	Table 17, 18, & 19

- Young's modulus remains constant.
- Stiffness eccentricity introduced by changing the area of elements 1& 2.
- Slip load eccentricity introduced by changing the yield strength of elements 1 & 2.

Table 15: Different Areas of Elements for Different Eccentricities

		0.3	0.5	0.75	0.9	1.2
1	Frame	131578.95	148543.69	164102.56	170866.14	180000
	Brace	394736.85	445631.07	492307.69	512598.43	540000
2	Frame	68421.05	51456.31	35897.44	29133.86	20000
	Brace	205263.15	154368.93	107692.31	87401.57	60000

Table 16: Frame Yield Strength for Different Earthquake Records

	El Centro	N-B-K	Taft	Romania
Frame 1 &2	0.05338	0.16587	0.016	0.05715

Table 17: Brace Yield Strength for Different Earthquake Records ($e_{pb} = e_s$)

	El Centro	N-B-K	Taft	Romania
Brace 1 & 2	0.01779	0.05529	0.00533	0.01905

Table 18: Brace Yield Strength for Different Earthquake Records ($e_{pb} = 0$)

		El Centro	N-B-K	Taft	Romania
$e_s = 0.3$	Brace 1	0.013523	0.04202	0.004053	0.014478
	Brace 2	0.026006	0.06236	0.007795	0.027842
$e_s = 0.5$	Brace 1	0.011979	0.03722	0.00359	0.012825
	Brace 2	0.034578	0.10745	0.010365	0.037022
$e_s = 0.75$	Brace 1	0.010843	0.03369	0.00325	0.011609
	Brace 2	0.049567	0.15402	0.014857	0.053068
$e_s = 0.9$	Brace 1	0.010414	0.03236	0.003121	0.011149
	Brace 2	0.061074	0.18978	0.018306	0.065388
$e_s = 1.2$	Brace 1	0.009885	0.03072	0.002963	0.010583
	Brace 2	0.088967	0.27645	0.026667	0.095250

Table 19: Brace Yield Strength for Different Earthquake Records ($e_{pb} = -e_s$)

		El Centro	N-B-K	Taft	Romania
$e_s = 0.3$	Brace 1	0.009253	0.02875	0.002773	0.009906
	Brace 2	0.034218	0.10633	0.010256	0.036635
$e_s = 0.5$	Brace 1	0.006164	0.01915	0.001847	0.006599
	Brace 2	0.051366	0.15961	0.015396	0.054993
$e_s = 0.75$	Brace 1	0.003892	0.01209	0.001167	0.004167
	Brace 2	0.081341	0.25275	0.024381	0.087086
$e_s = 0.9$	Brace 1	0.003033	0.00947	0.000909	0.003248
	Brace 2	0.104356	0.32427	0.031279	0.111726
$e_s = 1.2$	Brace 1	0.001977	0.00614	0.000593	0.002117
	Brace 2	0.160140	0.49886	0.048	0.17145

A.3.2 Torsionally Flexible Ten-storey Model

The following are the numerical input values of the torsionally flexible ten-storey model for DRAIN-2D program:

T=1.0 sec., Ω_0= 0.7, ξ=0.05, Δt = 0.01 sec., m=1, and ρ=100.
[All units are SI units, N and mm]

Table 20: Elements Properties $e_s = 0$

ELEMENT	ELEMENT TYPE	YOUNG'S MODULUS	AREA	YIELD STRENGTH
1	Frame	0.883648	100000	Table 16
	Brace	0.883648	300000	Table 17, 18, & 19
2	Frame	0.883648	100000	Table 16
	Brace	0.883648	300000	Table 17, 18, & 19

- Young's modulus remains constant.
- Stiffness eccentricity introduced by changing the area of elements 1& 2.
- Slip load eccentricity introduced by changing the yield strength of elements 1 & 2.

Table 21: Different Areas of Elements for Different Eccentricities

		0.3	0.5	0.75	0.9	1.2
1	Frame	1390625.5	157736.72	172815.53	178947.37	186330.9
	Brace	417187.5	473210.16	518946.59	536842.1	558992.7
2	Frame	60937.5	42263.28	27184.47	21052.63	13669.1
	Brace	182812.5	126789.89	81553.41	63157.89	41007.3

See table 16 for frame yield strength of Different Earthquake Records.

See table 17 for braces yield strength of Different Earthquake Records ($e_{pb} = e_s$)

Table 22: Distance Between The Resisting Elements and CM.

e_s	0.0	0.3	0.5	0.75	0.9	1.2
a	50	77	86.6	103	114	139

Table 23: Brace Yield Strength for Different Earthquake Records ($e_{pb} = 0$)

		El Centro	N-B-K	Taft	Romania
$e_s = 0.3$	Brace 1	0.0128	0.0398	0.00384	0.0137
	Brace 2	0.0292	0.0907	0.00875	0.0313
$e_s = 0.5$	Brace 1	0.0113	0.0.351	0.00338	0.0121
	Brace 2	0.0421	0.1308	0.0162	0.0451
$e_s = 0.75$	Brace 1	0.0103	0.0320	0.00308	0.0110
	Brace 2	0.0655	0.2034	0.01962	0.0701
$e_s = 0.9$	Brace 1	0.0099	0.0309	0.00298	0.0106
	Brace 2	0.0845	0.2626	0.0253	0.0905
$e_s = 1.2$	Brace 1	0.00955	0.0997	0.00286	0.0102
	Brace 2	0.1302	0.4044	0.0390	0.1394

Table 24: Brace Yield Strength for Different Earthquake Records ($e_{pb} = -e_s$)

		El Centro	N-B-K	Taft	Romania
$e_s = 0.3$	Brace 1	0.0078	0.0242	0.00233	0.00835
	Brace 2	0.0406	0.1262	0.01217	0.04347
$e_s = 0.5$	Brace 1	0.0048	0.0148	0.00143	0.00510
	Brace 2	0.0664	0.2064	0.0199	0.0711
$e_s = 0.75$	Brace 1	0.0028	0.00869	0.00084	0.002994
	Brace 2	0.1131	0.3515	0.0339	0.1211
$e_s = 0.9$	Brace 1	0.00209	0.0065	0.00063	0.00224
	Brace 2	0.1512	0.46997	0.0453	0.1619
$e_s = 1.2$	Brace 1	0.00131	0.00406	0.00039	0.0014
	Brace 2	0.1426	0.7537	0.0727	0.2598

A.3.3 Torsionally Rigid Ten-storey Model

The torsionally rigid ten-storey model has the same numerical input values as the ten-storey model with Ω_0=0.9, but it has additional two elastic resisting element in the orthogonal direction (elements 3 & 4) placed at distance d = 85 mm either side of the center of mass. These two elastic elements have the following numerical input values for DRAIN-2D program:

T=1.0 sec., Ω_0= 1.7, ξ=0.05, Δt = 0.01 sec., m=1, and ρ=100.
[All units are SI units, N and mm]

Table 25: Elements Properties $e_s = 0$

ELEMENT	ELEMENT TYPE	YOUNG'S MODULUS	AREA	YIELD STRENGTH
3	Frame	0.00001	25000	999999
4	Frame	0.00001	25000	999999

A.4 The Ratio ω_2/ω_1 for Single and Multi-storey Models:

For single-storey model the ratio ω_2/ω_1 has been calculated for Ω_0= 0.9 using equation 2-23.

For the multi-storey models the ratio ω_2/ω_1 has been calculated for Ω_0= 0.9 using SAP90 program.

Table 26: The Ratio ω_2/ω_1

e_s	1-Storey	5-Storey	10-Storey
0.3	0.718	0.69	0.718
0.5	0.588	0.588	0.588
0.75	0.46	0.48	0.46

Table 26: The Ratio ω_2/ω_1

e_s	1-Storey	5-Storey	10-Storey
0.9	0.398	0.36	0.397
1.2	0.302	0.34	0.33

A.4 T_θ max and $V_y$max of the Base Shear And Torque Time History:

For single storey model with two FDBF in the direction of excitation following properties apply:

T=1.0 sec., Ω_0= 0.9, ξ=0.05, Δt = 0.01 sec., m=1, and ρ=100.

$V_y$max = 2360.4 N

Table 27: Values of T_θ max for Different Eccentricities

e_s	0.0	0.3	0.5	0.75	0.9	1.2
T_θ max (N.mm)	212436	224238	243120.4	276166.8	299770.8	354060

APPENDIX B

SPECTRAL VELOCITY OF ROMANIA AND EL CENTRO EARTHQUAKE

ENERGY INPUT OF ELASTIC UNBRACED CASE:

For Romania earthquake:

$R_{elastic} = 4.9568$ kN

$\Delta_{max} = 0.125$ m

Elastic strain energy $E^e = 0.5\ R_{elastic}\ \Delta_{max}$

$E^e = 0.3098$ kN.m

Using spectral velocity:

$E^e = 0.5\ (m)\ (S_v^2)$

$E^e = 0.5 \cdot (1) \cdot (0.79^2) = 0.31205$ kN.m

The energy curves are normalized with respect to the frame elastic energy of symmetric unbraced case E_{el}.

$E_{el}(e=0\ \&\ KB/KF=0) = 0.5\ (RF)\ (\Delta_y)$

$\Delta_y = \Delta_{max}/4 = 0.03125$ m

$RF = R_{elastic}/4 = 1.2392$ kN

$E_{el}(e=0\ \&\ KB/KF=0) = 0.019$ kN.m

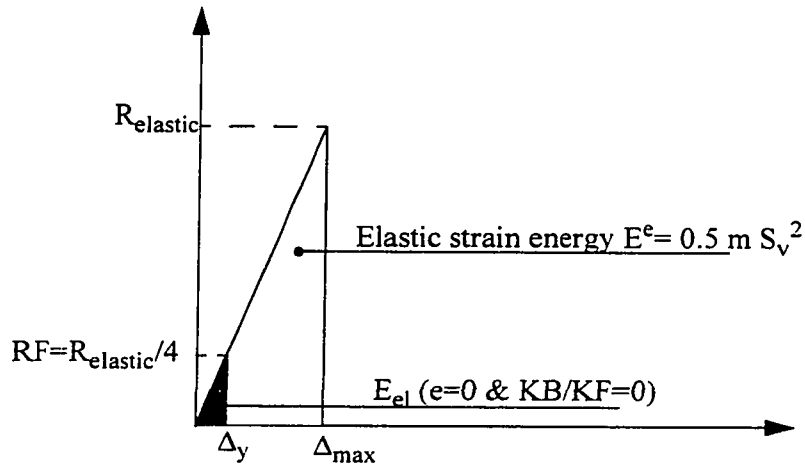

Figure B.1 Elastic strain energy and frame elastic strain energy of symmetric unbraced case

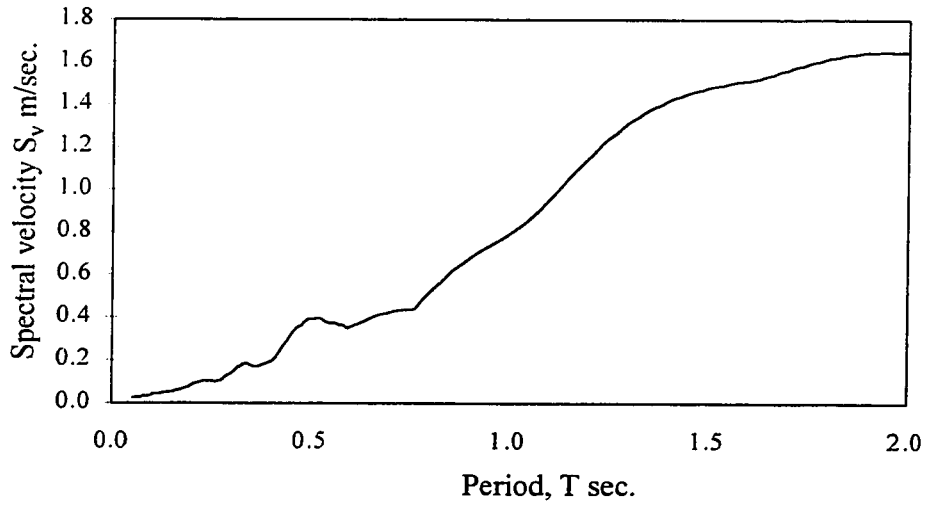

Figure B.2 Velocity Spectrum of 1977 Romania earthquake

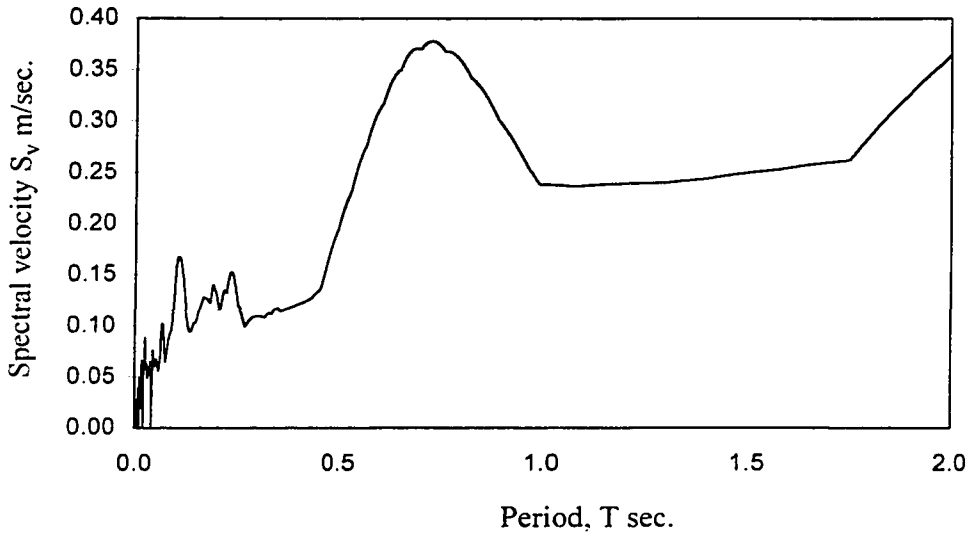

Figure B.3 Velocity spectrum of 1940 El Centro N-S

APPENDIX C

DISPLACEMENT PERFORMANCE OF THE SINGLE AND MULTI-STOREY MODELS DUE TO EACH EARTHQUAKE.

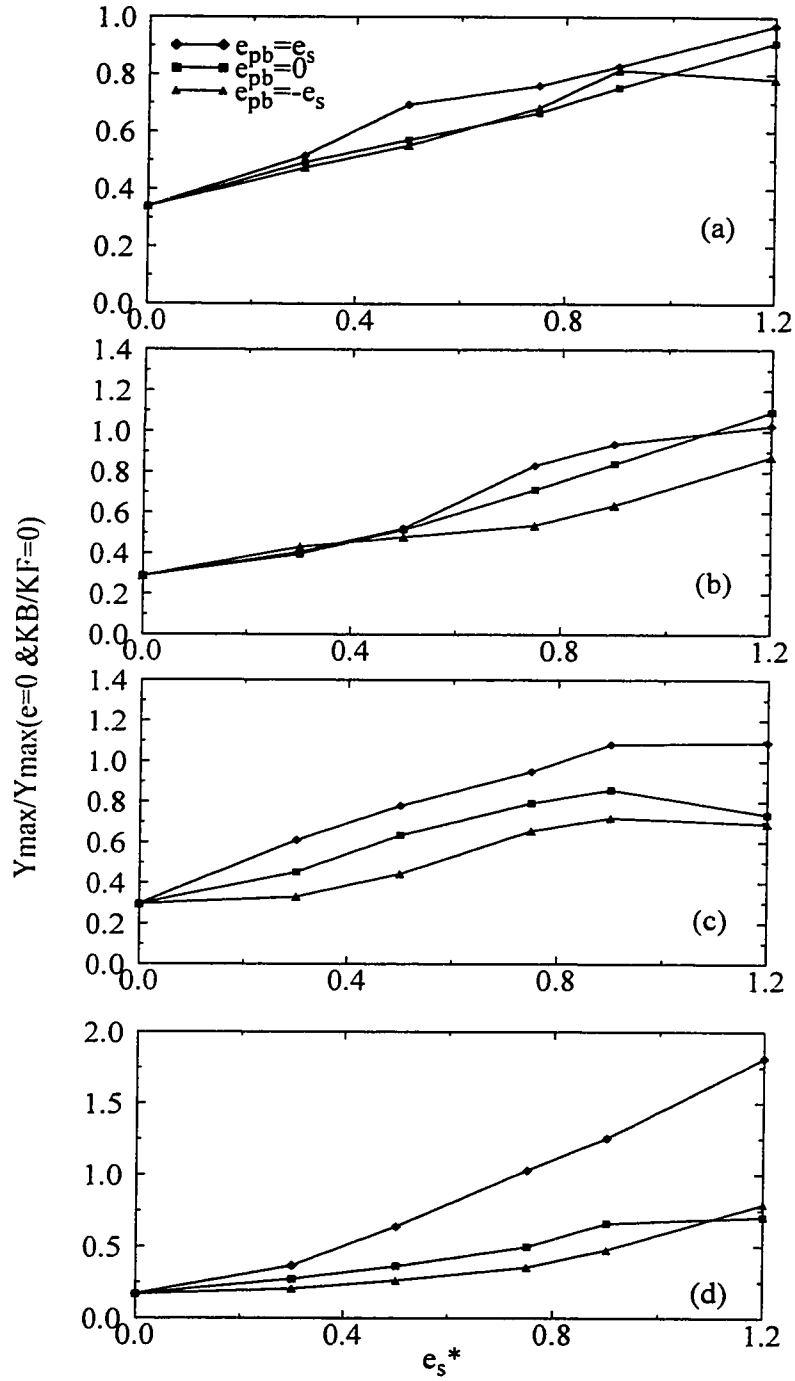

Figure C.1 Maximum response for the single-storey model (T =1 & Ω_0= 0.9)

(a) EL Centro (b) Newark-Blame-Kapur (c) Taft (d) Romania

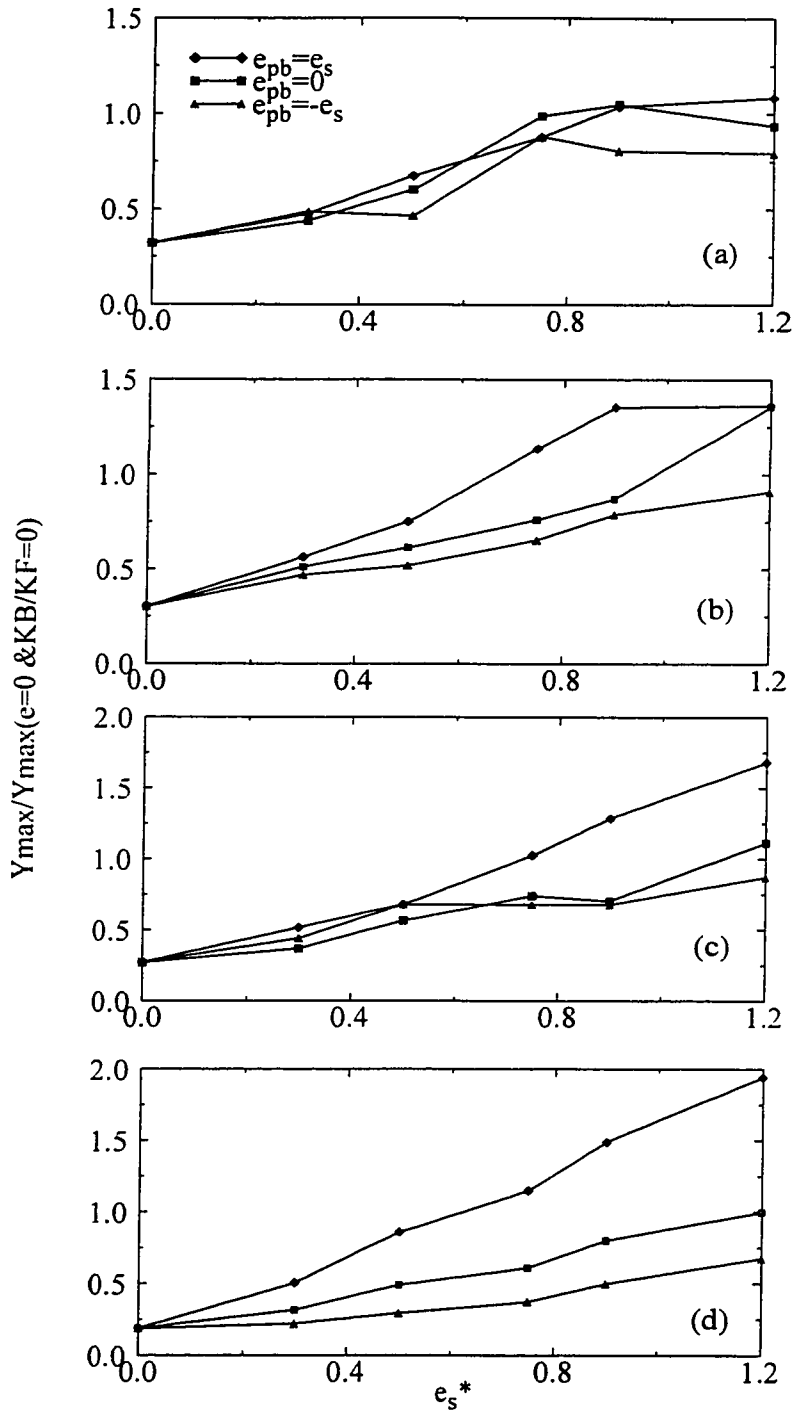

Figure C.2 Maximum response for the five-storey model (T =1 & Ω_0= 0.9)
(a) EL Centro (b) Newark-Blame-Kapur (c) Taft (d) Romania

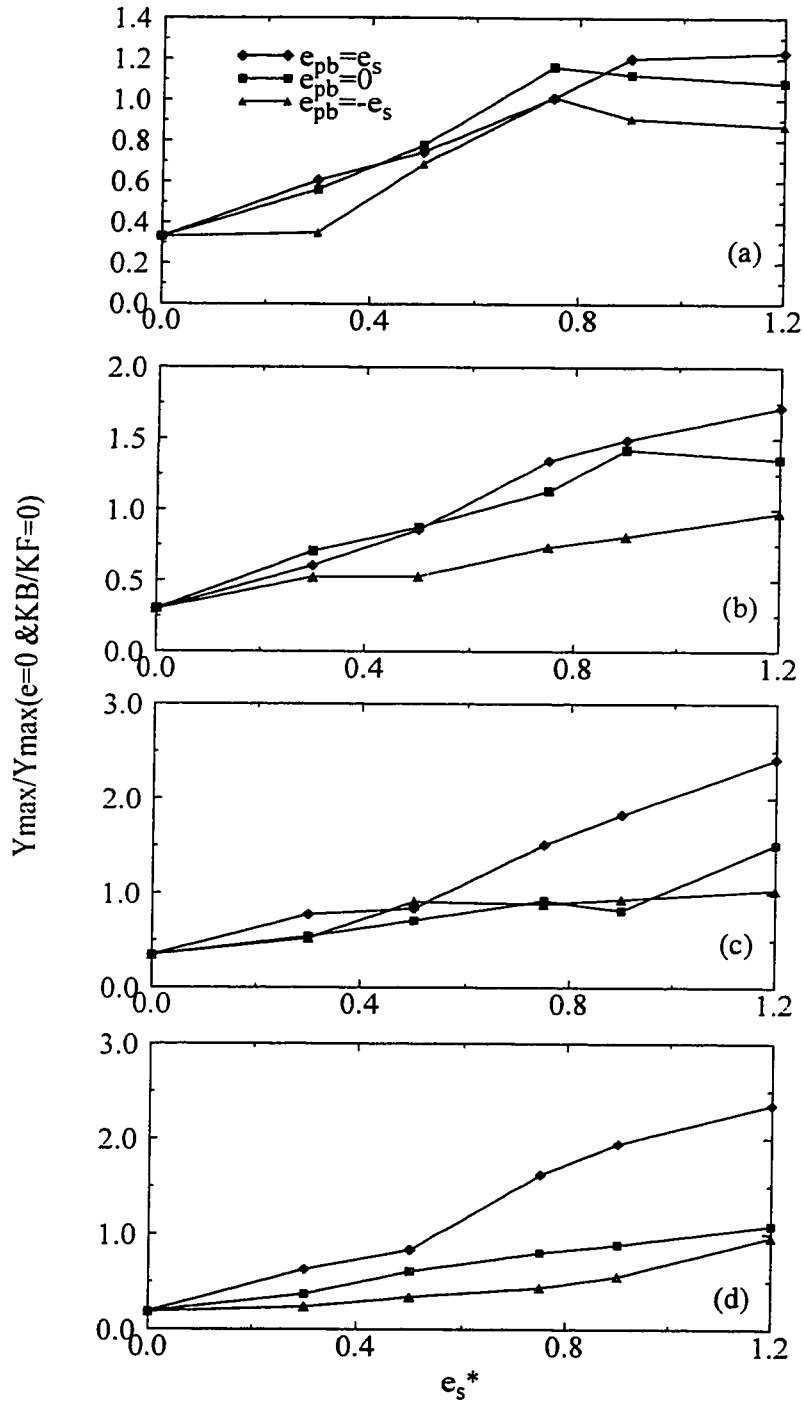

Figure C.3 Maximum response for the ten-storey model (T =1 & Ω_0= 0.9)
(a) EL Centro (b) Newark-Blame-Kapur (c) Taft (d) Romania

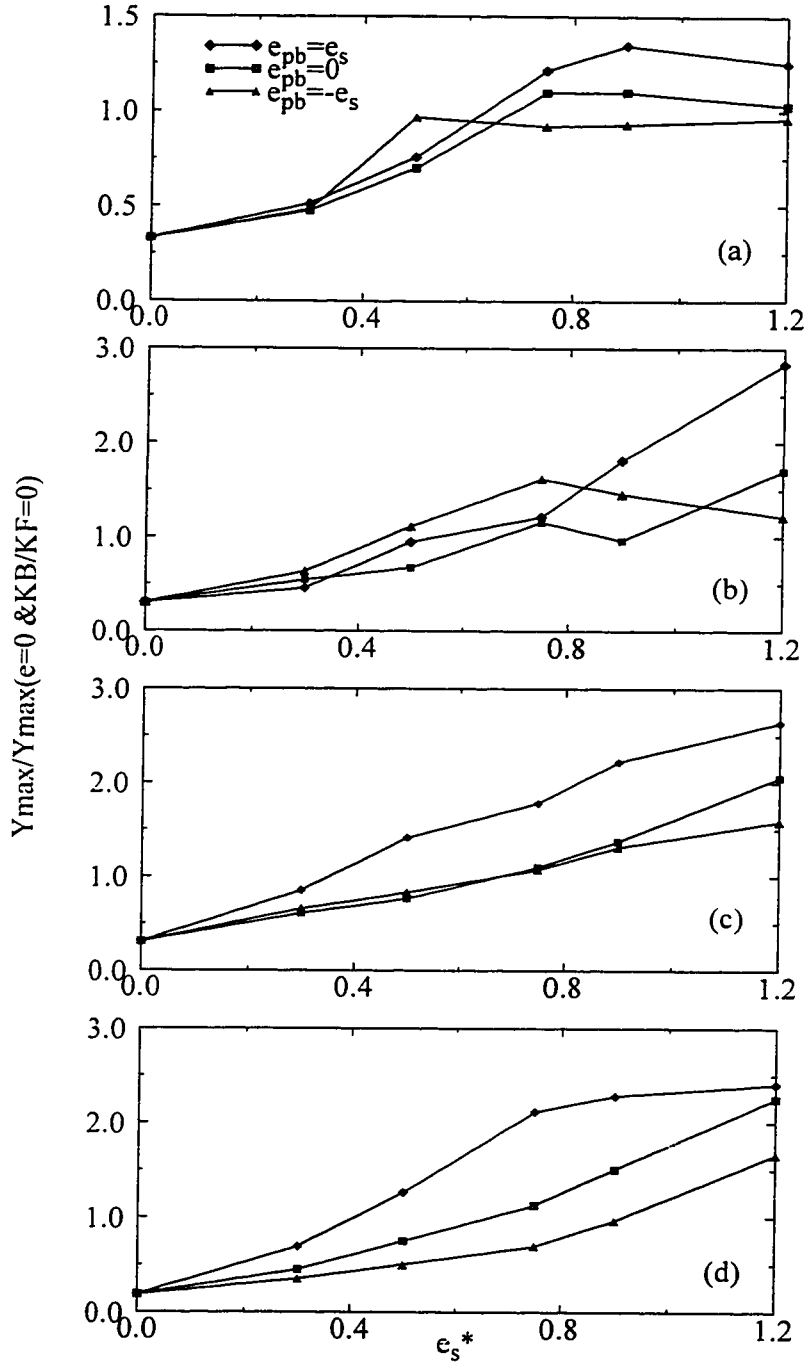

Figure C.4 Maximum response for the torsionally flexible ten-storey model (T=1 & Ω_0=0.7)(a) EL Centro (b) Newark-Blame-Kapur (c) Taft (d) Romania

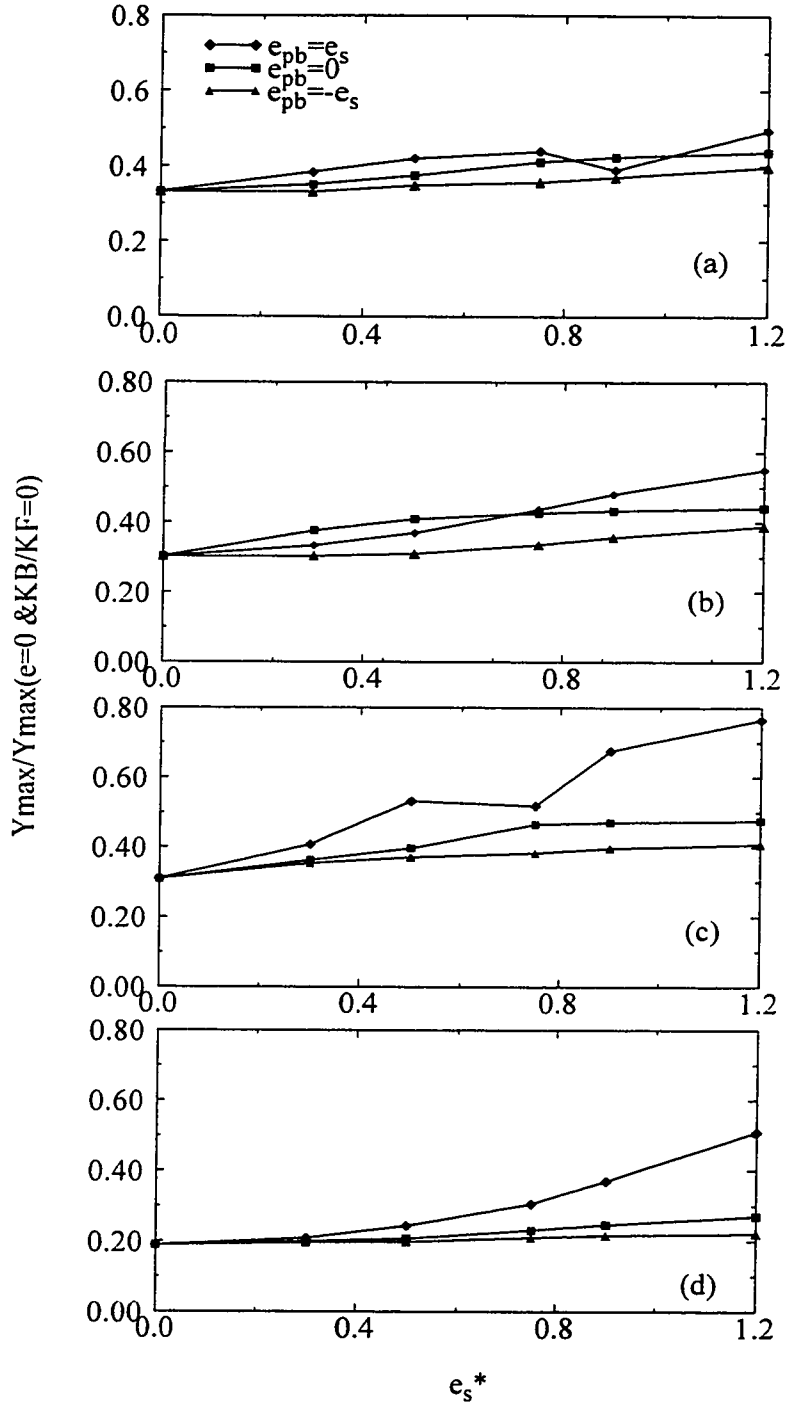

Figure C.5 Maximum response for the torsionally rigid ten-storey model (T=1 & Ω_0=1.7)(a) EL Centro (b) Newark-Blame-Kapur (c) Taft (d) Romania